University of Alberta

Pharmacokinetics and Dosimetry of Radiolabelled Iodoazomycin Arabinoside (IAZA)

by

Daria Stypinski ©

A thesis submitted to the Faculty of Graduate Studies and Research in partial fulfillment of the requirements for the degree of Doctor of Philosophy

in

Pharmaceutical Sciences

Faculty of Pharmacy and Pharmaceutical Sciences

Edmonton, Alberta

Spring 1998

National Library of Canada
Acquisitions and Bibliographic Services
395 Wellington Street
Ottawa ON K1A 0N4
Canada

Bibliothèque nationale du Canada
Acquisitions et services bibliographiques
395, rue Wellington
Ottawa ON K1A 0N4
Canada

Your file Votre référence

Our file Notre référence

The author has granted a non-exclusive licence allowing the National Library of Canada to reproduce, loan, distribute or sell copies of this thesis in microform, paper or electronic formats.

L'auteur a accordé une licence non exclusive permettant à la Bibliothèque nationale du Canada de reproduire, prêter, distribuer ou vendre des copies de cette thèse sous la forme de microfiche/film, de reproduction sur papier ou sur format électronique.

The author retains ownership of the copyright in this thesis. Neither the thesis nor substantial extracts from it may be printed or otherwise reproduced without the author's permission.

L'auteur conserve la propriété du droit d'auteur qui protège cette thèse. Ni la thèse ni des extraits substantiels de celle-ci ne doivent être imprimés ou autrement reproduits sans son autorisation.

0-612-29114-6

Canada

University Of Alberta

Faculty of Graduate Studies and Research

The undersigned certify that they have read, and recommended to the Faculty of Graduate Studies and Research for acceptance, a thesis entitled **Pharmacokinetics and Dosimetry of Radiolabelled Iodoazomycin Arabinoside (IAZA)** submitted by Daria Stypinski in partial fulfillment of the requirements for the degree of Doctor of Philosophy in Pharmaceutical Sciences.

Dr. Leonard I. Wiebe (Supervisor)

Dr. John R. Mercer (Co-supervisor)

Dr. Yun K. Tam

Dr. Stephen A. McQuarrie

Dr. Alexander J. B. McEwan

Dr. Donald Lyster (External Examiner)

Date: November 16, 1992

To my beloved mom and dad: Stanislawa and Daniel Stypinski.

ABSTRACT

Purpose: Radiolabelled iodoazomycin arabinoside ($^{123/125}$I-IAZA), a novel gamma-emitting imaging agent which preferentially binds to hypoxic cells, has already shown very promising results in about 100 patients as a marker of hypoxic regions in tumors. The objectives of this study were to determine human pharmacokinetics (PK) and dosimetry of ^{123}I-IAZA, and to use these data to develop a pharmacokinetic/pharmaco-dynamic (PK/PD) link-model to predict tissue oxygenation status from a scintigraphic image depicting total radioactivity. The effect of an inhalation anesthetic on the PK of ^{125}I-IAZA was also studied in an animal model.

Methods: The PK parameters of $^{125/123}$I-IAZA were determined in seven Sprague-Dawley rats (4 anesthetized with methoxyflurane and 3 non-anesthetized) and in six healthy volunteers. Blood and urine samples were analyzed using HPLC followed by highly sensitive gamma radiometry of the radiolabelled species. Human dosimetry analysis was derived from five anterior and posterior whole body scintigraphic images. The effect of exercise on the PK and dosimetry of ^{123}I-IAZA was studied in three volunteers subjected to the "Bruce" treadmill protocol.

Results: Non-anesthetized rats had three-fold higher clearance and three fold-shorter elimination phase half-lives for ^{125}I-IAZA than the anesthetized group, without any apparent differences in total radioactivity PK parameters. In humans, ^{123}I-IAZA was shown to have acceptable dosimetry, despite its relatively low clearance (239 ± 48 mL/min). Its V_{ss} was 0.716 ± 0.088 L/kg, with a rapid distribution ($t_{½\alpha}$ = 5.3 ± 4.2 min) and much slower elimination ($t_{½\beta}$ = 179 ± 24 min) phases. Total radioactivity $t_{½\beta}$ was 294 ± 27 min with 92 % renally eliminated (12 % as intact ^{123}I-IAZA). The PK/PD model incorporated ^{123}I-IAZA PK blood profile, tumor volume, perfusion, and

phenotype-specific intrinsic PK parameters (V_{max}, K_m, and cellular efflux of radioactivity) to determine the fraction of the dose reductively bound in the hypoxic cell compartment.

Conclusions: Disposition kinetics and favorable radiation dosimetry support the clinical use of ^{123}I-IAZA for imaging tissue hypoxia. The striking effects of anesthesia on the PK of ^{125}I-IAZA in rats bring into question the current practices of anaesthetizing animals during pre-clinical imaging studies. The PK/PD model developed utilizes the relationship between the pharmacokinetic parameters of ^{123}I-IAZA and total radioactivity to correlate signal intensity to hypoxic fraction.

Acknowledgements

I would like to express my deep gratitude to Dr. L.I. Wiebe for his guidance, encouragement, support and enthusiasm throughout the duration of my studies. He has been an excellent supervisor and a true mentor.

I wish also to express my appreciation to Dr J.R. Mercer and Dr. Y.K. Tam for years of advice and encouragement. In addition, I would like to say thank you to all the professors and staff of the Faculty of Pharmacy and Pharmaceutical Sciences for passing on the knowledge, for their personal involvement, friendship and advice throughout both my graduate and undergraduate years at this Faculty.

A very special thank you is also extended to all the human volunteers for their cooperation and patience, and to the staff of the Nuclear Medicine Department for their assistance in completing the human studies.

I especially thank and dedicate this work to my mother, Stanislawa, and my father, Daniel, for their love, encouragement, support, advice, understanding and patience over my entire life, and particularly over the course of my studies.

I also acknowledge the studentship awards from the Medical Research Council of Canada, the Alberta Heritage Foundation for Medical Research and the Sanofi Winthrop Medical Imaging Institute.

TABLE OF CONTENTS

1. INTRODUCTION 1
   1.1 Hypoxia 1
   1.2 The Ideal Hypoxia Radiopharmaceutical 2
   1.3 References 6

2. LITERATURE SURVEY OF THE PHARMACOKINETICS OF HYPOXIA RADIOPHARMACEUTICALS 8
   2.1 Misonidazole Analogues 8
      2.1.1 ^{3}H-Misonidazole (^{3}H-MISO) 8
      2.1.2 ^{82}Br-Bromomisonidazole (^{82}Br-BrMISO) 9
      2.1.3 ^{18}F-Fluoromisonidazole (^{18}F-FMISO) 9
      2.1.4 ^{131}I-Iodovinylmisonidazole (^{131}I-IvMISO) 12
   2.2 ^{99m}Tc-labelled 2-nitroimidazoles 12
   2.3 Iodoazomycin Nucleosides 13
      2.3.1 Iodoazomycin Riboside (IAZR) 14
      2.3.2 Iodoazomycin Galactoside (IAZG) 15
      2.3.3 Iodoazomycin Pyranoside (IAZP) 15
      2.3.4 Fluoroiodoazomycin Pyranoside (FIAZP) 15
      2.3.5 Iodoazomycin Arabinoside (IAZA) 16
   2.4 References 18

3. RATIONALE, HYPOTHESIS AND OBJECTIVES 23
   3.1 Rationale 23
   3.2 Hypotheses 23
   3.3 Objectives 24

4. HPLC AND RADIOMETRIC ASSAY OF RADIOLABELLED IAZA IN BLOOD AND URINE 25
   4.1 Introduction 25
   4.2 Experimental 26
      4.2.1 Reagents 26
      4.2.2 Blood Sample Collection and Preparation 26
      4.2.3 Solid Phase Extraction 27
      4.2.4 Urine Sample Preparation 27
      4.2.5 Instrumentation and Chromatographic Conditions 27
      4.2.6 Extraction Efficiency 28
   4.3 Results and Discussion 29
   4.4 References 35

5. COMPARISON OF ^{125}I-IAZA PHARMACOKINETICS IN ANESTHETIZED AND NON-ANESTHETIZED RATS 36
   5.1 Introduction 36
   5.2 Experimental 37
      5.2.1 Chemicals and Dose Preparation 37
      5.2.2 Catheter Cross-Contamination Effect 38
      5.2.3 Animal Models Preparation 38
      5.2.4 Sample Analysis 39
      5.2.5 Pharmacokinetic and Statistical Analysis 39
   5.3 Results 40

5.3.1 Catheter Washout Study 40
5.3.2 ^{125}I-IAZA and Total Radioactivity Pharmacokinetics 41
5.3.3 Metabolite Pharmacokinetics 43
5.3.4 Biodistribution (Group 2) 44
5.4 Discussion 45
5.5 References 49

6. PHARMACOKINETICS OF ^{123}I-IAZA IN HEALTHY SUBJECTS 52
6.1 Introduction 52
6.2 Experimental 53
6.2.1 Chemicals and reagents 53
6.2.2 Clinical protocol 53
6.2.3 Pharmacokinetic analysis 54
6.3 Results 55
6.3.1 Blood clearance of ^{123}I-IAZA and total radioactivity 55
6.3.2 Blood clearance of IAZA and total radioactivity corrected for physical decay 57
6.3.3 Total body clearance of ^{123}I-IAZA and total radioactivity 58
6.3.4 Disposition kinetics of radioiodinated metabolites of IAZA 59
6.3 Discussion 61
6.4 References 65

7. RADIATION DOSIMETRY OF ^{123}I-IAZA IN HEALTHY SUBJECTS 67
7.1 Introduction 67
7.2 Experimental 68
7.2.1 ^{123}I-IAZA Preparation 68
7.2.2 Clinical Protocol 68
7.2.3 Region of Interest Selection Protocol 69
7.2.4 Source Organ Activity 70
7.2.5 Total Body and All Body Activity Determination 72
7.2.6 Organ Mean Residence Time Determination 73
7.2.7 Remainder of the Body Mean Residence Time 73
7.2.8 Renal and GIT Excretion Fractions 73
7.2.9 Generation of Radiation Dose Estimates 74
7.3 Results and Discussion 74
7.3.1 Gamma Camera Imaging 74
7.3.2 Volunteer Dosimetry Results 76
7.3.3 Kinetic and Dosimetric Correlation 82
7.4 References 86

8. PHARMACOKINETICS AND RADIATION DOSIMETRY OF ^{123}I-IAZA IN HEALTHY VOLUNTEERS FOLLOWING "BRUCE" TREADMILL PROTOCOL 87
8.1 Introduction 87
8.2 Experimental 87
8.2.1 Chemicals and reagents 87
8.2.2 Clinical protocol 88
8.2.3 Pharmacokinetic and dosimetric analysis 89
8.3 Results and Discussion 90
8.3.1 Pharmacokinetics 90

8.3.2 Dosimetry 94
8.4 References 97

9. A PHARMACOKINETIC-PHARMACODYNAMIC MODEL TO QUANTIFY TISSUE HYPOXIA WITH ^{123}I-IAZA 100
9.1 Introduction 100
9.2 Theoretical Model Development 101
9.2.1 Physiological Pharmacokinetic Model of the Effect Compartment 101
9.2.2 Classical Pharmacokinetic Model of the Effect Compartment 102
9.2.3 Merging of the Classical and Physiological Models 104
9.2.4 In Vitro Data 106
9.3 Computer Simulations 108
9.4 Discussion 110
9.5 References 118

10. GENERAL DISCUSSION AND CONCLUSIONS 121
References 124

11. APPENDICES 125
Appendix 1: Whole blood concentrations of total adioactivity, ^{125}I-IAZA and radioactive metabolites in anesthetized and non-anesthetized rats after ^{125}I-IAZA administration. 125
Appendix 2: Blood sample collection times and corresponding concentrations of ^{123}I-IAZA and total radioactivity in volunteers 1 through 6. 127
Appendix 3: Blood sample collection times and corresponding concentrations of ^{123}I-IAZA and total radioactivity in volunteers CV1, CV2 and CV3 129
Appendix 4: Fractional mean residence times used for calculation of dosimetry estimates in healthy volunteers after i.v. administration of ^{123}I-IAZA. 130
Appendix 5: Consent form given to each volunteer prior to ^{123}I-IAZA administration. 131
Appendix 6: Instruction sheet supplied to each volunteer prior to the cardiac stress test study. 135
Appendix 7: Summary of all the currently available effective pharmacokinetic parameters of ^{123}I-IAZA and total radioactivity in patients and volunteers. 138

List of Tables

Table 4.1 Extraction efficiency values for IAZA in the matrices studied. **31**

Table 5.1 Pharmacokinetic parameters following a single i.v. ^{125}I-IAZA administration to anesthetized (Group 1) and non-anesthetized (Group 2) rats. **42**

Table 6.1 Volunteer demographics and doses for ^{123}I-IAZA study at rest. **54**

Table 6.2 Effective pharmacokinetic parameters of ^{123}I-IAZA and total radioactivity in healthy human volunteers after i.v. administration of ^{123}I-IAZA. **57**

Table 6.3 Decay corrected biologic pharmacokinetic parameters of IAZA and total radioactivity in healthy human volunteers after i.v. administration of ^{123}I-IAZA. **58**

Table 6.4 Relationship between mean values of ^{123}I-IAZA and total radioactivity dose fractions per mL of blood. **60**

Table 7.1 Radiation dose estimates for ^{123}I-IAZA in six volunteers using a 2 h bladder void time. The "reference adult" phantom was used for volunteers 1, 2, 3 and 5 (males). The "adult female" phantom used for volunteers 4 and 6 (females). **79**

Table 7.2 Radiation dose estimates for ^{123}I-IAZA in six volunteers using a 4.8 h bladder void time. The "reference adult" phantom was used for volunteers 1, 2, 3 and 5 (males). The "adult female" phantom used for volunteers 4 and 6 (females). **80**

Table 7.3 Dosimetry estimates comparison between ^{123}I-IAZA and several other radiopharmaceuticals. Dose estimates are for adults with a 2 h bladder void time. **81**

Table 7.4 MRT estimates for various organs for six healthy volunteers. Values based on whole body scintigraphic image analysis at five time points within a 24 h period after ^{123}I-IAZA administration. **83**

Table 7.5 Comparison of dosimetric and pharmacokinetic methods to estimate the effective total body MRT and the percent of total radioactivity eliminated in the urine of six volunteers. Percent dose in urine is based on biological elimination routes only, and does not include clearance due to physical decay of the radionuclide. **84**

Table 8.1 Volunteer demographics and doses for ^{123}I-IAZA cardiac stress test study. **88**

Table 8.2 Summary of pharmacokinetic parameters of ^{123}I-IAZA and total radioactivity in the three stressed volunteers. Also included are the arithmetic mean ± SD values for the six volunteers whose kinetic parameters have been determined at rest. **91**

Table 8.3 Radiation dose estimates for ^{123}I-IAZA in stressed volunteers CV1 and CV2, and mean and standard deviation values from the rest study in a group of six volunteers (Ref; Chapter 7, Tables 7.1 and 7.2). **96**

Table 11.1 Individual and mean concentrations of total radioactivity and ^{125}I-IAZA in anesthetized rats (group 1). All values represent percent injected dose per g of whole blood. **125**

Table 11.2 Individual and mean concentrations of total radioactivity and ^{125}I-IAZA in non-anesthetized rats (group 2). All values represent percent injected dose per g of whole blood. **126**

Table 11.3 Mean concentrations of total radioactivity, ^{125}I-IAZA and radioiodinated metabolites in anesthetized (group 1) and non-anesthetized (group 2) rats. All values represent percent injected dose per g of whole blood. **126**

Table 11.4 Target and actual blood sample collection times for volunteers 1 – 6. **127**

Table 11.5 ^{123}I-IAZA concentrations in blood samples of volunteers 1 – 6 following i.v. administration of ^{123}I-IAZA. **127**

Table 11.6 Total radioactivity concentrations in blood samples of volunteers 1 – 6 following i.v. administration of ^{123}I-IAZA. **128**

Table 11.7 Total radioactivity and ^{123}I-IAZA concentrations in blood samples of volunteers CV1, CV2 and CV3 following i.v. administration of ^{123}I-IAZA during Bruce treadmill protocol. **129**

Table 11.8 Fractional mean residence times of total radioactivity in source organs and in the remainder of the body ROI following ^{123}I-IAZA administration. **130**

Table 11.9 Summary of all the currently available pharmacokinetic parameters of ^{123}I-IAZA and total radioactivity in patients with cancer (n = 3) and in healthy volunteers (n = 9). Parameters are based on effective half-life determinations (i.e. no decay correction). **138**

List of Figures

Figure 2.1 Structure of 1-(5-iodo-5-deoxy-β-D-arabinofuranosyl) -2-nitroimidazole (IAZA). 16

Figure 4.1 IAZA calibration curve using analytical HPLC (injection volume = 25 μL, flow conditions: 60:40 H_2O:MeOH, 2 mL/min, λ = 325 nm, retention time 5.98 ± 0.25 min). Each point represents n = 5 samples. 29

Figure 4.2 IAZA stability in rat plasma samples. Values expressed as ratio of ^{125}I-IAZA fraction in the sample at the time of analysis to the fraction of ^{125}I-IAZA at the time of sample preparation. Key: (●) refrigerated sample; (▲) frozen sample (thawed at room temperature for 30 min prior to HPLC analysis). 30

Figure 4.3 HPLC chromatogram (upper panel) and corresponding radiometric plot (lower panel) of a representative human blood sample after single ^{123}I-IAZA i.v. administration. In the lower panel A represents polar radioactive metabolites, while B represents radioactive ^{123}I-IAZA. 33

Figure 4.4 HPLC chromatograms of representative cumulative 28 h human urine sample without the internal standard (upper panel) and after addition of 50 μg of the internal standard to 1 mL of urine (middle panel), and a corresponding radiometric plot (lowest panel) after single i.v. ^{123}I-IAZA dose administration. In the lowest panel A represents polar radioactive metabolites, while B represents radioactive ^{123}I-IAZA. 34

Figure 5.1 Radioactive contamination (CPM) in various catheter wash samples *vs.* sample wash number following a push of ^{125}I-IAZA (220 μCi). Key: Plot 1 (●) ten sequential 0.25 mL normal saline washes of the catheter; Plot 2 (O) five sequential 0.25 mL washes with rat whole blood; Plot 3 (▼) one 0.25 mL whole blood wash followed by one 0.2 mL normal saline wash (CPM not shown), followed by four more 0.25 mL whole blood washes. 41

Figure 5.2 Whole blood time course of ^{125}I-IAZA and total radioactivity in anesthetized and non-anesthetized rats. Key: (●) total radioactivity, anesthetized; (O) total radioactivity, non-anesthetized; (▼) ^{125}I-IAZA, anesthetized; (▲) ^{125}I-IAZA, non-anesthetized. 42

Figure 5.3 Mean blood disposition courses *vs.* time of (●) total radioactivity, (O) ^{125}I-IAZA and (▼) the radioactive metabolites of ^{125}I-IAZA. (A = anesthetized animals; B = non-anesthetized animals). 44

Figure 5.4 Organ accumulation of total radioactivity at 5 hours after ^{125}I-IAZA dose to non-anesthetized Sprague-Dawley rats. 45

Figure 6.1 Concentration-time profiles of ^{123}I-IAZA (solid symbols) and total radioactivity (open symbols) for volunteers 1-3 (A) and 4-6 (B) following an i.v. dose of ^{123}I-IAZA. Data are not decay corrected (i.e. effective parameters). 56

Figure 6.2 Plots of mean disposition of various radioactive components in human volunteers following ^{123}I-IAZA administration. Key: (O) total radioactivity; (●) ^{123}I-IAZA; (▼) radioactive metabolites. **60**

Figure 6.3 Representative concentration vs. time plot for ^{123}I-IAZA (●) and IAZA (O) (based on data from volunteer #2). **62**

Figure 7.1 Decay scheme for ^{123}I (from: Weber DA, Eckerman KF, Dillman LT, Ryman JC. MIRD: Radionuclide Data and Decay Schemes, Society of Nuclear Medicine, 1989.) **68**

Figure 7.2 Typical immediate anterior (A) and posterior (B) view and 22 h anterior (C) and posterior (D) view images following ^{123}I-IAZA i.v. administration to a volunteer. These images were obtained from volunteer # 3 (27 year old male) following the administration of 5.62 mCi of ^{123}I-IAZA into the right arm. **76**

Figure 8.1 Concentration-time profiles of ^{123}I-IAZA (solid symbols) and total radioactivity (open symbols) for volunteers 1 (circles), 2 (triangles) and 3 (squares), following ^{123}I-IAZA administration during "Bruce" treadmill protocol. **90**

Figure 8.2 ^{123}I-IAZA blood concentration versus time plots for the two groups of volunteers: (O) dose administration during "Bruce" protocol (n = 3); (●) dose administration at rest (n = 6). **93**

Figure 8.3 Plots of ^{123}I-IAZA (solid symbols) and total radioactivity (open symbols) for volunteer # CV2. ^{123}I-IAZA dose administered at rest (circles) and during "Bruce" treadmill protocol (triangles). **93**

Figure 8.4 Three representative SPECT image frames (numbers 36, 57 and 72, respectively) of the chest cavity in a 27 year old male volunteer (CV2) following 5.68 mCi ^{123}I-IAZA dose given i.v. during "Bruce" treadmill protocol. Images acquired 1.5 h after the radiopharmaceutical administration. **94**

Figure 9.1 A two compartment blood-flow limited physiological pharmacokinetic model of ^{123}I-IAZA. For hypoxia modeling, only the hypoxic cells and the rest of the body need to be considered in this simplest form of the physiological pharmacokinetic model. **101**

Figure 9.2 Classical PK/PD model to describe the profile of radioactivity in the hypoxic cells effect compartment following ^{123}I-IAZA administration. **103**

Figure 9.3 Michaelis-Menten plot of the initial binding rate of ^{125}I-IAZA to the EMT-6 tumor cell line. The maximum rate V_{max} is fixed at 650 pmol/10^6 cells/h while the Michaelis constant K_m is fixed at 26 μmol/L. **107**

Figure 9.4 Temporal change in the percent injected dose in a 200 mL blood pool (●) and in three hypothetical 200 g tumors with varying hypoxic fractions: (∇) 1 %, (O) 10 % and (▼) 30 % of tumor cells are hypoxic. Partitioning of activity between normoxic cells and blood is assumed to be one. **109**

Figure 9.5 Graded response intensity (●) in a hypothetical homogeneous tumor at eight hours after ^{123}I-IAZA administration to the patient. 109

Figure 9.6 A simplified scheme of the first major reversible and irreversible steps in the 2-nitroimidazole bioreductive pathway. 113

Figure 9.7 Effect of physical decay on the accumulation of radioactivity in a hypothetical 1 g mass of hypoxic EMT-6 tumor cells following ^{123}I-IAZA dose to a patient. Input parameters into the effect compartment are defined in the text. Biological efflux of radioactivity is assumed to be zero. Key: (●) no physical decay in the effect compartment; (O) 13.2 h decay of ^{123}I in the effect compartment; (▲) 1.83 h decay of ^{18}F in the effect compartment. 117

ABBREVIATIONS

%ID	percent of the injected dose
α	distribution rate constant (2 compartment model)
AB	all body ROI; AB = WB - Bladder
AIC	Akaike criterion
$AUC_{0-\infty}$	area under the curve from the time of dose administration to time infinity
AUC_{0-X}	area under the curve from the time of dose administration to time X
β	elimination rate constant (2 compartment model)
C_h	IAZA concentration in the hypoxic cells
Ci	curie
C_{in}	drug concentration in the afferent (arterial) blood perfusing a region in the body (i.e. the hypoxic cells)
Cl_{hy}	hypoxic cell clearance (defined per 1 g or 10^6 cells)
Cl_{int}	intrinsic clearance
Cl_{nr}	non-renal (metabolic) clearance
Cl_p	clearance by physical decay of the isotope
Cl_r	renal clearance
Cl_{TB}	total body clearance
C_o	drug concentration in the efferent (venous) blood perfusing a region in the body (i.e. the hypoxic cells)
CPM	counts per minute
DPM	disintegrations per minute
E	extraction ratio; $E = (f \times Cl_{int}) \div (Q + f \times Cl_{int})$
ED	Effective Dose
EDE	Effective Dose Equivalent
f	drug free fraction (unbound)
FR_A	measured fraction remaining
FR_P	model-predicted fraction remaining
GIT	gastrointestinal tract

HPLC	high performance liquid chromatography
i.v.	intravenous
IAZA	1-(5-iodo-5-deoxy-β-D-arabinofuranosyl) -2-nitroimidazole (iodoazomycin arabinoside)
k_{12}	transfer rate constant into the second (peripheral) compartment from the first (central) compartment
k_{1e}	uptake rate constant into the effect compartment
k_{21}	transfer rate constant from the second (peripheral) compartment into the first (central) compartment
K_A	global reaction rate constant
K_{elM}	elimination rate constant of the radioactive metabolites from the body
k_{eo}	elimination rate constant of radioactivity from the effect compartment
keV	kilo-electron volt
k_m	formation rate constant of the radioactive metabolites outside of the hypoxic cell compartment
K_M	Michaelis constant
k_{red}	intracellular reductive biotransformation rate
k_u	urinary elimination rate constant of IAZA
LLI wall	lower large intestinal wall
MBq	megabecquerel
M_c	amount of radioactive metabolites in the central compartment
MIRD	medical internal radiation dose
MISO	misonidazole
M_{hy}	amount of radioactive metabolites in the hypoxic cells
MRT	mean residence time, determined as: $MRT = \frac{t1/2}{0.693}$
MRT_{fr}	fractional organ MRT, determined as: $MRTfr = \frac{\text{Organ count (immediate)}}{\text{Whole Body count (immediate)}} \times MRT\,(\text{organ})$

P	octanol:water partition coefficient
PD	pharmacodynamic
PK	pharmacokinetic
PK/PD	pharmacokinetic/pharmacodynamic
Q	perfusion, defined as the blood flow through a region divided by the volume (or weight) of the region
RB	remainder of the body ROI
ROI	region of interest
S-value	a cumulative dosimetric parameter defined as: $\frac{\left(\begin{matrix}\text{mean \# of ionizing emis-}\\ \text{sions per nuclear transition}\end{matrix}\right)\times\left(\begin{matrix}\text{mean energy}\\ \text{per emission}\end{matrix}\right)\times\left(\begin{matrix}\text{absorbed}\\ \text{fraction}\end{matrix}\right)}{\text{mass of the target region}}$
SC	Schwartz criterion
S_{cr}	serum creatine
SD	standard deviation
T:B ratio	tumor to blood radio
$t_{1/2\alpha}$	distribution phase half-life (2 compartment model)
$t_{1/2\beta}$	elimination phase half-life (2 compartment model)
$t_{1/2b}$	biologic elimination half-life
$t_{1/2e}$	effective elimination half-life of a radiopharmaceutical, defined as $\frac{1}{t1/2e}=\frac{1}{t1/2b}+\frac{1}{t1/2p}$
$t_{1/2p}$	physical decay half-life of the isotope
TB	total body ROI; TB = WB - (GIT + Bladder)
TLC	thin layer chromatography
ULI wall	upper large intestinal wall
v:v	volume to volume ratio
V_β	volume of distribution determined by extrapolation of the terminal (elimination) phase in a 2 compartment model
V_c	central compartment volume of distribution
V_h	volume of distribution in the effective (i.e. hypoxic) compartment

V_{ss}	steady state volume of distribution
WB	whole body ROI
X_c	amount of IAZA in the central compartment
X_h	amount of IAZA in the hypoxic cells (effect compartment)
X_p	amount of IAZA in the peripheral compartment

1. Introduction

1.1 Hypoxia

The term hypoxia defines a state of oxygenation lying between the absolute absence of oxygen (anoxia) and the normal state of oxygenation of healthy, disease-free tissue. Normal oxygen levels are known to fluctuate both among and within the various tissues, even within tissues that are considered to have excellent perfusion. Since specific tissues may have a range of normal oxygen concentrations, the definition of hypoxia may be tissue-specific as well as function-specific. For example, radiobiological hypoxia defines a functionally-specific condition in which the oxygen concentration will be less than 1000 ppm, whereas cardiological hypoxia may include conditions in which oxygen concentrations are 10-100 times higher. Regardless of tissue, however, when oxygen demand required for normal cellular function exceeds the supply for extended periods of time, the cells will respond by down-regulating their metabolism (Woodrooffe *et al.*, 1995; Nunn *et al.*, 1995).

This decreased tissue oxygen tension resulting in cellular metabolic down-regulation is a common component of several clinically important diseases, including coronary insufficiency, cerebral vascular accident, peripheral vascular disease in diabetes mellitus, rheumatoid arthritis, alcohol-induced liver damage, and cancer. In addition, prolonged tissue hypoxia has been recently identified as the principal cause of allograft non-function shortly after organ transplant (Woodrooffe *et al,* 1995). With the exception of cancer, an important goal in these disease states is to identify the presence of the hypoxic cells and salvage the function of the tissue before the cells become necrotic and the damage irreversible.

In tumors, where rapid cellular division may often outgrow the blood supply, the presence of hypoxia has been linked to increased radioresistance. Although its potential for compromising radiation therapy was realized more than four decades ago (Thomlinson and Gray, 1955), the only direct evidence for the existence of radiobiologically hypoxic tumor fraction comes from highly invasive studies in experimental animals (Powers and Tolmach, 1964; Moulder and Rockwell, 1987; Hill, 1992; Chapman, 1984). In human tumors there is a wide variety of indirect evidence of tissue hypoxia based on: a) histomorphometric analysis (Thomlinson and Gray, 1955; Moore *et al.*, 1985); b) oxygen electrodes (Carter and Silver, 1960) and microelectrodes

(Höckel *et al.*, 1996); c) DNA strand breaks (Fairbairn *et al.*, 1995); d) oxyhemoglobin saturation in red blood cells in tumors (Mueller-Klieser *et al.*, 1981); e) correlation between low hemoglobin levels and radiotherapy response (Bush *et al.*, 1978); f) high-pressure oxygen and high oxygen-content gas breathing (Overgaard and Horsman, 1996); d) improved radiation response with co-administration of various radiosensitizers (for minireview see Overgaard and Horsman, 1996); and g) presence of a signal originating in certain human tumors after the administration of radiolabelled 2-nitoimidazole compounds (for minireview see Wiebe and Stypinski, 1996; Nunn *et al.*, 1995). This last group, the 2-nitroimidazoles, are often referred to as hypoxic cell markers by dint of their ability to scavenge electrons in oxygen-deficient (hypoxic), but not oxygen-rich (oxic), environments.

The term "hypoxic cell marker" is somewhat of a misnomer, since, generally, a tissue marker is taken to be a substance (usually a protein or glycoprotein) that is specific to a tissue (e.g. carcinoembryonic antigen from certain tumors) and can be found in blood samples due to abnormal expression and shedding. Although hypoxia does have many biochemical implications, including the stimulation of endothelin-1 expression in rats (Elton *et al.*, 1992), increased membrane expression of Glut-1 transporter (Clavo *et al.*, 1995), promotion of erythropoietin gene transcription and inhibition of CYP450 gene transcription (Woodrooffe *et al.*, 1995), a hypoxia-specific cell marker has not been identified to date. Thus, although 2-nitroimidazoles are commonly referred to as hypoxic cell markers, they are not expressed by the hypoxic tissue. In many of today's hypoxia-marking radiopharmaceuticals, the "marker" is normally a nitroimidazole-containing molecule that is labeled with a gamma emitting radioisotope covalently bound to a part of the molecule that is not involved in the oxygen-sensitive process (i.e. nitro radical anion formation).

1.2 The Ideal Hypoxia Radiopharmaceutical

The pharmacokinetic requirements for an ideal hypoxia marker are in many respects identical to the requirements of other radiopharmaceuticals. It must concentrate efficiently and selectively in target cells, while keeping the radiation dose to the patient within acceptable levels (Wiebe, 1984). To ensure this selectivity, the ideal marker should have a high, dose-independent, localization mechanism (i.e. initial binding rate) in hypoxic cells and negligible localization (binding) under aerobic conditions. On the

other hand, this uptake (binding) rate should be independent of oxygen concentration over a wide range of hypoxia, and should preferably be independent of cell derivation or function.

The ideal radiopharmaceutical must be cleared quickly from all normal tissues, including the blood, to minimize background radioactivity and at the same time produce a clear image of the target (hypoxic) tissue in the patient. At the same time, its elimination half-life must be long enough to allow for sufficient distribution into target areas which, by their definition, are regions of diminished blood supply. Ideally, the half-life of the terminal phase of the blood or plasma concentration vs. time curve should be less than 5 hours, but the lower half-life limit will be dependent on the relative lipophilicity of an agent since lipophilic agents will cross biological membranes faster than hydrophilic drugs. Consequently, the extent of the agent's distribution into the hypoxic region will be governed by physiochemical properties such as lipid-water partition and protein binding in plasma and tissue.

For any hypoxic cell marker the partition coefficient must be high enough to allow this agent to diffuse to both well-perfused and poorly-perfused tissues. Balance is essential, however, as has been shown with highly lipophilic 2-nitroimidazoles, which have low body clearance and high non-specific tissue binding (Biskupiak and Krohn, 1993). Furthermore, it is generally preferred to have renal clearance and urinary excretion of these compounds. This requires them to be relatively hydrophilic and of low molecular weight. Although an ideal partition coefficient cannot be narrowly defined, hypoxia radiosensitizers have been most promising if the octanol-water partition coefficient was in the 0.1-10 range (Brown and Workman, 1980); a range that also seems suitable for diagnostic radiopharmaceuticals.

An important characteristic of an ideal imaging agent is minimal protein binding in blood and normal tissue. The importance of low protein binding is apparent when one considers that the actual amount of drug reaching the hypoxic area will be between 1% and 10% of the total dose (Chapman *et al.*, 1983). Extraction of the radiopharmaceutical from circulating macromolecules will therefore critically affect the fraction that is actually available for diffusion across the plasma membrane. Therefore, it is essential that tissues, including blood, are quickly cleared of both the bound and unbound drug if a significant signal from the metabolically trapped marker is to be observed.

The apparent volume of distribution is a derivative property that is controlled by tissue and plasma protein binding, partition coefficient and, to a lesser extent, molecular weight. The latter is important in that some high molecular weight compounds have been shown to be confined to the vascular space, thereby providing volume of distribution values of about 7 % of body weight in man (Gibaldi and Perrier, 1982). To diffuse out of blood vessels and into areas remote from tissue capillaries, a pharmaceutical must have a volume of distribution equivalent to at least the total body water weight, or approximately 56 % of the total body weight in man. However, excessively large volumes of distribution are often associated with long elimination half-lives that arise not from slow clearance by liver or kidney, but from seepage of the drug from the peripheral tissue into the vasculature, over an indefinite period.

Complete renal elimination of the radioactive dose, with preferably no hepatic involvement, is another requirement of an ideal radiopharmaceutical. This would largely circumvent the formation of (radiolabelled) metabolites which complicate the tracer kinetics by having distribution and elimination patterns different than their parent compound. Additionally, they will degrade the image quality and contribute unnecessarily to the radiation dose to the patient, especially in case of biliary elimination, which deposits activity into the gastrointestinal tract (GIT). In the least, if there is metabolic degradation, the metabolites should not accumulate and be quickly eliminated renally.

Diagnostic hypoxia radiopharmaceuticals will only be administered intravenously (i.v.) either as a bolus or a rapid infusion. Therefore, at least two kinetic parameters, the absorption rate and bioavailability, will never be complicating components of the pharmacokinetic analysis of these diagnostic agents, despite the potential first pass metabolism in the heart and the lungs.

The final, though equally critical specification for a hypoxic cell marker is that the lowest achievable radiation dose compatible with the study to be performed be delivered to the patient by the radiolabel (Wiebe, 1984). The radiation dose will depend on the effective half-life ($t_{1/2e}$), which is a function of both the biological half-life ($t_{1/2b}$) of the radiopharmaceutical and the physical half-life ($t_{1/2p}$) of the radionuclide; it can be expressed as:

$$\frac{1}{t_{1/2e}} = \frac{1}{t_{1/2b}} + \frac{1}{t_{1/2p}} \qquad (1.1)$$

Ideally, the imaging agent should have an effective half-life sufficient for distribution to the tissue to occur and for the background radioactivity to clear, so that when imaging is complete, the residual radioactivity will be minimal. Clearly, the type and energy of the radiation emitted by the radionuclide, the cost of its production, and the time and complexity of procedures required to incorporate it into the pharmaceutical formulation are all important considerations in the development of an ideal imaging agent.

1.3 References

Biskupiak JE, Krohn KA. Second generation hypoxia imaging agents. J Nucl Med 1993;34:411-3.

Brown JM, Workman B. Partition coefficients as a guide to the development of radiosensitizers which are less toxic than misonodazole. Radiat Res 1980;82:171-90.

Bush RS, Jenkin RDT, Allt WEC, Beale FA, Bean H, Dembo AJ, Pringle JF. Definite evidence for hypoxic cells influencing cure in cancer therapy. Br J Cancer 1978;37(Suppl. 3):302-6.

Carter DB, Silver JA. Quantitative measurements of oxygen tension in normal tissues and in tumors of patients before and after radiotherapy. Acta Radiol 1960;53:233-56.

Chapman JD, Baer K, Lee J. Characteristics of the metabolism-induced binding of misonidazole to hypoxic mammalian cells. Cancer Res 1983;43:1523-8.

Chapman JD. The detection and measurement of hypoxic cells in solid tumors. Cancer 1984;54:2441-9.

Clavo AC, Brown RS, Wahl RL. Fluorodeoxyglucose uptake in human cancer cell lines is increased by hypoxia. J Nucl Med 1995;36:1625-32.

Elton TS, Oparil S, Taylor GR, Hicks PH, Yang R-H, Jin H, Chen YF. Normobaric hypoxia stimulates endothelin-1 gene expression in the rat. Am J Physiol 1992;263:R1260-4.

Fairbairn DW, Olive PL, O'Neill KL. The comet assay: a comprehensive review. Mutat Res 1995;339:37-59.

Gibaldi M, Perrier D. Pharmacokinetics. 2nd ed. New York: Marcel Dekker, Inc.; 1982.

Höckel M, Schlenger K, Mitze M, Schäffer U, Vaupel P. Hypoxia and radiation response in human tumors. Seminars in Radiation Oncology 1996;6:3-9.

Hill RP. Cellular basis of radiotherapy. In: The basic science of oncology. Tannock IF, Hill RP (editors). 2nd ed. New York: McGraw-Hill, Inc.; 1992. pp. 259-75.

Moore JV, Hasleton PS, Buckley CH. Tumor cords in 52 bronchial and cervical squamous cell carcinomas: inferences for their cellular kinetics and radiobiology. Br J Cancer 1985;51:407-13.

Moulder JE, Rockwell S. Tumor hypoxia: its impact on cancer therapy. Cancer Metas Rev 1987;5:313-41.

Mueller-Klieser W, Vaupel P, Manz R, Schmidseder R. Intracapilary oxyhemoglobin saturation of malignant tumors in humans. Int J Radiat Oncol Biol Phys 1981;7:1397-404.

Nunn A, Linder K, Strauss WH. Nitroimidazoles and imaging hypoxia. Eur J Nucl Med 1995;22:265-80.

Overgaard J, Horsman MR. Modification of hypoxia-induced radioresistance in tumors by the use of oxygen and sensitizers. Seminars in Radiation Oncology 1996;6:10-21.

Powers WE, Tolmach LJ. Demonstration of an anoxic component in a mouse tumor-cell population by *in vivo* assay of survival following irradiation. Radiology 1964;83:328-36.

Thomlinson RH, Gray LH. The histological structure of some human lung cancers and the possible implications for radiotherapy. Br J Cancer 1955;9:539-49.

Wiebe LI, Stypinski D. Pharmacokinetics of SPECT radiopharmaceuticals for imaging hypoxic tissues. Quarterly Journal of Nuclear Medicine 1996;40:270-84.

Wiebe LI. Radionuclides, radiotracers and radiopharmaceuticals for *in vivo* diagnosis. Radiation Physics and Chemistry 1984;24:365-72.

Woodrooffe AJM, Bayliss MK, Park GR. The effects of hypoxia on drug metabolizing enzymes. Drug Metab Rev 1995;27:471-95.

2. Literature Survey of the Pharmacokinetics of Hypoxia Radiopharmaceuticals[1]

2.1 Misonidazole Analogues

About two decades ago, misonidazole (MISO), originally developed as a trichomonacide, was first investigated as a radiosensitizer of viable but oxygen-deficient cancer cells. MISO kinetics received special attention in early clinical trials, when it was observed that its dose-limiting neurotoxicity was related to the area under the curve (AUC) of its plasma concentration vs. time plot, or, in other words, the duration and extent of total tissue exposure. Currently MISO is considered to be the prototype drug of the 2-nitroimidazole class of radiosensitizers and hypoxia markers.

2.1.1 ^{3}H-Misonidazole (^{3}H-MISO)

Since the dose of radiolabeled MISO required for imaging would be less that 1% of the radiosensitizing (therapeutic) dose (Jette *et al.*, 1986) dose-limiting side effects would not be a consideration. The first study which showed *in vitro* that radiolabelled MISO can be used as a marker of viable hypoxic cells was published in 1981 by a team from the Cross Cancer Institute and the Department of Radiology from the University of Alberta, led by J.D. Chapman (Chapman *et al.*, 1981). In 1985, the same group initiated a preliminary study using ^{3}H-MISO and autoradiography to detect the hypoxic cell fraction in soft tissue and lymph node tumors in cancer patients (Urtasun *et al.*, 1986). Blood and urine were monitored in one patient, showing a half-life of 8.7 $\pm$ 0.4 h for the first 24 h period, which is within the limits (8 -12 h) observed in patients who had received MISO at radiosensitizer doses (Jerabek *et al.*, 1986). Urine collected for the first 72 hours after administration contained 66% of the radioactive dose, but the amount of intact ^{3}H-MISO present was not determined, and no other kinetic data were given.

The study did demonstrate the feasibility of using a radiolabelled drug to identify and image hypoxic areas in humans, and soon ^{3}H-MISO was investigated as a potential hypoxia marker of diseases in non-cancerous tissues, such as cerebral ischemia

---

[1] A version of this section has been published in: Wiebe LI, Stypinski D. Pharmacokinetics of SPECT radiopharmaceuticals for imaging hypoxic tissues. The Quarterly Journal of Nuclear Medicine. 1996;40:270-284.

(Hoffman *et al.*, 1987). The use of tritium made the methods tedious and invasive, but these studies led to extensive work on synthesis and characterization of MISO derivatives labeled with gamma emitting radionuclides.

2.1.2 ^{82}Br-Bromomisonidazole (^{82}Br-BrMISO)

^{82}Br-BrMISO was developed simultaneously and independently by the groups of Krohn (Rasey *et al.*, 1982) and Wiebe (Jette *et al.*, 1983) in the early 1980's. This compound represents an interesting example of tracer kinetics that turned out to be, in large part, the pharmacokinetics of the free isotope (^{82}Br-bromide) rather than the labeled, active compound. In 1983 Jette *et al.* (1983) reported a study of ^{82}Br-BrMISO in BALB/c mice bearing EMT-6 tumors. Intraperitoneal injection of ^{82}Br-BrMISO produced persistently high blood radioactivity, with 6.7 % of the dose in the blood stream at 30 min and a plasma half-life of 10-18 hours. Most of the radioactivity had accumulated in the kidneys, but surprisingly, hepatic radioactivity was even lower than in GIT and spleen. The high blood radioactivity resulted in continuously high tissue background, so that tumor-to-blood (T:B) ratios only reached 0.7. Although the authors attributed the high background radioactivity to debromination of ^{82}Br-BrMISO and/or its major metabolite (O-demethylated bromomisonizadole; ^{82}Br-BrDeMISO), they did not find any debrominated MISO or DeMISO in blood samples, most likely due to the lack of sensitive assay techniques. The half-life of cold BrMISO was determined to be approximately 40 min, from BrMISO concentration data values that fluctuated inconsistently with time and had large standard deviations for averaged data. BrDeMISO, the principal metabolite, exhibited formation-dependent kinetics (Wiebe and Stypinski, 1996), with an apparent elimination half-life of 60 min.

2.1.3 ^{18}F-Fluoromisonidazole (^{18}F-FMISO)

^{18}F-FMISO was synthesized and evaluated in early 1980's by the group of Krohn (Jerabek *et al.*, 1984; Jerabek *et al.*, 1986). It was created to non-invasively image hypoxia using positron emission tomography (PET). This compound, and its tritiated analogue (^{3}H-FMISO), have been extensively studied first as markers of hypoxic myocardium in the dog model (Martin *et al.*, 1989; Caldwell *et al.*, 1995; Shelton *et al.*, 1988; Cerqueira *et al.*, 1988) and increasingly as tumor hypoxia markers (Rasey *et al.*,

1987; Koh *et al.*, 1995; Casciari and Rasey, 1995; Rasey *et al.*, 1990; Rasey *et al.*, 1989; Rasey *et al.*, 1996; Yeh *et al.*, 1996; Casciari *et al.*, 1995).

In order to determine the compatibility of FMISO with PET imaging procedures, the pharmacokinetics of ^{3}H-FMISO were studied in a dog model (Martin *et al.*, 1989). Through the four hours of the experiment, and thus during the blood and urine sample collection, all the animals, including the controls, were maintained under surgical plane anesthesia with thiamyl sodium and halothane. Although the results were reported as ^{3}H-FMISO kinetics, only total radioactivity scintillation counting of samples was performed. However, in the results section the authors did mention that based on TLC analysis of several blood and urine samples more than 80 % of urine radioactivity and virtually 100 % of blood radioactivity was due to intact ^{3}H-FMISO. Based on these data, ^{3}H-FMISO had a bi-exponential plasma elimination profile with a very rapid distribution phase followed by an elimination phase with a 275 $\pm$ 50 min half-life, and an elimination phase-extrapolated volume of distribution (V_{β}) of 0.65 $\pm$ 0.21 L/kg. Since the terminal phase half-life was longer than the duration of the experiment, it would have been beneficial to continue the study longer to verify whether the second phase was truly the elimination phase or, in fact, another distribution phase. In addition, a control study in non-anesthetized animals would verify whether the surgical plane anesthesia had any effect on the pharmacokinetic parameters.

Human kinetics of ^{18}F-FMISO have been determined in eight cancer patients by Koh *et al.* (1991). In this study both the sample collection times and duration were variable, with the longest study ending with the collection of a 180 min sample. The plasma disposition profile was again bi-exponential with a rapid distribution phase, and a long terminal phase, with a calculated half-life of 380 $\pm$ 50 min. These results were also based on total radioactivity scintillation counting of plasma samples. In a different study Casciari *et al.* (1995) analyzed plasma samples of two patients at 120 - 160 min after ^{18}F-FMISO administration, and found that about 85 % of radioactivity was due to the intact parent compound. The entire model for tumor hypoxic fraction determination developed in that report (Casciari *et al.*, 1995) was based on the assumption that total radioactivity counts can be substituted directly into the input function of the tumor hypoxic cells. This assumption is only valid if the disposition profiles of the tracer and the parent compound parallel each other, that is, when there is either no metabolism or when the metabolite profile is formation rate-limited. However, by using this single

point determination, Casciari *et al.* (1995) have only determined the change in the input function value based on the assumption that 15 % of blood activity is in the form of diffusable metabolites. Since the authors have assumed that this 15 % is constant, they have thus presumed the existence of parallel profiles between tracer and ^{18}F-FMISO terminal phase disposition in these patients.

Recently, ^{18}F-fluoroerythronitroimidazole (^{18}F-FETNIM), a new hydrophilic analogue of FMISO, has been synthesized and evaluated by the same group (Yang *et al.*, 1995). This compound showed a better T:B ratio than FMISO, making it a potential new hypoxic cell marker, and, since it is also more hydrophilic than MISO, a potential new radiosensitizer.

Although ^{18}F-MISO and ^{18}F-FETNIM have been synthesized with the goal of creating a non-invasive hypoxia imaging agent for PET, ^{18}F-MISO kinetics is not very compatible with this imaging technology (Nunn *et al.*, 1995). The $t_{1/2p}$ of the ^{18}F isotope is only 110 min, while the $t_{1/2b}$ of the second phase is more than six hours. Generally, in order to allow for background radioactivity to clear, it is considered beneficial to wait at least three biologic half-lives of the imaging agent before image acquisition (Parliament *et al.*, 1992). Eighteen hour image acquisition is impossible for ^{18}F-PET studies, where even 90 to 120 min images are of limited quality (Nunn *et al.*, 1995). This inability to wait until the background activity clears may have been partly responsible for the unusually high (97%) number of hypoxic-fraction-containing tumors detected by ^{18}F-FMISO in a study of 37 patients with cancers of various types (Rasey *et al.*, 1996). Numerous oxygen microelectrode studies have reported a wide range of hypoxic tumor fractions, ranging from 27.8 % for a study of cervical cancer in 18 patients (Höckel *et al.*, 1991) to 100 % for a study of 5 patients with glioblastoma and 5 patients with brain metastases (Rampling *et al.*, 1994).

In addition to radionuclide half-life considerations, the PET imaging modality is expensive and not as widely available in medical centers as single photon gamma camera imaging. For this reason, a gamma emitting iodinated or a technetium labeled tracer would be better, as ^{123}I and ^{99m}Tc are both less expensive, require less expensive imaging equipment and each have longer $t_{1/2p}$.

2.1.4 ^{131}I-Iodovinylmisonidazole (^{131}I-IvMISO)

^{131}I-IvMISO was developed in 1991 in an effort to prepare a MISO analogue that would have the physico-chemical properties of MISO and be more radiochemically stable than BrMISO (Biskupiak *et al.*, 1991). The tracer kinetics of ^{131}I-IvMISO, as determined in a 4 h study in an anesthetized dog model, showed a bi-phasic blood clearance curve, with a very fast initial distribution phase followed by a more gradual elimination phase which had a half-life of 4.6 ± 0.3 h (Martin *et al.*, 1993). Although metabolic studies were not reported, the authors observed that liver concentrated much of the radioactivity, indicating that extensive hepatic extraction and/or metabolic biotransformation may have been occurring. Since only tracer kinetic data were available, the impact of these processes on pharmacokinetic parameters cannot be predicted from the information available. The presence of high liver activity was perceived as a potential problem in cardiac imaging and the work on ^{131}I-IvMISO was not continued.

2.2 ^{99m}Tc-labelled 2-nitroimidazoles

^{99m}Tc is considered to be the ideal radionuclide for routine imaging in nuclear medicine. Some of its "ideal" physical characteristics are its decay mode, which has a high yield of 140 keV gamma photons, no alpha or beta particle emissions, a 6 h decay half-life, and inexpensive availability from the ^{99}Mo/^{99m}Tc generator. The carrier molecule will ideally be formulated into a convenient "kit" preparation, where the labeling and preparation of the radiopharmaceutical will take only minutes and can be done by any radiopharmacist. The biggest problem with ^{99m}Tc is its chemistry. Technetium is a metal and therefore its chemistry is complex. It links with the carrier molecules through co-ordinate bonds and can exist in any of 7 oxidation states. ^{99m}Tc binds to small molecules by forming large chelate adducts, altering both the chemical properties and biodistribution of the resulting co-ordination complex (Wiebe, 1984).

It is not surprising, therefore, that although ^{99m}Tc-labelled complexes that selectively bind to hypoxic cells have the potential to become ideal hypoxia radiopharmaceuticals, most of the reported ^{99m}Tc compounds have been disappointing as scintigraphic hypoxia markers (eg. Treher *et al.*, 1986; Linder *et al.*, 1993). However, some recently synthesized ^{99m}Tc-labelled 2-nitroimidazoles and related agents have been more promising (DiRocco *et al.*, 1992; Rumsey *et al.*, 1993; Kusuoka *et al.*, 1994; Rumsey *et*

al., 1995a; Archer *et al.*, 1995; DiRocco *et al.*, 1993; Stone *et al.*, 1995; Fukuchi *et al.*, 1996; Ng *et al.*, 1995; Shi *et al.*, 1995). One such compound is a technetium complex of 2-nitroimidazole-derivatized propylene amine oxime, also referred to as BMS-181321.

Initially, the uptake of BMS-181321 by hypoxic myocardium (eg. Rumsey *et al.*, 1993; Kusuoka *et al.*, 1994;) and brain (DiRocco *et al.*, 1993) has been determined in experiments in which the hearts and the brains were excised from the animals before imaging. Although the hypoxic myocardium does selectively retain BMS-181321, two more recent studies in intact animals (Rumsey *et al.*, 1995; Shi *et al.*, 1995), have shown that the very high liver uptake (4 times that of the ischemic region) makes it very unlikely that the agent will ever be used clinically (Patterson and Eisner, 1995).

The study by Kusuoka *et al.* (1994) not only compared the uptake of BMS-181321 in different myocardial perfusion states, but also, in the same environments, compares this agent with ^{99m}Tc labeled perfusion agent HMPAO and with ^{99m}Tc labeled PAO-6-Me. PAO-6-Me is an analogue of BMS-181321 but without the 2-nitroimidazole group. This was a very carefully prepared experiment which proved that BMS-181321 is fairly quickly taken up by the ischemic myocardium, while its analogue PAO-6-Me is completely washed out. Interestingly, HMPAO also showed a slightly elevated uptake in the ischemic myocardium. In this model, BMS-181321 is not effective for imaging ischemic regions unless it is administered before the onset of ischemia. However, since this was a single pass experiment, perhaps the poor uptake of the marker following its administration after the onset of ischemia could be attributed to the very short contact time with the ischemic tissue. Because of the poor perfusion in the ischemic region the marker may require several minutes to reach this area.

Recently, HL91, a new analogue of BMS-181321 but without the 2-nitroimidazole group has been reported to accumulate in the hypoxic myocardial tissue, and this agent appears to have minimal hepatic uptake (Fukuchi *et al.*, 1996b). Unfortunately, there are no reports on the pharmacokinetics or the full tracer kinetics of any ^{99m}Tc-labelled hypoxia imaging agents in the current literature.

2.3 Iodoazomycin Nucleosides

Sugar-labeled 2-nitroimidazoles were developed collaboratively by the groups of Wiebe and Chapman at the University of Alberta and the Cross Cancer Institute,

Edmonton. These compounds were designed to provide a balance between the lipophilic effect of the iodo substituent (a radiolabel that contributes substantial lipophilicity to small molecules) and the hydrophilic properties of the sugar hydroxyl groups. It was known that at least one related compound, azomycin riboside, was not only a radiosensitizer but also a competitor for transport by the equilibrative NBMPR-sensitive nucleoside transporter (Jarvis *et al.*, 1982). Despite speculation about the undesirable impact of such transport (Biskupiak and Krohn, 1993), experimental evidence for transport of the iodinated analogue has not been reported; preliminary data (Wiebe *et al.*, unpublished), suggest that transport is unlikely to be an issue in pharmacokinetic analysis and imaging.

2.3.1 Iodoazomycin Riboside (IAZR)

IAZR was the first radioiodinated azomycin nucleoside synthesized (Jette *et al.*, 1986). Although potentially suited for use as a radiopharmaceutical on the basis of *in vitro* sensitizer and oxygen-dependent binding properties, it is an excellent example of a potentially useful marker which was not suitable for imaging because of its pharmacokinetics.

The biodistribution of ^{125}I-IAZR was reported in 1986 (Wiebe *et al.*, 1986). The agent had a T:B ratio of 5.5 at 24 h. Blood clearance was reported to be rapid, with <5 % of injected radioactivity in blood at 30 min after injection and 0.19 ± 0.02 % after 2 h. This value remained steady over the next several hours (0.23 % at 6 h), and fell to 0.03 % by 24 h. Precise tracer kinetic interpretations of these data were not possible due to the large standard errors reported for the later (24 and 48 h) measurements. Similarly, no useful pharmacokinetic parameters could be calculated from this study, although HPLC analysis of plasma and of urine was conducted to determine the contribution of ^{125}I-iodide and ^{125}I-IAZR to total activity. It is interesting to note that the relative ratio of ^{125}I-iodide and ^{125}I-IAZR in plasma remained constant. This ^{125}I-IAZR\$^{125}$I-iodide plasma concentration equilibrium is surprising, given the substantial de-iodination and the anticipated differences in clearance rates for these substances. The data obtained from urine studies were insufficient to determine the renal clearance of ^{125}I-iodide and ^{125}I-IAZR, although they did establish that urine was a route of elimination.

2.3.2 Iodoazomycin Galactoside (IAZG)

IAZG was synthesized in late 1980's in an attempt to improve on the biodistribution of IAZR by replacing the pentose sugar with a hexose sugar (Mercer *et al.*, 1990; Mannan, 1991). However, IAZG still had a relatively high clearance with substantial de-iodination, as evident from the results in an 8 h biodistribution study. At the same time, its maximum T:B ratio in EMT-6 tumor tissue of BALB/c mice was only 1.56 at 4 h.

2.3.3 Iodoazomycin Pyranoside (IAZP)

^{123}I-labeled IAZP has been used in a limited clinical study (Parliament *et al.*, unpublished) because of its apparent resistance to de-iodination relative to other radioiodinated sugar-coupled 2-nitroimidazoles (Mannan, 1991). Perhaps partially because of its resistance to deiodination, ^{125}I-IAZP achieved surprisingly high T:B ratios of 13.9 at 24 hours and much higher absolute uptake into tumor tissue when compared to its more extensively studied arabinoside analogue ^{125}I-IAZA (Mannan *et al.*, 1992). Total blood radioactivity was measured to construct a blood clearance plot, but the pharmacokinetic parameters of ^{125}I-IAZP have not been determined. The tracer kinetic plot could not be resolved by exponential analysis, but it would appear that it could be acceptably characterized by three exponential equations. Unfortunately, the terminal phase is really only determined by the single 24 h data point, since the 12 hour data point is still within the "intermediate" phase, so that the feathering technique cannot be used to extrapolate the remaining components' lines. As it is, it is not possible to estimate the half-life of this terminal phase, except to say that it begins sometime between 12 and 24 h.

2.3.4 Fluoroiodoazomycin Pyranoside (FIAZP)

The latest of this class of compounds to be synthesized and evaluated as a potential hypoxia marker was FIAZP (Mannan *et al.*, 1992). This agent could be potentially radiolabeled at either the fluorine or the iodine position, making it compatible with both ^{123}I-SPECT (single photon emission computerized tomography) and ^{18}F-PET technology. Surprisingly, ^{125}I-FIAZP did not have as good a T:B ratio as did its analogue ^{125}I-IAZP. ^{125}I-FIAZP T:B ratio at 24 h was only 5.9 in the EMT-6 tumor bearing BALB/c mice. The blood disposition profile was very similar to that of ^{125}I-IAZP, with similarly low de-iodination, as evident by the insubstantial thyroid uptake of free

radioiodine. The major problem with this agent was the high liver uptake, with the liver-to-blood ratio of 7.13 at 24 h.

2.3.5 Iodoazomycin Arabinoside (IAZA)

IAZA (Figure 2.1), a sugar coupled 2-nitroimidazole and a conjugation isomer of IAZR was synthesized by the group of L.I. Wiebe (Mannan *et al.*, 1991; Mercer *et al.*, 1990). It is the first SPECT hypoxia radiopharmaceutical to proceed to the clinical study stage. Preliminary clinical data were published by Parliament *et al.*, (1992). Patients with advanced malignant tumors were given ^{123}I-IAZA (10 mg; ~6mCi) as an i.v. infusion over 20 min. Blood samples collected from 3 patients showed biexponential plasma clearance tracer kinetic profiles. The half-life of the distribution phase was determined to be 22.6 ± 8.7 min, while the half-life of the elimination phase was 9.8 ± 4.1 h. Based on these results and on an earlier study of MISO retention in hypoxic cells (Chapman *et al.*, 1983), the authors concluded that the optimal time for imaging with this agent would be at approximately 24 h post infusion, at which time the hypoxic tissue-to-background ratio would be at a maximum of 5.6.

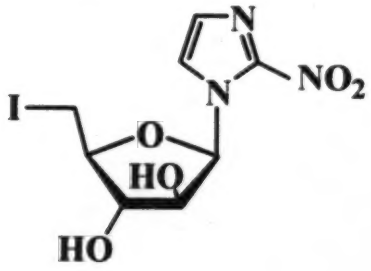

Figure 2.1 Structure of 1-(5-iodo-5-deoxy-β-D-arabinofuranosyl) -2-nitroimidazole (IAZA).

The plots of relative blood activity *vs.* time after ^{123}I-IAZA infusion presented by Parliament *et al.*, (1992) showed that the clearance of radioactivity in one of these patients was much slower than in the other two. This would explain the large standard deviation in the half-life values obtained. The importance of renal function in pharmacokinetic studies of renally cleared agents is shown in this study, in which the

patient with the longest elimination half-life also had impaired renal function (Cr_S = 165 μmol/L) at the time of imaging with ^{123}I-IAZA.

The presence of radioactivity in the thyroid and liver at short time intervals after injection reported by Parliament *et al.*, (1992) are evidence that the tracer kinetic data are representative of the pharmacokinetics of ^{123}I-IAZA, its radiolabeled metabolites and ^{123}I-iodide. Other published reports also refer to the clearance of total blood activity, so little is actually known about pharmacokinetics of radioiodinated IAZA (Mannan, 1991; Mercer *et al.*, 1990; Mannan *et al.*, 1991; Chapman *et al.*, 1996; Urtasun *et al.*, 1996).

Parliament *et al.*, (1992) also addressed the importance of clearance of both the covalently-bound (hypoxia-specific binding) and non-covalently-bound fractions of an imaging agent. They pointed out that for an imaging agent to be successful, the ratio of drug concentration in target tissue to drug concentration in normal tissue must increase with time, that is, the drug must be cleared at a much slower rate from hypoxic areas than from all other tissues in the body. Consequently, provided that this agent is metabolically trapped in hypoxic tissue, its biological half-life will determine the imaging time. A hypothetical model was developed to compare the tissue accumulation of two markers, both eliminated by bi-exponential kinetics and identical in all parameters except the half-life of the terminal phase ($t_{1/2\beta}$). In this model, a plot of relative concentration of the markers shows that, assuming a differential binding ratio between hypoxic and oxic tissues of approximately 10, it will require at least three biological half-lives for optimum image of the area of interest. The plot of tumor-to-normal tissue ratio *vs.* time will result in a sigmoidal curve which will reach its maximum tumor-to-normal tissue ratio after three biological half-lives.

Radiolabelled IAZA has been also investigated as a potential marker of hypoxic tissue in rheumatoid arthritis (McEwan *et al.*, 1996a; McEwan *et al.*, 1996b), in peripheral vascular disease of diabetic patients (Al-Arafaj *et* al., 1994), and in cerebral ischemia (Lythgoe *et al.*, 1997). This agent has also been evaluated as a potential marker of hypoxia formed as a by-product of photodynamic therapy in tumors (Moore *et al.*, 1993; Biskupiak and Krohn, 1993).

2.4 References

Al-Arafaj A, Ryan EA, Hutchison K, Mannan RH, Mercer JR, Wiebe LI, McEwan AJB. An evaluation of iodine 123 iodoazomycin arabinoside as a marker of localized tissue hypoxia in patients with diabetes mellitus. Eur J Nucl Med 1994;21:1338-42.

Archer CM, Edwards B, Kelly JD, King AC, Burke JF, Riley ALM. Technetium labelled agents for imaging tissue hypoxia *in vivo*. In: Technetium and rhenium in chemistry and nuclear medicine. Nicolini M, Bandoli G, Mazzi U (editors). Ditoriali (Italy): Padova SGE; 1995. pp. 535-45.

Biskupiak JE, Grierson JR, Rasey JS, Martin GV, Krohn KK. Synthesis of an (iodovinyl)misonidazole derivative for hypoxia imaging. J Med Chem 1991;34:2165-8.

Biskupiak JE, Krohn KA. Second generation hypoxia imaging agents. J Nucl Med 1993;34:411-3.

Caldwell JH, Revenaugh JR, Martin GV, Johnson PM, Rasey JS, Krohn KA. Comparison of flourine-18-fluorodeoxyglucose and tritiated fluoromisonidazole uptake during low-flow ischemia. J Nucl Med 1995;36:1633-8.

Casciari JJ, Graham MM, Rasey JS. A modeling approach for quantifying tumor hypoxia with [F-18]fluoromisonidazole PET time-activity data. Med Phys 1995;22:1157-39.

Casciari JJ, Rasey JS. Determination of the radiobiologically hypoxic fraction in multicellular spheroids from data on the uptake of [^{3}H]fluoromisonidazole. Radiat Res 1995;141:28-36.

Cerqueira M, Martin G, Embree L, Caldwell J, Krohn K, Rasey J. Enhanced binding of fluoromisonidazole in isolated adult rat myocytes during hypoxia. (Abstract). J Nucl Med 1988;29:807.

Chapman JD, Baer K, Lee J. Characteristics of the metabolism-induced binding of misonidazole to hypoxic mammalian cells. Cancer Res 1983;43:1523-8.

Chapman JD, Coia LR, Stobbe CC, Engelhardt EL, Fenning MC, Schneider RF. Prediction of tumour hypoxia and radioresistance with nuclear medicine markers. Br J Cancer 1996;74(Suppl. 27):S204-S208.

Chapman JD, Franko AJ, Sharplin J. A marker for hypoxic cells in tumors with potential clinical applicability. Br J Cancer 1981;43:546-50.

DiRocco RJ, Bauer A, Kuczynski BL, Pirro JP, Linder KE, Narra RK, Nunn AD. Imaging regional hypoxia with a new technetium-labeled imaging agent in rabbit myocardium after occlusion of the left anterior descending coronary artery. (Abstract). J Nucl Med 1992;33:865.

DiRocco RJ, Kuczynski BL, Pirro JP, Bauer A, Linder KE, Ramalingam K, Cyr JE, Chan YW, Raju N, Narra RK, Nowotnik DP, Nunn AD. Imaging ischemic tissue at risk of infarction during stroke. J Cereb Blood Flow Metab 1993;13:755-62.

Fukuchi K, Kusuoka H, Watanabe Y, Fujiwara T, Nishimura T. Ischemic and reperfused myocardium detected with technetium-99m-nitroimidazole. J Nucl Med 1996;37:761-6. (a)

Fukuchi K, Kusuoka H, Yutani K, Hasegawa S, Nishimura T. Assessment of reperfused myocardium using new hypoxia avid imaging agent Tc-99m HL91.(Abstract). J Nucl Med 1996;37:94P. (b)

Hőckel M, Schlenger K, Knoop C, Vaupel P. Oxygenation of carcinomas of the uterine cervix: evaluation by computered O_2 tension measurements. Cancer Res 1991;51:6098-102.

Hoffman JM, Rasey JS, Spence AM, Shaw DW, Krohn KA. Binding of the hypoxia tracer [^{3}H]misonidazole in cerebral ischemia. Stroke 1987;18:168-76.

Jarvis SM, Chapman JD, Ngan-Lee J, Rutledge KA, Barr PJ, Paterson RP. Azomycin riboside, a sugar homologue of misonidazole with favorable radiosensitizing properties. Cancer Res 1982;42:4358-63.

Jerabek PA, Patrick TB, Kilbourn MR, Dischino DD, Welch MJ. Synthesis and biodistribution of ^{18}F-labeled fluoronitroimidazoles: potential *in vivo* markers of hypoxic tissues. Appl Radiat Isot 1986;37:599-605.

Jerabek RH, Dischino DD, Kilborn MR, Welch MJ. Synthesis of fluorine-18 labeled hypoxic cell sensitizer. (Abstract). J Nucl Med 1984;25:P23.

Jette DC, Wiebe LI, Chapman JD. Synthesis and *in vivo* studies of the radiosensitizer 4-[82Br]bromomisonidazole. Int J Nucl Med Biol 1983;10:205-10.

Jette DC, Wiebe LI, Flanagan RJ, Lee J, Chapman JD. Iodoazomcin riboside (1-(5'-iodo-5-deoxyribofuranosyl]-2-nitroimidazole), a hypoxic cell marker. 1. Synthesis and *in vitro* characterization. Radiat Res 1986;105:169-79.

Koh W-J, Bergman KS, Rasey JS, Peterson LM, Evans ML, Graham MM, Grierson JR, Lindsley KL, Lewellen TK, Krohn KA, et al. Evaluation of oxygenation status during fractionated radiotherapy in nonsmall cell lung cancers using [F-18]fluoromisonidazole positron emission tomography. Int J Radiat Oncol Biol Phys 1995;33:391-8.

Koh W-J, Rasey JS, Evans ML, Grierson JR, Lewellen TK, Graham MM, Krohn KA, Griffin TW. Imaging hypoxia in human tumors with [F-18]fluoromisonidazole. Int J Radiat Oncol Biol Phys 1991;22:199-212.

Kusuoka H, Hashimoto K, Fukuchi K, Nishimura T. Kinetics of a putative hypoxic tissue marker, technetium-99m-nitroimidazole (BMS181321), in normoxic, hypoxic, ischemic and stunned myocardium. J Nucl Med 1994;35:1371-6.

Linder KE, Raju N, Cyr J, Chan Y-W, Ramalingam K, Nowotnik DP, Nunn AD. The synthesis of nitroimidazole BATO (boric acid adducts of technetium dioxime) derivatives and their in vitro evaluation as potential hypoxia imaging radiopharmaceuticals.(Abstract). J Labelled Compds Radiopharm 1993;32:13-4.

Lythgoe MF, Williams SR, Wiebe LI, McEwan AJB, Gordon I. Autoradiographic imaging of cerebral ischemia using a combination of blood flow and hypoxic markers in an animal model. Eur J Nucl Med 1997;24:16-20.

Mannan RH, Mercer JR, Wiebe LI, Kumar P, Somayaji VV, Chapman JD. Radioiodinated azomycin pyranoside (IAZP): a novel non-invasive marker for the assessment of tumor hypoxia. J Nucl Biol Med 1992;36:60-7.

Mannan RH, Mercer JR, Wiebe LI, Somayaji VV, Chapman JD. Radioiodinated 1-(2-fluoro-4-iodo-2,4-dideoxy-β-L-xylopyranosyl)-2-nitroimidazole: a novel probe for the non-invasive assessment of tumor hypoxia. Radiat Res 1992;132:368-74.

Mannan RH, Somayaji VV, Lee J, Mercer JR, Chapman JD, Wiebe LI. Radioiodinated 1-(5-iodo-5-deoxy-β-D-arabinofuranosyl) -2-nitroimidazole (iodoazomycin arabinoside: IAZA), a novel marker of tissue hypoxia. J Nucl Med 1991;32:1764-70.

Mannan RH. Novel non-invasive markers of tumor hypoxia. Edmonton, Alberta, Canada: *PhD. Thesis*, University of Alberta; 1991.

Martin GV, Biskupiak JE, Caldwell JH, Rasey JS, Krohn KA. Characterization of iodovinylmisonidazole as a marker for myocardial hypoxia. J Nucl Med 1993;34:918-24.

Martin GV, Caldwell JH, Rasey JS, Grunbaum Z, Cerqueira M, Krohn KA. Enhanced binding of the hypoxic cell marker [3H]Fluoromisonidazole in ischemic myocardium. J Nucl Med 1989;30:194-201.

McEwan AJB, Skeith KJ, Mannan RH, Davies N, Jamali F, Wiebe LI. Hypoxia-targeted ^{123}I-iodoazomycin arabinoside imaging of the adjuvant arthritis in rat model. CANM Annual Scientific Meeting 1996; Quebec City, PQ. (b)

McEwan AJB, Skeith KJ, Mannan RH, Davies N, Jamali F, Wiebe LI.^{123}I-iodoazomycin arabinoside - a possible marker of hypoxia in rheumatoid arthritis. CANM Annual Scientific Meeting 1996; Quebec City, PQ. (a)

Mercer JR, Mannan RH, Somayaji VV, Lee J, Chapman JD, Wiebe LI. Sugar-coupled 2-nitroimidazoles: novel *in vivo* markers of hypoxic tumor tissue. In: Advances in Radiopharmacology, Proceedings of the Sixth International Symposium on Radiopharmacology, Maddelena DJ, Snowdon GM, Boniface GR (editors). U Wollongong. Wollongong Writing Services (Australia), 1990; 104-113.

Moore RB, Chapman JD, Mercer JR, Mannan RH, Wiebe LI, McEwan AJ, McPhee MC. Measurement of PDT-induced hypoxia in Dunning prostate tumors by iodine-123-iodoazomycin arabinoside. J Nucl Med 1993;34:405-10.

Ng CK, Sinusas AJ, Zaret BL, Soufer R. Kinetic analysis of technetium-99m-labeled nitroimidazole (BMS-181321) as a tracer of myocardial hypoxia. Circulation 1995;92:1261-8.

Nunn A, Linder K, Strauss WH. Nitroimidazoles and imaging hypoxia. Eur J Nucl Med 1995;22:265-80.

Parliament MB, Chapman JD, Urtasun RC, McEwan AJ, Golberg L, Mercer JR, Mannan RH, Wiebe LI. Non-invasive assessment of human tumour hypoxia with ^{123}I-iodoazomycin arabinoside: preliminary report of a clinical study. Br J Cancer 1992;65:90-5.

Patterson RE, Eisner RL. Value of objective assessment of new radiopharmaceuticals. J Nucl Med 1995;36:1086-7.

Rampling R, Cruickshank G, Lewis AD, Fitzsimmons SA, Workman P. Direct measurement of pO_2 distribution and bioreductive enzymes in human malignant brain tumors. Int J Radiat Oncol Biol Phys 1994;29:427-31.

Rasey JS, Grunbaum Z, Magee S, Nelson NJ, Olive PL, Durand RE, Krohn KA. Characterization of radiolabeled fluoromisonidazole as a probe for hypoxic cells. Radiat Res 1987;111:292-304.

Rasey JS, Koh W-J, Evans ML, Peterson LM, Lewellen TK, Graham MM, Krohn KA. Quantifying regional hypoxia in human tumors with positron emission tomography of [18F]fluoromisonidazole: a pretherapy study of 37 patients. Int J Radiat Oncol Biol Phys 1996;36:417-28.

Rasey JS, Koh W-J, Grierson JJ, Grunbaum Z, Krohn KA. Radiolabelled fluoromisonidazole as an imaging agent for tumor hpoxia. Int J Radiat Oncol Biol Phys 1989;17:985-91.

Rasey JS, Krohn KA, Freauff S. Bromomisonidazole: synthesis and characterization of a new radiosensitizer. Radiat Res 1982;91:542-54.

Rasey JS, Nelson NJ, Chin L, Evans ML, Grunbaum Z. Characteristics of the binding of labeled fluoromisonidazole in cells *in vitro*. Radiat Res 1990;122:301-8.

Rumsey WL, Cyr JE, Raju N, Narra RK. A novel [^{99m}]technetium-labeled nitroheterocycle capable of identification of hypoxia in heart. Biochem Biophys Res Commun 1993;193:1239-46.

Rumsey WL, Kuczynski B, Patel B, Bauer A, Narra RK, Eaton SM, Nunn AD, Strauss HW. SPECT imaging of ischemic myocardium using a Technetium-99m-nitroimidazole ligand. J Nucl Med 1995;36:1445-50.

Shelton ME, Welch MJ, Dence CS, Hwang D-R, Bergmann SR. [F-18]fluoromisonidazole: a potential marker of salvageable myocardium. (Abstract). J Nucl Med 1988;29:807.

Shi CQX, Sinusas AJ, Dione DP, Singer MJ, Young LH, Heller EN, Rinker BD, Wackers FJT, Zaret BL. Technetium-99m-nitroimidazole (BMS181321): a positive imaging agent for detecting myocardial ischemia. J Nucl Med 1995;36:1078-86.

Stone CK, Mulnix T, Nickles RJ, Renstrom B, Nellis SH, Liedtke AJ, Nunn AD, Kuczynski BL, Rumsey WL. Myocardial kinetics of a putative hypoxic tissue marker, ^{99m}Tc-labeled nitroimidazole (BMS-181321), after regional ischemia and reperfusion. Circulation 1995;92:1246-53.

Treher EN, Gougoutas J, Malley M, Nunn AD, Unger SE. New technetium radiopharmaceuticals: boric acid adducts of vicinal dioxime complexes.(Abstract). J Labelled Compds Radiopharm 1986;23:1118-9.

Urtasun RC, Koch CJ, Franko AJ, Raleigh JA, Chapman JD. A novel technique for measuring human tissue pO_2 at the cellular level. Br J Cancer 1986;54:453-7.

Urtasun RC, Parliament MB, McEwan AJ, Mercer JR, Mannan RH, Wiebe LI, Morin C, Chapman JD. Measurement of hypoxia in human tumours by non-invasive spect imaging of iodoazomycin arabinoside. Br J Cancer 1996;74 (Suppl. 27):S209-12.

Wiebe LI, Jette DC, Chapman JD, Flanagan RJ, Meeker BE. Iodoazomcin riboside (1-(5'-iodo-5-deoxyribofuranosyl]-2-nitroimidazole), a hypoxic cell marker. *In vivo* evaluation in experimental tumors. In: Nuclear Medicine and Clinical Oncology. Winkler C (editor). Berlin/Heidelberg/New York: Springer-Verlag, 1986; 402-7.

Wiebe LI, Stypinski D. Pharmacokinetics of SPECT radiopharmaceuticals for imaging hypoxic tissues. Quarterly Journal of Nuclear Medicine 1996;40:270-84.

Wiebe LI. Radionuclides, radiotracers and radiopharmaceuticals for *in vivo* diagnosis. Radiation Physics and Chemistry 1984;24:365-72.

Yang DJ, Wallace S, Cherif A, Li C, Gretzer MB, Kim EE, Podoloff DD. Development of F-18-labeled fluoroerythronitroimidazole as a PET agent for imaging tumor hypoxia. Radiology 1995;194:795-800.

Yeh S-H, Liu R-S, Wu L-C, Yang DJ, Yen S-H, Chang C-W, Yu T-W, Chou K-L, Chen KY. Fluorine-18 fluoromisonidazole tumour to muscle retention ratio for the detection of hypoxia in nasopharyngeal carcinoma. Eur J Nucl Med 1996;23:1378-83.

3. Rationale, Hypothesis and Objectives

3.1 Rationale

Currently, all the literature reported pharmacokinetic parameters of radiolabelled 2-nitroimidazole hypoxic cell markers are based on tracer kinetic analysis. ^{123}I-IAZA, which to date has been used in over 100 patients, is no exception. However, based on the biodistribution patterns, it is clear that radioactive metabolites do form. Therefore, tracer kinetics cannot be treated as synonymous with the radiopharmaceutical's pharmacokinetics. To further complicate the issue, this lack of delineation of true pharmacokinetic parameters has led to effect-compartment modeling of hypoxic tissue fraction using tracer kinetic data. This substitution is only valid if the concentration *vs.* time plots of total radioactivity and the radiopharmaceutical parallel one another; a circumstance which can be neither predicted nor assumed. It was therefore proposed that the pharmacokinetics of ^{123}I-IAZA should be studied in detail.

At the same time, ^{123}I-IAZA is a radiopharmaceutical, and therefore some radiation safety concerns exist about its use in patients. Considering that a diagnostic marker of tissue hypoxia has potential applicability in numerous diseases, there is a good possibility that a successful agent may become a routine diagnostic tool. Thus, it was also proposed that the radiation dose to the human from ^{123}I-IAZA administration be estimated.

Finally, all current pre-clinical imaging protocols routinely call for either continuous or intermittent use of anesthetics. The inherent assumption is that anesthetics do not change the pharmacokinetics of the investigated pharmaceuticals, but currently there is a profusion of evidence in the literature that they, in fact, do. Therefore, it was proposed that the effect of anesthetic use on ^{125}I-IAZA be studied in an animal model under conditions that would normally be used in an imaging study.

3.2 Hypotheses

1. Tracer kinetics of radioiodine are not consistent with the pharmacokinetics of radioiodinated IAZA.
2. Use of anesthetic in pre-clinical studies may change the pharmacokinetics of ^{125}I-IAZA in certain species during imaging protocols.

3. In humans with normal renal function ^{123}I-IAZA has appropriate pharmacokinetic parameters as a hypoxia marker, with total radioactivity excreted mainly via the kidneys.
4. ^{123}I-IAZA has favorable radiation dosimetry in humans for routine use as a diagnostic agent.
5. Exercise protocols, required during certain cardiac imaging studies, do not affect ^{123}I-IAZA biodistribution in a normal population.
6. Hypoxic tissue fraction can be theoretically predicted from a scintigraphic image.

3.3 Objectives

1. Develop a sensitive, specific and convenient assay for measuring $^{123/125}$I-IAZA in biological matrices.
2. Evaluate the pharmacokinetic profiles of ^{125}I-IAZA and total radioactivity in anesthetized and non-anesthetized rats.
3. Delineate the pharmacokinetics of ^{123}I-IAZA in healthy volunteers.
4. Estimate the human internal radiation dosimetry from ^{123}I-IAZA administration to the healthy volunteers.
5. Determine the effect of cardiac stress test on the pharmacokinetics and dosimetry of ^{123}I-IAZA in healthy volunteers.
6. Develop a pharmacokinetic/pharmacodynamic (PK/PD) model capable of estimating percent regional hypoxia from a scintigraphic image.

4. HPLC and Radiometric Assay of Radiolabelled IAZA in Blood and Urine[2]

4.1 Introduction

In its standard clinical application IAZA is administered to humans in a very low chemical dose (1 to 10 mg typical) and with levels of radioactivity suitable for nuclear medicine imaging (185 MBq of ^{123}I typical). The low dose causes the drug levels in blood to rapidly fall below the level of UV detection in HPLC. In addition, the radioactivity levels become too low for detection by standard HPLC flow-through radiometric detectors. The challenge was to develop a sensitive and reproducible assay which would allow the detection of unchanged IAZA in blood and urine.

A semi-quantitative analysis of radioiodinated ^{123}I-IAZA was reported previously, based on measurement of total radioactivity in serial blood samples taken from cancer patients. These data were used to estimate the pharmacokinetics of ^{123}I-IAZA (Parliament *et al.*, 1992). Counting the blood samples for total radioactivity is a common method of pharmacokinetic analysis of radiolabelled agents (Wiebe and Stypinski, 1996). However, this scintigraphic method is a nonspecific assay which cannot distinguish between ^{123}I-IAZA and its ^{123}I-labelled metabolites. In practice both total blood activity, as determined by direct gamma counting of blood, and selective counting of $^{123/125}$I-IAZA as described in the present assay, are clinically relevant. While ^{123}I-IAZA alone is metabolically trapped in hypoxic tissues, total radioactivity from ^{123}I-IAZA and its radioactive metabolites in blood and surrounding tissues constitutes background interference which must be reduced before clear scintigraphic tissue images can be obtained. It is therefore important to distinguish between intact $^{123/125}$I-IAZA and radiolabelled metabolites including free radioiodine produced by de-iodination of the radiopharmaceutical. Consequently, a very specific assay that combines the selectivity of HPLC and the sensitivity of gamma counting has now been developed.

This assay has been used, with minor modifications, to determine the concentration of ^{125}I-IAZA in mouse (Stypinski *et al.*, 1993) and rat (Stypinski *et al.*, unpublished), and ^{123}I-IAZA in human blood samples (Stypinski *et al.*, 1997submitted). A similar reverse isotope dilution technique (Wolfe, 1992) has been developed to determine the concentration of $^{123/125}$I-IAZA in urine of rats and human volunteers.

---

[2] A version of this chapter has been accepted for publication: Stypinski D, Wiebe LI, Mercer JR. J Pharm Biomed Anal, 1997(in press).

4.2 Experimental

4.2.1 Reagents

IAZA was synthesized and radiolabelled by an exchange reaction with Na[^{123}I]I or Na[^{125}I]I, based on procedures described previously (Mannan *et al.*, 1991). Water (Caledon Laboratories, Georgetown, Canada) and methanol (Fisher Scientific, Montreal, Canada) were HPLC grade. Sterile normal saline was supplied by Baxter Corporation (Toronto, Canada) in 100 mL i.v. bags.

4.2.2 Blood Sample Collection and Preparation

Prior to the collection of the blood samples, the internal standard (cold IAZA; 30 μg in 250 μL normal saline) was added to the collection tubes. In the animal studies the collection tubes were Fisherbrand® 1.5 mL microcentrifuge tubes (Fisher Scientific), while for human studies 9 mL SST Vacutainer® blood collection tubes (Becton Dickenson) were used. To prevent clotting of blood, heparin sodium (Hepalean®, Organon Teknika) was used in the animal studies. Clot formation and centrifugation in the absence of heparin sodium were used for human blood samples in order to speed up sample preparation. The tubes were weighed before and after blood sample collection to determine the blood volume. A 1:1 w/v relationship was assumed.

After coagulation, the human blood samples were centrifuged (15 min at 1528 g) in a Beckman Model TJ-6 Centrifuge. A small aliquot of serum (50 - 80 μL) was withdrawn for the determination of total radioactivity in the serum fraction. The remainder of the serum was separated from the clot for further analysis, while the clot was counted for total radioactivity. Rat blood samples were centrifuged for 5 min in a Brinkman Model 5412 centrifuge, with packed cells and the supernatant separately counted for total radioactivity. Mouse blood samples were not centrifuged, instead whole blood was counted to determine total radioactivity. All human blood samples were handled using a protocol approved by the University of Alberta biosafety and radiation safety committees, and clinical samples were obtained through a protocol approved by the Alberta Cancer Board research ethics committee.

4.2.3 Solid Phase Extraction

Disposable Waters™ SepPak cartridges (C18, Classic, Short body) were used for cleanup and isolation of $^{123/125}$I-IAZA in human serum, rat plasma, and mouse whole blood samples. Each cartridge was first conditioned with methanol (4 mL) followed by water (5 mL). Immediately thereafter, the samples were manually loaded onto the cartridge with a 1 or 5 mL syringe, depending on sample size. Water (3 mL) was pushed through the cartridge, effectively eluting most of the unwanted components. This eluent was discarded, and methanol (2 mL) was passed through the cartridge. This methanol fraction, which contained $^{123/125}$I-IAZA, was collected for further analysis. In the animal studies, where ^{125}I-IAZA (^{125}I decay $t_{1/2}$ = 60 d) was used, these samples were evaporated to dryness and reconstituted with normal saline (250 μL). For human samples where ^{123}I-IAZA (^{123}I decay $t_{1/2p}$ = 13.2 h) was used, the methanol eluent fractions were collected into 3 mL serum collection Vacutainer® tubes that had been pre-calibrated to allow for the determination of the volume of the eluent, thereby bypassing the evaporation and reconstitution steps. All the samples were analyzed using HPLC.

4.2.4 Urine Sample Preparation

Aliquots of urine (5 mL) were first counted for total radioactivity. Prior to HPLC analysis, aliquots (1 mL) were filtered through a sterile Acrodisc® 0.2 μm low protein binding disposable filter to remove any possible particulate matter, spiked with several micrograms of cold IAZA, and injected onto the HPLC directly without any dilution. ,

4.2.5 Instrumentation and Chromatographic Conditions

The HPLC system consisted of a U6K manual injector (Waters), a single M45 pump (Waters), and a scanning ultraviolet detector (Waters Millipore Lambda-Max Model 401 LC Spectrophotometer). The eluent from the HPLC was collected using a fraction collector (FRAC-100, Pharmacia). The chromatographic data acquisition was performed with IBM-compatible PC with Baseline 810 data processing software (Waters, Mississagua, Canada).

The mobile phase used for blood sample analysis was a pre-mixed, degassed water-methanol solution (3:2, v/v), and for urine sample analysis pre-mixed, degassed water-methanol solution (7:3, v/v). In both cases the flow rate was 2 mL/min. The

chromatographic separation was achieved using a reverse-phase analytical column (Waters, μBondpack Radial-Pak C18 Cartridge). The detector was set at $\lambda = 325$ nm, which is the λ_{max} of IAZA as determined by PU 8740 UV/VIS Scanning Spectrophotometer (Phillips). All samples were analyzed in triplicate. HPLC system stability was tested at the beginning, during and at the end of each day by injecting standard IAZA in normal saline.

For radiometry, HPLC serial eluent fractions were collected with careful recovery of the eluent volume that contained the IAZA peak as indicated by the UV detector. The duration of sample collection was 1.25 min (blood) and 1.65 min (urine) corresponding to a sample volume of 2.5 mL and 3.3 mL, respectively. All HPLC samples were counted for radioactivity using a Gamma 8000 (Beckman) gamma scintillation counter. Counter background radioactivity was determined by counting several empty sample vials along with each sample set.

4.2.6 Extraction Efficiency

A calibration plot of UV absorption against IAZA amount was established by analyzing 25 μL samples of five different IAZA concentrations over the 15 - 100 μg/mL range. All the samples were analyzed in triplicate.

Whole blood extraction efficiency studies were performed with blank blood samples (no IAZA dose to the donor) collected from rat and human volunteers. Cold IAZA internal standard (30 μg in 250 μL of normal saline) was mixed *in vitro* with donor whole blood and subsequently analyzed using the solid phase extraction procedure and HPLC analysis as described above. In addition, plasma (rats) and serum (human) extraction efficiencies were determined in a similar manner for blank rat plasma and human serum, by adding the internal standard to each, followed by solid phase extraction and HPLC analysis. The exact volumes of each matrix are given in Table 4.1.

The extraction efficiency from all of the matrices was calculated by comparing the HPLC UV absorbance peak of the internal standard in normal saline versus that determined for the internal standard added to the matrix and extracted using the SepPak extraction procedure, normalized for any dilution.

4.3 Results and Discussion

The calibration curve of IAZA, shown in Figure 4.1, was found to be linear over the 0.375 - 2.50 μg (1.06 - 7.04 nmol) range, with a calculated regression line with a slope of 0.0160, f(0) = -0.0207; the correlation coefficient (r^2) was 0.99. The calibration curve of the internal standard IAZA was used to determine the extraction efficiency. It is important to note that the extraction efficiency is independent of the amount of $^{123/125}$I-IAZA in the samples. For each assay, 30 μg of internal standard IAZA was added to the matrix. Therefore, the contribution of $^{123/125}$I-IAZA (cold and radiolabelled dose) to the total IAZA (from dose and internal standard) amount in the sample was insignificant. Under our experimental conditions, even for samples taken at 1 min after $^{123/125}$I-IAZA administration, the $^{123/125}$I-IAZA concentration in the samples accounted for less than 1.0 % of the total IAZA (from dose and internal standard) in that sample. Consequently, the extraction efficiency of any sample will depend only on the sample matrix.

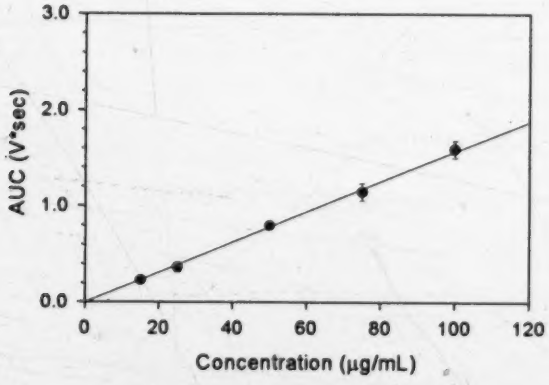

Figure 4.1 IAZA calibration curve using analytical HPLC (injection volume = 25 μL, flow conditions: 60:40 H_2O:MeOH, 2 mL/min, λ = 325 nm, retention time 5.98 ± 0.25 min). Each point represents n = 5 samples.

Radiolabelled IAZA was found to be stable in plasma for at least one month when stored either refrigerated or frozen (Figure 4.2). Furthermore, there was no difference in the efficiency of extraction of IAZA from plasma samples stored for 24 hours at room

temperature when compared to extraction from samples stored at refrigerator temperature. For *in vivo* studies, samples were routinely refrigerated within 30 minutes of collection and brought to room temperature only at the time of analysis. The final volume of each MeOH fraction, following SepPak extraction, was adjusted to 2 mL and, therefore, the samples were always analyzed in the linear range of the calibration curve (1.11 ± 0.11μg/200 μL injection for a 36.9 ± 3.6% extraction efficiency).

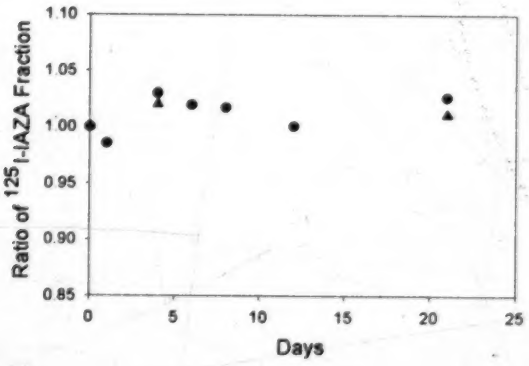

Figure 4.2 IAZA stability in rat plasma samples. Values expressed as ratio of ^{125}I-IAZA fraction in the sample at the time of analysis to the fraction of ^{125}I-IAZA at the time of sample preparation. Key: (●) refrigerated sample; (▲) frozen sample (thawed at room temperature for 30 min prior to HPLC analysis).

The results of the extraction efficiency studies are summarized in Table 4.1. With the exception of the mouse blood samples, all relative standard deviation values were < 10 %. For the mouse, whole blood samples were loaded directly onto the SepPak cartridge, and the presence of cellular debris may have introduced greater variability to the assay. Since rat plasma samples were less than one tenth the size of the human serum samples, the lower extraction efficiency from the rat plasma may reflect sample loss during sample transfers rather than sample loss during the SepPak extraction procedure; however, the wash eluent from rat plasma has not been analyzed to verify this observation. Similarly, the greater extraction efficiency value from the rat whole blood reflects the volume expansion of the supernatant once the internal standard, in

250 μL of normal saline, was added to whole blood (200 - 500 μL for rats, 5 -10 mL for human). The low extraction efficiency from the whole blood in humans suggests that almost 63 % of the analyte was retained in the clot. This has been confirmed by collecting blood samples from seven volunteers within 1-3 min of ^{123}I-IAZA administration, and counting the clot and the serum. The radioactivity in the clot was 62.6 ± 1.4 % of total sample radioactivity. In addition, for one of the volunteers, the water wash, the SepPak cartridge and the volume not accommodated by the 1.0 mL hold-up volume of the cartridge were collected. All of the activity in the serum sample was accounted for, with negligible loss to the SepPak cartridge and the volume of serum not accommodated by the cartridge. The percent radioactivity in the water wash was negligible initially, but increased with time after administration of the radiopharmaceutical. This increase was most likely due to the presence of radiolabelled water-soluble metabolites of ^{123}I-IAZA.

	Whole blood	Serum	Plasma
Human	0.369 ± 0.036 (5 -10 mL) (n = 25)	0.997 ± 0.071 (2.5 - 5 mL) (n = 7)	ND[a]
Rat	0.564 ± 0.055 (0.2 - 0.5 mL) (n = 6)	ND	0.823 ± 0.013 (0.1 - 0.25 mL) (n = 4)
Mouse	0.462 ± 0.106 (0.75 -1.0 mL) (n = 2)	ND	ND

[a]ND not determined for reasons explained in the text

Table 4.1 Extraction efficiency values for IAZA in the matrices studied.

A representative chromatogram and radiochromatogram of a human blood sample is shown in Figure 4.3. ^{123}I-IAZA from the blood samples along with the added IAZA internal standard eluted at 5.98 ± 0.25 min. The presence of the internal standard allowed UV detection of the appropriate fraction containing ^{123}I-IAZA and provided a guide for the collection of the eluent for subsequent gamma counting. The chromatograms from mouse and rat blood samples containing ^{125}I-IAZA and the internal standard were similar to those in Figure 4.3. Due to the distance between the UV

detector and fraction collector, there was an approximate 30 seconds delay between the UV and gamma counter measurement of the same eluent fraction.

A representative chromatogram and radiochromatogram of a human urine sample is shown in Figure 4.4. In the case of urine, cold IAZA was added just prior to the HPLC injection, and served only to identify the location of the ^{123}I-IAZA peak. The HPLC retention time of IAZA in urine was 11.2 ± 0.5 min. It was necessary to increase the retention time of IAZA in urine samples to improve the separation of this peak from the interfering UV peak from an endogenous component of urine which overlapped the IAZA peak when the solvent and flow conditions described for blood were used. The amount of ^{123}I-IAZA in urine samples was calculated by determining the radioactivity due to the ^{123}I-IAZA in a known volume of sample, correcting for radioactive decay from the time of ^{123}I-IAZA administration to the subject and multiplying by the total volume of urine collected. Rat urine containing ^{125}I-IAZA produced similar chromatograms.

Decay corrections were made based on first-order decay of ^{123}I, using the equation:

$$A = A_0 \times e^{-\left(\frac{0.693 \times t}{t_{1/2p}}\right)} \qquad (4.1)$$

where A is the activity at the time of measurement (in the gamma counter), A_0 is the activity at the time of sample collection from the patient, $t_{1/2p}$ is the 13 h physical decay half-life of ^{123}I, and t is the time elapsed between sample collection and measurement. Since ^{125}I has a 60 day decay half-life and since same-day or next-day processing and counting of samples was used, no decay correction was necessary for these samples.

A biologic system can be assumed to be unable to differentiate between the radioactive and cold IAZA. It is the ratio of radiolabelled to total (radiolabelled and cold) IAZA that determines the specific activity of the dose. Thus, the minimum detection limit of this assay depends not so much on the chemical amount of the agent in the blood, as on the specific activity of the radiolabelled compound (MBq/mg). In the human studies, for example, the specific activity of the administered ^{123}I-IAZA dose varied by more than tenfold, with a nominal dose of 185 MBq of radioactivity administered in anywhere from 0.1 mg to 1.2 mg of cold IAZA carrier (Stypinski *et al.*, 1997submitted). As a result, the minimum detection limit of the assay for ^{123}I-IAZA, as determined from the last sample of the volunteer who received the smallest chemical dose (0.1 mg), was 7.46 pg (21 fmol) per mL of serum. The actual detection limit for

this assay is determined by the detection limit for radioactive counting. In the human blood sample analysis this limit was set arbitrarily at three times the background count rate. The background (38 ±11 CPM) was determined from a blank blood sample collected from each volunteer before the administration of ^{123}I-IAZA. Since the counting efficiency of the gamma counter for ^{123}I was 0.4, this cut-off count rate (114 ± 33 CPM) corresponded to a detection limit of about 645 DPM/mL (10.8 Bq/mL) of serum. In general, this assay was sensitive enough to trace activity up to the point where greater than 99 % of the predicted area under the concentration *vs.* time curve had been accounted for in all volunteers who received ^{123}I-IAZA (Stypinski *et al.*, 1997submitted).

The detection limit for ^{125}I-IAZA was similar; ^{125}I analysis has the advantages of practically no loss of counts from radioactive decay during processing (^{125}I $t_{1/2p}$ = 60 days) and better counting efficiency of the gamma counter (> 0.75).

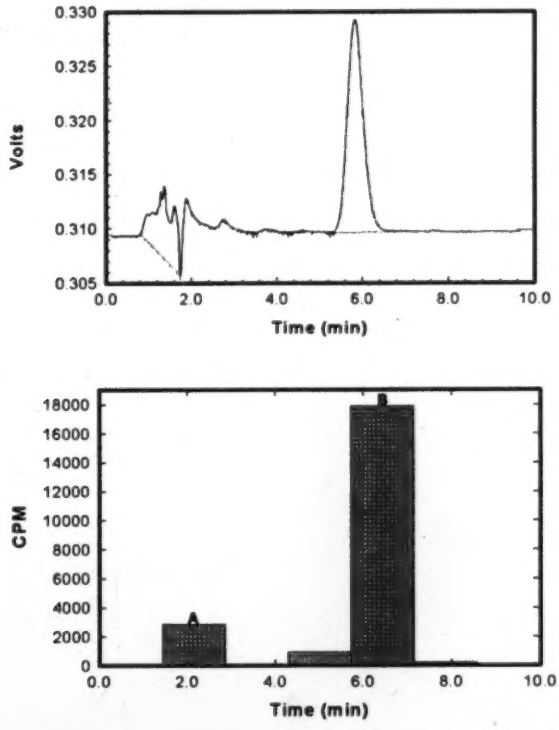

Figure 4.3 HPLC chromatogram (upper panel) and corresponding radiometric plot (lower panel) of a representative human blood sample after single ^{123}I-IAZA i.v. administration. In the lower panel A represents polar radioactive metabolites, while B represents radioactive ^{123}I-IAZA.

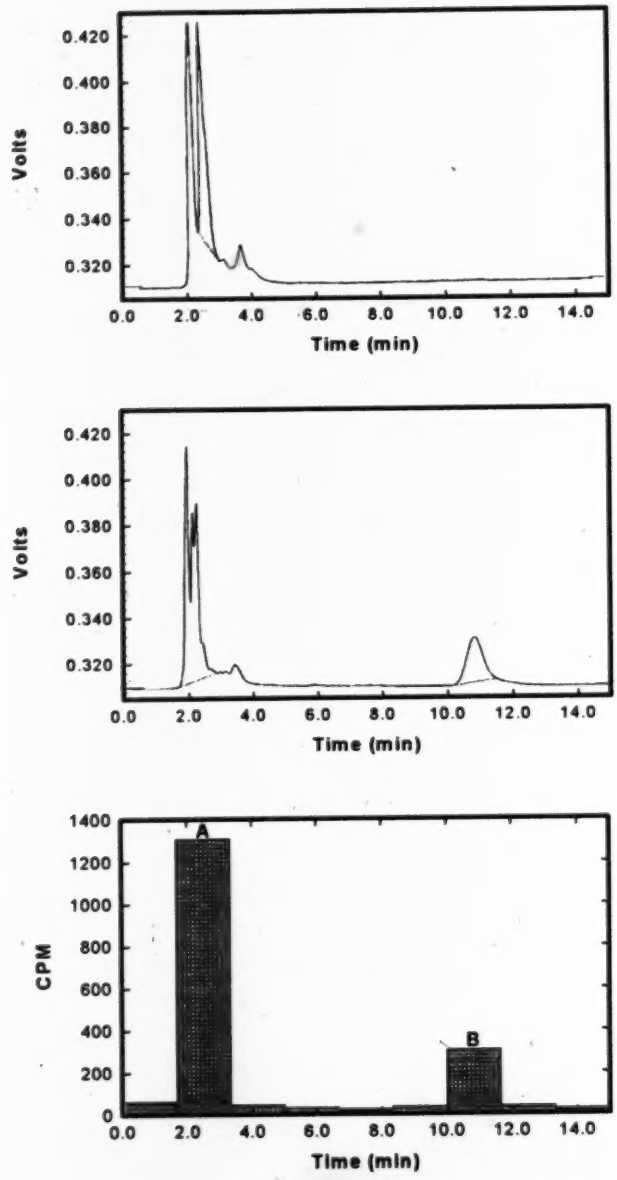

Figure 4.4 HPLC chromatograms of representative cumulative 28 h human urine sample without the internal standard (upper panel) and after addition of 50 μg of the internal standard to 1 mL of urine (middle panel), and a corresponding radiometric plot (lowest panel) after single i.v. ^{123}I-IAZA dose administration. In the lowest panel A represents polar radioactive metabolites, while B represents radioactive ^{123}I-IAZA.

4.4 References

Mannan RH, Somayaji VV, Lee J, Mercer JR, Chapman JD, Wiebe LI. Radioiodinated 1-(5-iodo-5-deoxy-*B*-D-arabinofuranosyl) -2-nitroimidazole (iodoazomycin arabinoside: IAZA), a novel marker of tissue hypoxia. J Nucl Med 1991;32:1764-70.

Parliament MB, Chapman JD, Urtasun RC, McEwan AJ, Golberg L, Mercer JR, Mannan RH, Wiebe LI. Non-invasive assessment of human tumour hypoxia with ^{123}I-iodoazomycin arabinoside: preliminary report of a clinical study. Br J Cancer 1992;65:90-5.

Stypinski D, Wiebe LI, Mercer JR. ^{125}I-IAZA - a novel hypoxic cell marker. Annual Meeting of the Canadian Society of Nuclear Medicine, Prairie Provinces Chapter 1993; Saskatoon, Saskachewan.

Stypinski D, Wiebe LI, McEwan AJ, Tam YK, Mercer JR. Radiopharmacokinetics of ^{123}I-IAZA in healthy volunteers. 1997(Submitted).

Wiebe LI, Stypinski D. Pharmacokinetics of SPECT radiopharmaceuticals for imaging hypoxic tissues. Quarterly Journal of Nuclear Medicine 1996;40:270-84.

Wolfe RR. Radioactive and stable isotope tracers in biomedicine. Principles and practice of kinetic analysis. 1st ed. New York, NY: Wiley-Liss, Inc.; 1992.

5. Comparison of ^{125}I-IAZA Pharmacokinetics in Anesthetized and Non-anesthetized Rats

5.1 Introduction

The effects of various anesthetics on drug metabolizing enzymes, renal function, cardiac output and perfusion have been well documented (Sawyer *et al.*, 1971; Brown, 1972; Ichimura *et al,*. 1984; Doursout and Chelly, 1988; Trevor and Miller, 1989; LaBella and Queen, 1992). In recognition of these changes, the use of anesthetized and acutely-instrumented animals in pharmaceutical investigation has been considered of limited value, unless, as for example in Ngo *et al.* (1995), it can be shown that the anesthetic does not affect the disposition of the agent under investigation. Generally, current pre-clinical pharmacokinetic protocols allow for a minimum of 24 h recovery time between surgical procedures and the administration of the pharmaceutical.

Pre-clinical diagnostic imaging studies present a technical problem, however, as they require the animal to be completely immobilized, necessitating the use of anesthesia during image acquisition. While the anesthetic of choice is in our laboratory methoxyflurane, other commonly used anesthetics include halothane (Caldwell *et al.*, 1995; DiRocco *et al.*, 1993), a combination of sodium thiamylal and halothane (Shi *et al.*, 1995; Martin *et al.*, 1992), ketamine (Yang *et al.*, 1995), a combination of ketamine and xylazine (Moore et al., 1993), or sodium pentobarbital (Rumsey *et al.*, 1995). Occasionally, the choice of anesthetic used during the imaging is not mentioned (Yang *et al.*, 1995; Archer *et al.*, 1995; Rasey *et al.*, 1989).

Although all of these anesthetic agents can affect both the biodistribution and clearance of the radiophramceuticals under investigation, generally no attempts have been made to assess the impact of the co-administered anesthetic on these kinetic parameters. Moreover, the lack of specific assays for radiopharmaceuticals further complicates the analysis, as data are usually obtained from total radioactivity counts of biologic samples; that is, from a tracer kinetic analysis which is incapable of distinguishing between the disposition of the radiopharmaceutical and its radioactive metabolites (Wiebe and Stypinski, 1996; Stypinski *et al.*, 1997submitted).

An HPLC/radiometric assay has recently been developed for the analysis of radiolabelled iodoazomycin arabinoside (IAZA) in blood and urine samples (Stypinski *et*

al., 1997in press). This assay is now applied to determine the impact of methoxyflurane anesthesia on the pharmacokinetics of ^{125}I-IAZA in a rat model which has been previously implemented in the imaging studies with ^{123}I-IAZA (McEwan *et al.*, 1996).

5.2 Experimental

5.2.1 Chemicals and Dose Preparation

Water (Caledon Laboratories, Georgetown, Canada) and methanol (Fisher Scientific, Montreal, Canada) were HPLC grade. Sterile normal saline (Baxter Corporation, Toronto, Canada) was supplied in 100 mL i.v. bags, and heparin sodium (Hepalean7, Organon Teknika) in 10 mL vials. Methoxyflurane (Metofane®) was supplied by Janssen Pharmaceutica (Mississauga, Ontario, Canada).

IAZA was synthesized by Dr. Elena Atrazheva (Faculty of Pharmacy and Pharmaceutical Sciences, University of Alberta) using published procedures (Mannan, 1991; Mannan *et al,* 1991). The modified radiolabelling procedure based on Mannan (1991) was as follows. Five mCi (185 MBq) of no-carrier-added ^{125}I-NaI, supplied by Amersham in 11 μL of 0.1 N NaOH solution, was transferred into a glass Reacti-vial together with a 50 μL methanol wash. The solvent was removed with a gentle stream of nitrogen with the reaction vial heated at 35° C. Pivalic acid (3-4.5 mg) and IAZA (0.6 and 0.05 mg for anesthetized and non-anesthetized study, respectively) dissolved in 75 μL methanol were added to the reaction vial and all of the solvent was again evaporated to dryness under a stream of nitrogen while heated at 43° C. The Reacti-vial was sealed and the reaction allowed to proceed for 75 min at 78° C. After the reaction was completed, the product was allowed to cool to the room temperature and the contents were dissolved with 100 μL methanol. The reaction yield was determined using HPLC (10μm, 60:40 water:methanol, 2 mL/min flow rate) equipped with a Waters C-18 Radial-Pak reverse phase column (μBondpack Radial-Pak C18 Cartridge, 8mm I.D.) with the radioactive eluent being monitored by a NaI(Tl) 5 cm crystal scintillation detector. The product was purified in 2 injections using a preparative Whatman Partisil M9 10/25 ODS reverse phase HPLC column (30:70 water:methanol, 2 mL/min flow rate), with the ^{125}I-IAZA peak collected and evaporated to dryness overnight under a

gentle stream of nitrogen. The reaction yields were > 99% and 20 % for the syntheses involving 0.6 mg and 0.05 mg of IAZA, respectively.

Specific activity determination was performed on the final product reconstituted with 2.0 mL MeOH. Four 3 μL samples of the product were analyzed for IAZA concentration using analytical HPLC. For the determination of the radiochemical yield, a 2 μL sample was withdrawn and further diluted with 200 μL of MeOH. Next, four 2 μL aliquots were withdrawn into small gamma counting vials, diluted with 2 mL of water and counted using a Gamma 8000 (Beckman) gamma scintillation counter. The specific activity for the anesthetized study was 6.4 mCi/mg and for the non-anesthetized study 24mCi/mg. The radiochemical purity was ≥ 97 %.

Final dose calibration for the animal study was performed by evaporating the product to dryness, and reconstituting to the desired concentration with normal saline.

5.2.2 Catheter Cross-Contamination Effect

Since both ^{125}I-IAZA dose administration and blood sample collection were to be performed using the same indwelling jugular vein catheter, contamination from the dose to the first sample had to be assessed and minimized. Several *in vitro* determinations were performed by connecting the catheter (30 cm) and the silastic tubing (2.5 cm), as required in the surgical procedure, and passing a dose of ^{125}I-IAZA through the two tubes. Next, the tubes (catheter and silastic) were washed using several different procedures. These generally involved washing the tubes with various amounts of normal saline wash and blank (^{125}I-IAZA free) heparinized rat blood samples (0.25 mL). The saline was pushed through the tubes, while the blood samples were withdrawn through the line with a syringe. Both the saline washes and blood samples were counted for ^{125}I radioactivity in the Gamma 8000 (Beckman) gamma scintillation counter.

5.2.3 Animal Models Preparation

Male Sprague-Dawley rats (436-532 g) were surgically implanted with a jugular vein catheter while under surgical plane anesthesia with methoxyflurane. Group 1 (n = 4) animals were maintained under surgical plane anesthesia with methoxyflurane for the additional two hours required for the duration of the experiment. Group 2 (n = 3)

animals were allowed to recover for 24 h from the catheter implant surgery prior to ^{125}I-IAZA administration.

A dose of ^{125}I-IAZA (0.219 ± 0.030 mCi) was administered i.v. via the jugular catheter, and blood samples were collected from the same catheter for two hours (group 1) or five hours (group 2). Group 1 blood collection times were: 1, 1.5, 2, 2.5, 3, 4, 5, 7, 10, 15, 20, 30, 45, 60, 90 and 120 min. Group 2 blood collection times were: 2.5, 5, 10, 20, 30, 45, 60, 90, 120, 240 and 300 min. In each case a blank blood sample was also taken just prior to ^{125}I-IAZA administration. Cumulative urine samples were collected and included urine directly removed from the urinary bladder after the animal was euthanised with sodium pentobarbital.

5.2.4 Sample Analysis

Blood and urine samples were analyzed using a reverse isotope dilution method published elsewhere (Stypinski *et al.*, 1997in press). During blood sample processing the ^{125}I-IAZA-containing methanol fractions eluted from the disposable WatersJ SepPak cartridges (C18, Classic, Short body) were evaporated to dryness overnight under a gentle stream of nitrogen and reconstituted with normal saline (250 μL) prior to HPLC analysis. The urine samples were counted for total radioactivity and 1 mL aliquots were cleaned of particulate contaminants with a sterile Acrodisc® 0.2 μm low protein binding disposable filter prior to HPLC analysis.

All of the samples were analyzed using analytical HPLC (μBondpack Radial-Pak C18 Cartridge, 2 mL/min flow rate, 60:40 water:methanol for blood and 70:30 water:methanol for urine) with eluent fractions collected and counted for ^{125}I. The location of the ^{125}I-IAZA radiometric peak was matched with the location of the cold IAZA internal standard as determined by the UV detector.

5.2.5 Pharmacokinetic and Statistical Analysis

All the data were fitted with both compartmental and non-compartmental analysis using WinNonlin v 1.1 (Scientific Consulting, Inc.). The two compartment model with the iteratively reweighted least squares weighing option was chosen as the best model to fit both data sets, based on observed and calculated correlation function values, AIC and SC measures, and linearity of the partial derivatives plots.

Radiolabelled metabolite disposition profiles were estimated by subtracting the plots of percent of injected dose (%ID) per gram of blood for ^{125}I-IAZA from that of total radioactivity. The fraction of injected radioactive dose remaining (FR_P) in the body at 300 min was predicted using the following relationship:

$$FR_P = AUC_{300-\infty} \div AUC_{0-\infty} \quad (5.1)$$

$AUC_{300-\infty}$ and $AUC_{0-\infty}$ were determined for total radioactivity using the two compartment open model. The actual fraction of dose remaining (FR_A) in the body was determined for the animals in group 2 by dissecting the major organs and the carcass, placing tissue samples in the pre-weighed gamma counter vials, re-weighing and counting for total radioactivity. The "goodness-of-fit" of the model used was verified by comparing the ratio of FR_P to FR_A. In addition, the mass balance of total radioactivity was determined for the animals in group 2 by summing the activities in the urine, dissected organs and carcass.

Statistical analysis to detect differences in the kinetic parameters between the anesthetized and recovered animals was conducted using Student's t test with the 0.05 power of significance. Parameters are reported as arithmetic mean ± SD.

5.3 Results

5.3.1 Catheter Washout Study

Some of the data from the catheter contamination studies are presented in Figure 5.1. Plot 1 represents contamination in 10 serial 0.25 mL normal saline washes, clearly showing evidence of significant ^{125}I activity even after 2.5 mL of normal saline has passed through the catheter. Plots 2 and 3 (Figure 5.1) show that in the first blank sample there is an unacceptable level of leftover dose, as about 23 % of radioactivity that would normally be found in the first collected blood sample (based on a pilot tail-vain administration with 480000 CPM in the first sample) would originate from the catheter contamination. However, the activity in the second sample decreases significantly. For Plot 2, where there was no normal saline wash between the two collected samples, only 2 % of the activity in the first sample would be due to the leftover dose in the catheter. Since blood left in the catheter during sample collection

would be normally washed with normal saline (or heparinized normal saline) to prevent clotting and cross contamination between samples, Plot 3 simulates this scenario by flushing the line with 0.2 mL normal saline between the first and second samples. This further decreases the contamination to an even more acceptable level of below 1 %.

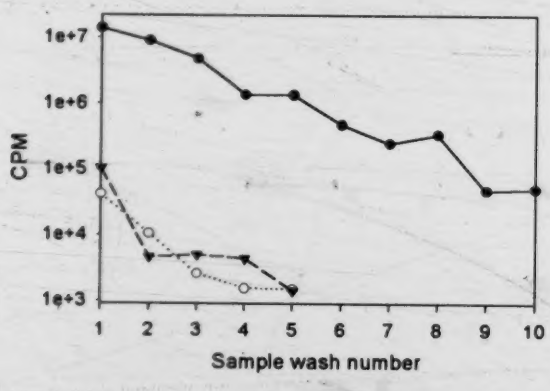

Figure 5.1 Radioactive contamination (CPM) in various catheter wash samples *vs.* sample wash number following a push of ^{125}I-IAZA (220 μCi). Key: Plot 1 (●) ten sequential 0.25 mL normal saline washes of the catheter; Plot 2 (O) five sequential 0.25 mL washes with rat whole blood; Plot 3 (▼) one 0.25 mL whole blood wash followed by one 0.2 mL normal saline wash (CPM not shown), followed by four more 0.25 mL whole blood washes.

5.3.2 ^{125}I-IAZA and Total Radioactivity Pharmacokinetics

Figure 5.2 depicts whole blood concentrations of ^{125}I-IAZA and total radioactivity, expressed as %ID/mL *vs.* time curves, following i.v. ^{125}I-IAZA doses to anesthetized and non-anesthetized rats. The individual and mean concentration values are presented in Tables 11.1 and 11.2 of Appendix 1. The pharmacokinetic parameters for both groups of animals are summarized in Table 5.1. Although there are no significant differences between the two treatment groups in the disposition of total radioactivity, ^{125}I-IAZA had a considerably lower clearance rate in the anesthetized animals than in those allowed to recover for 24 hours from the anesthetic effect. The observed three-fold difference was not due to any distribution changes, as the V_{ss} did not alter significantly, but was

due to the impaired elimination, which decreased from a half-life of 0.59 hours to 1.63 hours for groups 2 and 1, respectively.

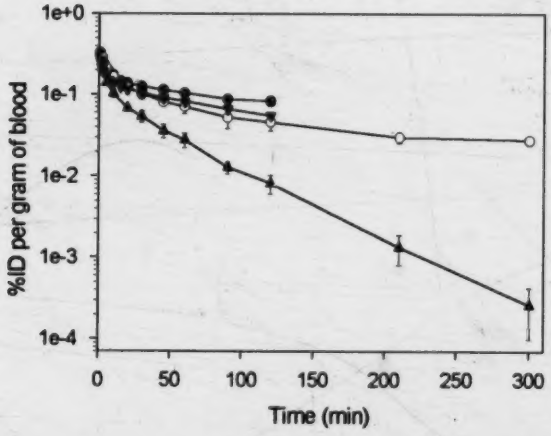

Figure 5.2 Whole blood time course of ^{125}I-IAZA and total radioactivity in anesthetized and non-anesthetized rats. Key: (●) total radioactivity, anesthetized; (O) total radioactivity, non-anesthetized; (▼) ^{125}I-IAZA, anesthetized; (▲) ^{125}I-IAZA, non-anesthetized.

	Total Radioactivity		^{123}I-IAZA	
	Group 1	Group 2	Group 1	Group 2
$t_{1/2\alpha}$ (min)	3.67 ± 1.15	9.22 ± 0.85	3.06 ± 1.44	4.54 ± 3.28
$t_{1/2\beta}$ (h)	2.45 ± 0.68	2.56 ± 0.50	1.63 ± 0.30	0.59 ± 0.09
MRT (h)	3.42 ± 0.96	3.25 ± 0.75	2.26 ± 0.39	0.69 ± 0.09
Cl_{TB} (mL/h/kg)	402 ± 110	595 ± 180	646 ± 52	2180 ± 350
V_{ss} (L/kg)	1.31 ± 0.16	1.86 ± 0.26	1.45 ± 0.10	1.55 ± 0.25

Table 5.1 Pharmacokinetic parameters following a single i.v. ^{125}I-IAZA administration to anesthetized (Group 1) and non-anesthetized (Group 2) rats.

Since the animals in group 1 were maintained under anesthesia throughout the experiment, sampling continued for only two hours, at which time the rats were euthanised. Because ^{125}I-IAZA had a long elimination half-life in this group, the $AUC_{0\text{-}120min}$ of ^{125}I-IAZA and of total radioactivity constituted only 59 ± 6 % and 47 ±11 % of $AUC_{0\text{-}\infty}$, respectively. For group 2 animals, the sample collection continued until more than eight elimination half-lives of ^{125}I-IAZA have passed. The $AUC_{0\text{-}300\ min}$ of ^{125}I-IAZA in this experiment was greater than 99 % of the $AUC_{0\text{-}\infty}$, while for total radioactivity $AUC_{0\text{-}300\ min}$ accounted for 71 ± 8 % of $AUC_{0\text{-}\infty}$. Consequently, only the renal clearance of ^{125}I-IAZA from group 2 was determined at 589 ± 44 mL/h/kg, with only 27 ± 2 % of radioactivity eliminated as ^{125}I-IAZA at 5 hours. In group 1 animals, of the 15 % of dose eliminated in urine by 2 hours more than 70 % was due to ^{125}I-IAZA.

5.3.3 Metabolite Pharmacokinetics

Graphs A and B of Figure 5.3 show the mean disposition of the radioactive metabolites of ^{125}I-IAZA in the anesthetized and recovered animals, respectively. In each case the metabolite plot was derived by subtracting the mean ^{125}I-IAZA plot from that of mean total radioactivity. The data used to construct each graph is presented in Table 11.3 of Appendix 1.

There is a significant difference in the relative blood concentration ratios of total radioactivity and radioactive metabolites between the two treatment groups. In graph A (group 1), where the metabolite concentrations are lower, the radioactive metabolites contribute only 38 ± 14 % to the total radioactivity predicted $AUC_{0\text{-}\infty}$. Furthermore, even by 120 min the plot of metabolites does not appear to reach linearity. In graph B (group 2), the radioactive metabolite contribution to the total radioactivity $AUC_{0\text{-}\infty}$ is 79 ± 3 %. As well, in this graph the terminal phase of the radioactive metabolites disposition plot eventually overlaps with that of total radioactivity. At 300 min, the blood concentration of intact ^{125}I-IAZA contributes less than 1 % to the total blood radioactivity concentration.

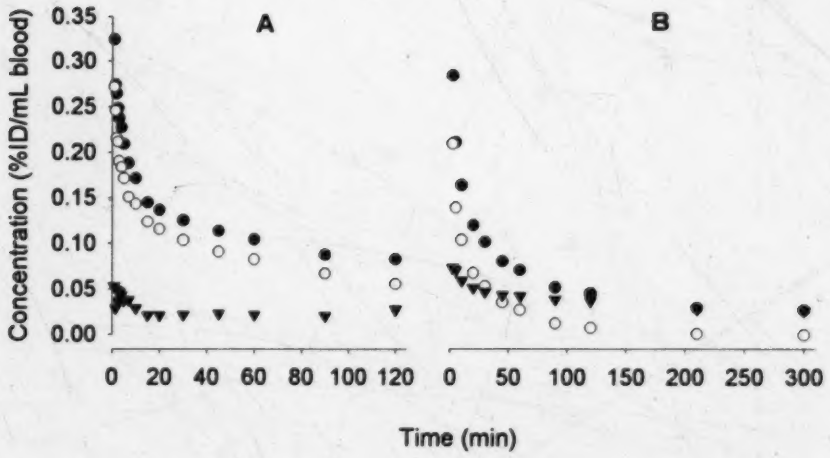

Figure 5.3 Mean blood disposition courses *vs.* time of (●) total radioactivity, (O) ^{125}I-IAZA and (▼) the radioactive metabolites of ^{125}I-IAZA. (A = anesthetized animals; B = non-anesthetized animals).

5.3.4 Biodistribution (Group 2)

Organs, urine and carcasses of rats in group 2 were counted for total radioactivity to determine the fate of the radioactive dose. Figure 5.4. summarizes the distribution of the radioactivity to the major organs, with kidneys and stomach concentrating the greatest fraction of the dose per gram wet weight. About half (49 ± 4 %) of the dose was found in the urine (28 ± 2 % as un-metabolized ^{125}I-IAZA), 15 ± 0.5 % in the large intestine, 3.5 ± 1 % in the small intestine and only about 0.04 % of the dose localized in the thyroid gland. Approximately 95 ± 5 % of the injected radioactivity was recovered. The correlation between the model predicted fraction of dose remaining in the body at 300 min and the actual activity found in the carcass ($FR_P \div FR_A$) was 0.92 and 1.1 for rats 1 and 3, respectively. Rat 2 had the poorest correlation ($FR_P \div FR_A = 1.5$), with the 2 compartment model overestimating by 10 % the actual amount of radioactivity left in the body.

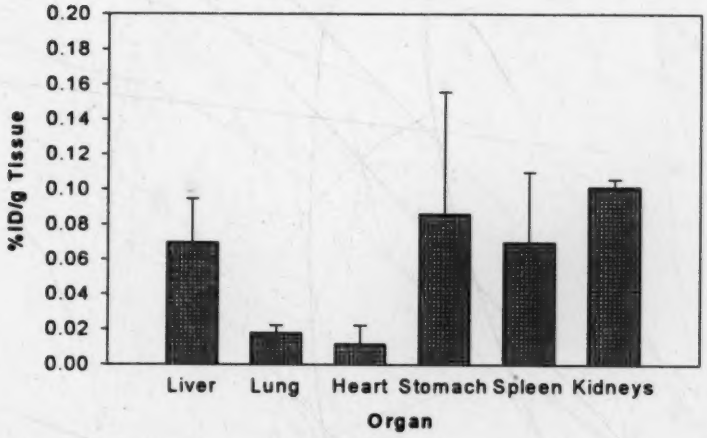

Figure 5.4. Organ accumulation of total radioactivity at 5 hours after ^{125}I-IAZA dose to non-anesthetized Sprague-Dawley rats.

5.4 Discussion

This experiment has shown that the pharmacokinetics of ^{125}I-IAZA in rats changes when the rats are anesthetized with methoxyflurane. This is not unexpected, in view of the literature reports on the use of anesthetics in experimental animals. Diethyl ether, halothane, methoxyflurane, enflurane, isoflurane, pentobarbital and thiamylal have all been shown to affect the cardiovascular system, enzyme activity, protein binding, and hepatic and renal function in humans and experimental animals (Maguire *et al.*, 1988; Sawyer *et al.*, 1971; Doursout and Chelly, 1988; Kenna and Jones, 1995; Liu *et al.*, 1993; Brown, 1972; LaBella and Queen, 1992; Watkins and Klassen, 1986). Although methoxyflurane is the most rapidly and extensively metabolized inhalation anesthetic in both humans and experimental animals, it appears to have the least effect on liver histology and function (Cale *et al.*, 1962). In certain rare cases, however, it has been linked to hepatotoxicity caused by bioactivation to an unidentified toxic metabolite(s). This anesthetic has repeatedly been reported to be nephrotoxic in rats, leading to dose dependent renal function impairment, which has been directly related to inorganic

fluoride levels in serum. Furthermore, methoxyflurane surgical plane anesthesia has been shown to decrease cardiac output by as much as 39 % in Hormel miniature swine (Sawyer *et al.*, 1971), although it is generally recognized that the cardiovascular effects are species specific and subject to experimental design, and are therefore very difficult to predict.

In this experimental design neither the Cl_r of ^{125}I-IAZA in group 1 nor the metabolic profiles in the two treatment groups have been fully investigated. It is difficult, therefore, to state conclusively if, and to what extent, any of the metabolic pathways were affected, or to what extent perfusion changes to liver and kidneys were responsible for the three-fold decrease in ^{125}I-IAZA Cl_{TB} in the anesthetized animals.

However, based on the data from group 2 rats, ^{125}I-IAZA has a high average Cl_{TB} of 18.2 mL/min in a 500 g rat, with Cl_r contributing about 4.9 mL/min and metabolic Cl_{nr} constituting the remaining 13.3 mL/min. Assuming that the hepatic artery and portal vein together deliver about 14 % of the cardiac output to the liver [11.8 mL/min/250 g rat (Bernareggi and Rowlad, 1991)], and assuming that the cardiac output of a 500 g Sprague-Dawley rat is approximately 130 mL/min [range: 95.8 mL/min for 250 g rat (Bernareggi and Rowlad, 1991; Kawai *et al.*, 1994) to 150 mL/min for 641 g rat (Le Blanc and Rakusan, 1987)], then liver perfusion (Q) and the liver extraction ratio ($E = Cl_{nr} \div Q$), will be 16 mL/min and 0.83, respectively. This makes ^{125}I-IAZA a high extraction drug, which will be much more sensitive to changes in Q than to changes in intrinsic clearance (Cl_{int}) or the free fraction (f) in blood. Consequently, decreased perfusion to both the liver and the kidneys is most likely responsible for the dramatic decrease in the observed clearance of ^{125}I-IAZA.

Since group 2 animals each received a 3.75 times lower chemical dose of IAZA than group 1, Michaelis-Menten type dose-dependent kinetics must be addressed as a potential alternative explanation for the observed decrease in Cl_{TB} of the anesthetized animals. Currently, there is no evidence that ^{125}I-IAZA metabolism is saturable in any of the animal species studied, and in humans linear kinetics of ^{125}I-IAZA have been shown in the clinically studied dose range of 0.1 to 10 mg for a 70 kg normal adult (Stypinski *et al.*, 1997submitted). Furthermore, since ^{125}I-IAZA is a high E drug administered to the rats by i.v. injection, a 3.75 change in dose would not be expected to change the kinetic parameters as dramatically as was observed in this study. It is unlikely, therefore, that saturable metabolism alone would be responsible for the

dramatic decrease in clearance between the two groups studied, especially in view of the well documented evidence of the cardiovascular effects of anesthetics.

Another important observation was the lack of an apparent relationship between the blood profiles of ^{125}I-IAZA and total radioactivity in the recovered animals, as seen in Figure 5.2. In group 2, ^{125}I-IAZA had a much faster elimination phase than did total radioactivity, indicating formation of some poorly eliminated metabolites. The cumulative profile of radioactive metabolites in Figure 5.3 (B) shows that in the terminal phase, the total radioactivity concentration is determined by these metabolites and not by ^{125}I-IAZA. Consequently, total radioactivity kinetic parameters cannot possibly serve as indicators of ^{125}I-IAZA kinetics.

It is interesting to note, therefore, the excellent correlation between total radioactivity and ^{125}I-IAZA kinetics in the anesthetized animals. Since the plots of ^{125}I-IAZA and total radioactivity are parallel, Figure 5.3 (A) shows that only very little amounts of metabolite(s) are being formed and accumulation is not as apparent as in Figure 5.3 (B). Under these experimental conditions (group 1) it is ^{125}I-IAZA which determines the total radioactivity pharmacokinetics, and consequently, total radioactivity parameters are a very good indicator of ^{125}I-IAZA kinetics under methoxyflurane anesthesia.

It is perhaps coincidental that ^{125}I-IAZA kinetic parameters under anesthesia, with the exception of distribution phase, do not show any statistically significant differences from those of total radioactivity in recovered animals. The alpha phase contributes only 3.3 % to the total $AUC_{0-\infty}$, and is therefore very easy to miss if not enough samples are taken within the first ten minutes of dose administration. If only total radioactivity gamma counting of biological samples were used to assess the impact of anesthesia on ^{125}I-IAZA kinetics, the very small observable difference between total radioactivity profiles of the two treatment groups could easily be missed, leading to the erroneous conclusion that ^{125}I-IAZA is unaffected by the use of anesthesia in the imaging procedure.

The statistically significant (t-test $p < 0.05$) increase in the $t_{1/2\alpha}$ of total radioactivity in group 2 animals may be partially attributed to the increased formation rate of the radioactive metabolic species. Since total radioactivity is the sum of ^{125}I-IAZA and all of its radioactive metabolites in blood, the alpha phase of total radioactivity is not a true distribution phase. It consists of at least three distinguishable characteristics: (a) distribution and (b) elimination of ^{125}I-IAZA, both of which cause the slope of total

radioactivity alpha phase to be negative, and (c) formation of radioactive metabolic species, which will act on the slope in the opposite (positive) direction. However, this interpretation must be made cautiously, since there is a large range of values in the distribution phase of ^{125}I-IAZA in group 2 animals, and, furthermore, the two groups represent small samples.

In addition to the differences in the blood kinetic parameters of ^{125}I-IAZA in anesthetized and non-anesthetized animals there are interesting interspecies differences in the organs which accumulate radioactivity following ^{125}I-IAZA administration. Mannan (1991) has shown that in normal mice, 4 h after dose administration the stomach accumulated the most radioactivity, followed by the liver, carcass and the kidney. The spleen was one of the organs which accumulated the least radioactivity from all the tissues. In group 2 rats the kidney appeared to accumulate the most activity on an average DPM/g basis, followed by the stomach, spleen and the liver. Although there was some accumulation of activity in the thyroid gland, at five hours post injection it accounted for only 0.04 % of total radioactive dose, and, therefore, eight times less than the four hour thyroid uptake in the BALB/c EMT-6 tumor bearing mice.

These results show that the PK of ^{125}I-IAZA are both species specific and subject to experimental design. While the use of methoxyflurane anesthesia did not affect tracer kinetics in Sprague-Dawley rats, the clearance of ^{125}I-IAZA was almost 3.5 times lower in the anesthetized animals than in the non-anesthetized group. The ultimate consequence could be a positive diagnosis resulting from ^{125}I-IAZA accumulation, indicating hypoxia in a region of an anesthetized animal that would not normally accumulate ^{125}I-IAZA to such extent if the animal were not anesthetized. The difference would be due to the much slower metabolism of ^{125}I-IAZA, leading to its longer residence time in the blood.

5.5 References

Archer CM, Edwards B, Kelly JD, King AC, Burke JF, Riley ALM. Technetium labelled agents for imaging tissue hypoxia *in vivo*. In: Technetium and rhenium in chemistry and nuclear medicine. Nicolini M, Bandoli G, Mazzi U (editors). Ditoriali (Italy): Padova SGE; 1995. pp. 535-45.

Bernareggi A, Rowlad M. Physiologic modeling of cyclosporin kinetics in rat and man. J Pharmacokinet Biopharm 1991;19:21-50.

Brown BR. Effects of inhalation anesthetics on hepatic glucuronide conjugation: a study of the rat *in vitro*. Anesthesiology 1972;37:483-8.

Caldwell JH, Revenaugh JR, Martin GV, Johnson PM, Rasey JS, Krohn KA. Comparison of flourine-18-fluorodeoxyglucose and tritiated fluoromisonidazole uptake during low-flow ischemia. J Nucl Med 1995;36:1633-8.

Cale JO, Parks CR, Jenkins MT. Hepatic and renal effects of methoxyflurane in dogs. Anesthesiology 1962;23:248-50.

DiRocco RJ, Kuczynski BL, Pirro JP, Bauer A, Linder KE, Ramalingam K, Cyr JE, Chan YW, Raju N, Narra RK, Nowotnik DP, Nunn AD. Imaging ischemic tissue at risk of infarction during stroke. J Cereb Blood Flow Metab 1993;13:755-62.

Doursout MF, Chelly JE. Effects of basal anaesthesia on cardiac function. Br J Anaesth 1988;60:119S-22S.

Ichimura F, Yokogawa K, Yamana T, Tsuji A, Yamamoto K, Murakami S, Mizukami Y. Physiological pharmacokinetic model for distribution and elimination of pentazocine.II. Study in rabbits and scale-up to man. International Journal of Pharmaceutics 1984;19:75-88.

Kawai R, Lemaire M, Steimer JL, Bruelisauer A, Niederberger W, Rowland M. Physiologically based pharmacokinetic study on a cyclosporin derivative, SDZ IMM 125. J Pharmacokinet Biopharm 1994;22:327-65.

Kenna JG, Jones RM. The organ toxicity of inhaled anesthetics. Anesth Analg 1995;81:S51-S66.

LaBella FS, Queen G. General anesthetics inhibit cytochrome P450 monooxygenases and arachidonic acid metabolism. Can J Physiol Pharmacol 1992;71:48-53.

Le Blanc PR, Rakusan K. Effects of age and isoproternol on the cardiac output and regional blood flow in the rat. Can J Cardiol 1987;3:246-50.

Liu PT, Ioannides C, Shavila J, Symons AM, Parke DV. Effects of ether anaesthesia and fasting on various cytochromes P450 of rat liver and kidney. Biochem Pharmacol 1993;45:871-7.

Maguire TA, Swanton JG, Temple DJ. *In situ* liver perfusion techniques: the significance of the anaesthetic procedure used. Eur J Drug Metab Pharmacokinet 1988;13:35-40.

Mannan RH. Novel non-invasive markers of tumor hypoxia. Edmonton, Alberta, Canada: *PhD. Thesis*, University of Alberta; 1991.

Mannan RH, Somayaji VV, Lee J, Mercer JR, Chapman JD, Wiebe LI. Radioiodinated 1-(5-iodo-5-deoxy-β-D-arabinofuranosyl) -2-nitroimidazole (iodoazomycin arabinoside: IAZA), a novel marker of tissue hypoxia. J Nucl Med 1991;32:1764-70.

Martin GV, Biskupiak JE, Caldwell JH, Rasey JS, Krohn KA. Characterization of iodovinylmisonidazole as a marker for myocardial hypoxia. J Nucl Med 1993;34:918-24.

Martin GV, Caldwell JH, Graham MM, Grierson JR, Kroll K, Cowan MJ, Lewellen TK, Rasey JS, Casciari JJ, Krohn KA. Noninvasive detection of hypoxic myocardium using fluorine-18-fluoromisonidazole and positron emission tomography. J Nucl Med 1992;33:2202-8.

Martin GV, Caldwell JH, Rasey JS, Grunbaum Z, Cerqueira M, Krohn KA. Enhanced binding of the hypoxic cell marker [3H]Fluoromisonidazole in ischemic myocardium. J Nucl Med 1989;30:194-201.

McEwan AJB, Skeith KJ, Mannan RH, Davies N, Jamali F, Wiebe LI. Hypoxia-targeted ^{123}I-iodoazomycin arabinoside imaging of the adjuvant arthritis in rat model. CANM Annual Scientific Meeting1996; Quebec City, PQ.

Moore RB, Chapman JD, Mercer JR, Mannan RH, Wiebe LI, McEwan AJ, McPhee MC. Measurement of PDT-induced hypoxia in Dunning prostate tumors by iodine-123-iodoazomycin arabinoside. J Nucl Med 1993;34(3):405-10.

Ngo LY, Tam YK, Coutts RT. Lack of residual effects on diethyl ether, methoxyflurane, and sodium pentobarbital on lidocaine metabolism in a single-pass isolated rat liver perfusion system. Drug Metabolism and Disposition 1995;23:525-8.

Rasey JS, Koh W-J, Grierson JJ, Grunbaum Z, Krohn KA. Radiolabelled fluoromisonidazole as an imaging agent for tumor hypoxia. Int J Radiat Oncol Biol Phys 1989;17:985-91.

Rumsey WL, Kuczynski B, Patel B, Bauer A, Narra RK, Eaton SM, Nunn AD, Strauss HW. SPECT imaging of ischemic myocardium using a Technetium-99m-nitroimidazole ligand. J Nucl Med 1995;36:1445-50.

Sawyer DC, Lumb WV, Stone HL. Cardiovascular effects of halothane, methoxyflurane, pentobarbital and thiamylal. J Appl Physiol 1971;30:36-43.

Shi CQX, Sinusas AJ, Dione DP, Singer MJ, Young LH, Heller EN, Rinker BD, Wackers FJT, Zaret BL. Technetium-99m-nitroimidazole (BMS181321): a positive imaging agent for detecting myocardial ischemia. J Nucl Med 1995;36:1078-86.

Stypinski D, Wiebe LI, McEwan AJ, Tam YK, Mercer JR. Radiopharmacokinetics of ^{123}I-IAZA in healthy volunteers. 1997(Submitted).

Stypinski D, Wiebe LI, Mercer JR. A rapid and simple assay to determine the blood and urine concentration of 1-(5-[$^{123/125}$I]iodo-5- deoxyarabinofuranosyl)-2-nitroimidazole, a marker of tissue hypoxia. Journal of Pharmaceutical and Biomedical Analysis 1997(in Press).

Trevor AJ, Miller RD. General anesthetics. In: Basic and clinical pharmacology. Katzung BG (editor). 4th ed. San Mateo, CA: Appleton & Lange; 1989. pp. 304-14.

Watkins JB, Klassen CD. Chemically-induced alteration of UDP-glucuronic acid concentration in rat liver. Drug Metabolism and Disposition 1986;35:4139-52.

Wiebe LI, Stypinski D. Pharmacokinetics of SPECT radiopharmaceuticals for imaging hypoxic tissues. Quarterly Journal of Nuclear Medicine 1996;40:270-84.

Yang DJ, Wallace S, Cherif A, Li C, Gretzer MB, Kim EE, Podoloff DD. Development of F-18-labeled fluoroerythronitroimidazole as a PET agent for imaging tumor hypoxia. Radiology 1995;194:795-800.

6. *Pharmacokinetics of ^{123}I-IAZA in Healthy Subjects*[3]

6.1 Introduction

The pharmacokinetics of a radiopharmaceutical (radiopharmacokinetics) present an additional consideration to classical pharmacokinetics, in that the first order physical decay of the radioisotope is superimposed on the physiological elimination of the compound. For isotopes commonly used in diagnostic nuclear medicine, such as ^{123}I (physical decay half-life, t_{sp}= 13.2 h), ^{99m}Tc (t_{sp}= 6 h) or ^{18}F (t_{sp}= 110 min), t_{sp} will contribute significantly to calculated pharmacokinetic parameters. Furthermore, if sample radiometry does not include isolation of each radioactive species (e.g. parent compound, chemical degradation products and metabolites), and results are expressed in terms of total radioactivity in blood or plasma, then only bulk tracer kinetics are determined. Although useful in determining the effective half-life of total radioactivity, and, hence, in predicting the radiation dose to the patient, these studies cannot be used to determine any other kinetic parameters (Gibaldi and Perrier, 1982). Unfortunately the distinctions between tracer kinetics and pharmacokinetics have not always been taken into consideration with radiopharmaceuticals, and these terms have often been used interchangeably even in specific areas such as predicting the kinetics of a radiopharmaceutical in the effect compartment (Casciari *et al.*, 1995).

The hypoxia marker ^{123}I-IAZA has already been used in over 100 patients, but to date only its tracer kinetics have been studied and reported (Parliament *et al.*, 1992; Urtasun *et al.*, 1996). In addition, the pre-clinical kinetic data comes from tracer kinetics studies in mice (Mercer *et al.*, 1990; Mannan, 1991; Mannan *et al.*, 1991).

The present report is the first of its kind in the area of hypoxia markers, in that it discusses both the tracer kinetics and the pharmacokinetics of ^{123}I-IAZA in healthy volunteers. The pharmacokinetic parameters of unlabeled IAZA, without the superimposed first order physical decay, are also presented. In addition, the tracer kinetic parameters uncorrected for physical decay are presented, as they provide information on the trends in the biological elimination of radioactivity from the patient's

---

[3] A version of this chapter has been submitted for publication: Stypinski D, Wiebe LI, McEwan AJ, Tam YK, Mercer JR. 1997(submitted).

body. Finally, the tracer kinetics of radioactive metabolites of ^{123}I-IAZA will be discussed.

6.2 Experimental

6.2.1 Chemicals and reagents

IAZA was synthesized by Dr. Elena Atrazheva at the Faculty of Pharmacy and Pharmaceutical Sciences, University of Alberta, and radiolabelled by Mr. Ron Schmidt at the Cross Cancer Institute in Edmonton, using published procedures (Mannan, 1991; Mannan *et al.*, 1991).

6.2.2 Clinical protocol

The research project was conducted in accordance with the tenets of the Declaration of Helsinki (1964) and was approved by the Alberta Cancer Board research ethics committee, and by the University of Alberta radiation safety committee. Six healthy volunteers (Table 6.1), four males and two females aged 26 to 54, participated with informed consent. The exclusion criteria were:

1. Females of childbearing potential
2. History of hepatitis B
3. History of hepatitis C
4. HIV
5. Chronic liver disease
6. Acute renal disease
7. Diabetes Mellitus
8. Cancer

Prior to the study, blood was drawn for hematology and for hepatic and renal function tests. At the time of injection each volunteer was given an oral dose of 0.6 mL of Lugol's solution (USP) in orange juice to block thyroid uptake of free radioiodide.

Each subject received a nominal 5 mCi dose of ^{123}I-IAZA, with the actual chemical dose of IAZA varying among the volunteers (Table 6.1). The routine clinical dose is 1 mg per 70 kg person. The dose was administered as a slow (1-3 min) i.v. injection in the arm. Venous blood samples (9 mL) were drawn from an indwelling catheter in the contralateral arm into SST Vacutainer® tubes containing 30 μg of non-radiolabelled IAZA dissolved in 250 μL of sterile normal saline at 1, 5, 15, 30, 45 min and 1, 2, 4, 6,

8, 12, 22, and 28 h post injection. After allowing the blood in the tubes to clot at room temperature for 30 min they were refrigerated prior to analysis. The volunteers collected urine in clean plastic containers for 28 h after injection. The volumes (and pH for urine) of all specimens were recorded. Urine samples were refrigerated throughout the collection period and until analysis. Both blood and urine samples were analyzed using a radiometric/HPLC assay described in Chapter 4 of this thesis and in Stypinski *et al.* (1997in press). In addition, anterior and posterior whole body images at five different time periods post injection were also acquired for each volunteer; these will be reported in Chapter 7 as part of the human radiation dosimetry of ^{123}I-IAZA.

Volunteer #	Sex	Age (years)	Weight (kg)	Height (cm)	Surface area (m^2)	IAZA dose (mg)
1	M	28	86	183	2.09	0.87
2	M	32	95	164	2.01	0.10
3	M	26	75	186	1.98	0.19
4	F	54	73	170	1.83	0.83
5	M	27	85	178	2.03	0.91
6	F	53	68	168	1.77	1.2
Mean ± SD		37 ± 13	80 ± 10	175 ± 9.0	1.95 ± 0.12	0.68 ± 0.44

Table 6.1 Volunteer demographics and doses for ^{123}I-IAZA study at rest.

6.2.3 Pharmacokinetic analysis

Blood clearance profiles for ^{123}I-IAZA and total radioactivity were analyzed using WinNonlin version 1.1 (Scientific Consulting, Inc.). Data for each volunteer were fitted both as (1) experimental at the time of sample collection (^{123}I-IAZA kinetics) and (2) decay corrected to injection time (IAZA kinetics). Only ^{123}I-IAZA was measured directly in blood by the radiometric assay; IAZA concentration in a sample was determined by decay-corrected extrapolation of ^{123}I-IAZA concentration. Interpretation of the kinetic parameters of IAZA was based on the assumption that the kinetics of ^{123}I-IAZA are linear and that there is no difference in the biologic fate of radiolabelled and unlabelled IAZA. Both compartmental and noncompartmental analyses were performed. The choice of model was based on observed and calculated correlation function values, AIC and SC measures, and linearity of the partial derivatives plots. Compartmental analysis used the iteratively reweighted least squares weighing option.

The kinetic parameters of iodinated metabolites were obtained by subtracting the decay corrected plot of IAZA from that of total radioactivity decay corrected to injection time. These data were analyzed using a one compartment open model (WinNonlin v 1.1) with uniformly weighed concentrations. Radioactive metabolite kinetics were determined by superimposing the first order physical decay of ^{123}I isotope on the formation and elimination half-lives of the iodinated metabolites.

For the calculation of the zero (AUC) and first (AUMC) statistical moments, the linear trapezoidal rule was used, with extrapolation to infinite time using the terminal phase half-life. The renal clearance (Cl_r) of IAZA was calculated from the urine samples by standard pharmacokinetic methods assuming first order elimination (Gibaldi and Perrier, 1982). Systemic clearance (Cl_{TB}) for IAZA is defined as the sum of Cl_r and nonrenal biologic (metabolic) clearance (Cl_{nr}), while for ^{123}I-IAZA Cl_{TB} is defined as the sum of Cl_r, Cl_{nr} and clearance due to physical decay of ^{123}I (Cl_p). Both Cl_{TB} of ^{123}I-IAZA and Cl_{TB} of unlabelled IAZA are determined from their respective concentration *vs.* time plots using the formula

$$Cl_{TB} = \frac{Dose}{AUC} \qquad (6.1)$$

Cl_p was calculated as the difference between Cl_{TB} of unlabelled IAZA and Cl_{TB} of ^{123}I-IAZA. All data are reported as arithmetic mean ± standard deviation (SD).

6.3 Results

6.3.1 Blood clearance of ^{123}I-IAZA and total radioactivity

The pharmacokinetic parameters of ^{123}I-IAZA and total radioactivity after ^{123}I-IAZA i.v. administration are summarized in Table 6.2. The actual blood concentration values of each volunteer are given in Tables 11.5 and 11.6 of Appendix 2. The blood concentrations of both ^{123}I-IAZA and of total radioactivity declined rapidly in a biexponential fashion for all volunteers except volunteer # 6, in whom the distribution phase was not observed (Figure 6.1). In all others, the distribution phase was rapid, with $t_{1/2\alpha}$ of 5.34 ± 4.25 min and only a very small contribution (0.84 - 12.7 %) to the overall AUC. This large variation in the $t_{1/2\alpha}$ values reported was largely due to

mechanical problems with early blood sample collection in the volunteers. The actual blood sample collection times are reported in Table 11.4 of Appendix 2. The terminal $t_{1/2\beta}$ of ^{123}I-IAZA varied from 150 to 214 min in individual subjects. The steady state volume of distribution (V_{ss}) was 71.6 ± 9.5 % of total body weight (TBW), and, based on TBW to ideal body weight ratio for the volunteers, was relatively insensitive to body mass composition. The observed AUC for ^{123}I-IAZA ranged from 99.0 % (Volunteer # 2) to 99.8 % (Volunteer # 6) of the predicted AUC extrapolated to infinity.

^{123}I-IAZA and total radioactivity had practically identical distribution phases, but, as shown in Table 6.2, the elimination phase half-life of total radioactivity was significantly longer (294 ± 30 min) than that of ^{123}I-IAZA (179 ± 27 min). The observed total radioactivity AUC ranged from 96.7 % to 97.9 % of the predicted AUC extrapolated to infinity.

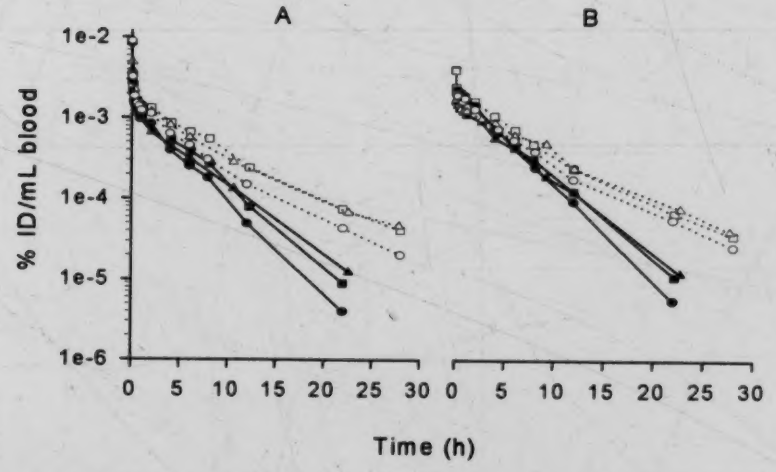

Figure 6.1 Concentration-time profiles of ^{123}I-IAZA (solid symbols) and total radioactivity (open symbols) for volunteers 1-3 (A) and 4-6 (B) following an i.v. dose of ^{123}I-IAZA. Data are not decay corrected (i.e. effective parameters).

6.3.2 Blood clearance of IAZA and total radioactivity corrected for physical decay

Since the choice of radioactive label changes the kinetic parameters of the imaging agent, the pharmacokinetics of unlabelled IAZA were also determined as they are independent of the choice of the radiolabel. The short distribution half-life was not significantly influenced by the correction for physical decay of ^{123}I isotope. The terminal $t_{1/2\beta}$ was more affected, and ranged from 185 to 294 min (Table 6.3). The elimination profile of IAZA was again biexponential for all volunteers except for volunteer # 6, for whom it was essentially monoexponential. Other pharmacokinetic parameters, such as Cl_{TB} and V_{ss} are reported in Table 6.3. The kinetic parameters for total radioactivity, corrected for physical decay of ^{123}I, are also found in Table 6.3.

	^{123}I-IAZA					Total Radioactivity				
V #	$t_{1/2\alpha}$ (min)[a]	$t_{1/2\beta}$ (min)[a]	V_{ss} (L/kg)[a]	Cl_{TB} (mL/min)[a]	Cl_r (mL/min)[a]	$t_{1/2\alpha}$ (min)[b]	$t_{1/2\beta}$ (min)[b]	V_{ss} (L/kg)[b]	Cl_{TB} (mL/min)[b]	Cl_r (mL/min)[b]
1	4.4	183	0.760	257	33	4.7	308	0.707	140	82
2	11	214	0.787	280	33	8.0	324	0.652	142	74
3	2.0	150	0.763	294	32[c]	2.0	264	0.839	173	76[c]
4	0.93	173	0.572	173	27	1.3	277	0.639	119	72
5	8.5	197	0.770	233	24	6.9	322	0.808	150	83
6	--[d]	156	0.641	194	22	--[d]	266	0.829	147	96
Mean	5.3	179	0.716	239	29	4.6	294	0.746	145	80
± SD	± 4.2	± 24	± 0.088	± 48	± 4.9	± 2.9	± 27	± 0.091	± 17	± 9.0

[a] Coefficient of variation (%) for each parameter is: $t_{1/2\alpha}$ (range = 11-141, mean = 47); $t_{1/2\beta}$ (range = 1.2-3.2 , mean = 2.0); V_{ss} (range = 2.5-4.5, mean = 3.5); Cl_{TB} (range = 1.8-3.1, mean = 2.5).
[b] Coefficient of variation (%) for each parameter is: $t_{1/2\alpha}$ (range = 25-99 , mean = 49); $t_{1/2\beta}$ (range = 2.3-4.0, mean = 3.3); V_{ss} (range = 3.5-7.0, mean = 5.4); Cl_{TB} (range = 2.6-5.4, mean = 4.1).
[c] Incomplete urine collection for V # 3 (last sample not collected).
[d] Distribution phase not determined.

Table 6.2 Effective pharmacokinetic parameters of ^{123}I-IAZA and total radioactivity in healthy human volunteers after i.v. administration of ^{123}I-IAZA.

	IAZA					Total Radioactivity				
V #	$t_{1/2\alpha}$ (min) [a]	$t_{1/2\beta}$ (min) [a]	V_{ss} (L/kg) [a]	Cl_{TB} (mL/ min) [a]	Cl_r (mL/ min) [a]	$t_{1/2\alpha}$ (min) [b]	$t_{1/2\beta}$ (min) [b]	V_{ss} (L/kg) [b]	Cl_{TB} (mL/ min) [b]	Cl_r (mL/ min) [b]
1	4.4	238	0.858	200	33	4.6	508	0.802	86	82
2	11	294	1.344	211	33	8.3	546	1.085	87	74
3	2.0	185	0.743	243	32 [c]	2.0	397	0.807	118	76 [c]
4	0.93	221	0.697	137	27	1.3	426	0.772	77	72
5	9.0	261	0.904	176	24	9.4	546	0.977	91	83
6	-- [d]	194	0.729	156	22	-- [d]	395	0.937	99	96
Mean ± SD	5.5 ± 4.4	232 ± 41	0.879 ± 0.241	187 ± 39	29 ± 4.9	5.1 ± 3.6	471 ± 72	0.897 ± 0.124	93 ± 14	80 ± 9.0

[a] Coefficient of variation (%) for each parameter is: $t_{1/2\alpha}$ (range = 11-135, mean = 46); $t_{1/2\beta}$ (range = 1.5-3.9, mean = 2.5); V_{ss} (range = 2.5-4.5, mean = 3.5); Cl_{TB} (range = 1.9-3.1, mean = 2.5).
[b] Coefficient of variation (%) for each parameter is: $t_{1/2\alpha}$ (range = 25-77, mean = 44); $t_{1/2\beta}$ (range = 3.7-6.4, mean = 5.1); V_{ss} (range = 3.5-6.9, mean = 5.5); Cl_{TB} (range = 2.6-5.6, mean = 4.2).
[c] Incomplete urine collection for V # 3 (last sample not collected).
[d] Distribution phase not determined.

Table 6.3 Decay corrected biologic pharmacokinetic parameters of IAZA and total radioactivity in healthy human volunteers after i.v. administration of ^{123}I-IAZA.

6.3.3 Total body clearance of ^{123}I-IAZA and total radioactivity

The decay corrected clearance values for IAZA and total radioactivity, and the effective clearance values for ^{123}I-IAZA and total radioactivity, are reported in Tables 6.3 and 6.2, respectively. Cl_{TB} of ^{123}I-IAZA in blood was 239 ± 53 mL/min, while for IAZA it was 187 ± 43 mL/min. Biological elimination of the parent drug constituted 15.5 % eliminated intact in the urine and the remaining 84.5 % metabolized. Since Cl_r is a physiological process not influence by physical decay of the isotope, Cl_r is the same for ^{123}I-IAZA and IAZA. During the residence of the radiolabelled drug in the body 22 % of the dose underwent physical decay.

More than 92 % of total radioactivity was eliminated in urine within 28 hours. Of the remaining 8 %, 3 % was still distributed in tissues at 28 h while 5 % was localized in the large intestine, as determined by scintigraphic imaging. During its residence in the

body, 37 % of total radioactivity was eliminated by physical decay of ^{123}I to ^{123}Te. Consequently, the effective Cl_{TB} of total radioactivity was 239 ± 53 mL/min, while its biological Cl_{TB} was 187 ± 43 mL/min.

6.3.4 Disposition kinetics of radioiodinated metabolites of IAZA

By subtracting the $AUC_{0-\infty}$ of ^{123}I-IAZA from the $AUC_{0-\infty}$ of total radioactivity, it was estimated that 43 ± 9 % of total radioactivity $AUC_{0-\infty}$ was due to radioactive metabolites. Table 6.4 shows how the ^{123}I-IAZA fraction of blood radioactivity decreases with time. Within 15 min, 33 % of the radioactivity in blood will be in the form of radioactive metabolites. This accumulation of radioactive metabolites is due to their longer $t_{1/2\beta}$ and lower Cl_{TB} compared to ^{123}I-IAZA.

The plot of formation and elimination of radioiodinated metabolites, constructed using the values in Table 6.4, is shown in Figure 6.2. It is apparent from this plot that the iodine containing metabolites never actually reach the log-linear part of the elimination phase, although accumulation clearly does take place during the 28 hours of sample collection. A one compartment open model analysis with first order input function (WinNonlin v. 1.1) showed that the formation and elimination half-lives of the radioiodinated metabolites are practically identical, at 245 and 246 min, respectively, resulting in very large standard errors relative to the estimated values. The formation and elimination half-lives of the non-radiolabeled iodinated metabolites, calculated by subtraction of decay corrected IAZA from total radioactivity, were determined to be 345 and 346 min, respectively.

Time (h)	^{123}I-IAZA (%ID/mL)	Tot RA* (%ID/mL)	IAZA:Tot RA
0.08	3.74E-03	4.49E-03	0.832
0.25	1.68E-03	2.51E-03	0.670
0.50	1.46E-03	2.22E-03	0.658
0.75	1.38E-03	2.14E-03	0.644
1.00	1.30E-03	2.06E-03	0.629
2.00	1.02E-03	1.79E-03	0.573
4.00	6.38E-04	1.34E-03	0.475
6.00	3.98E-04	1.01E-03	0.394
8.00	2.48E-04	7.59E-04	0.326
10.00	1.55E-04	5.71E-04	0.271
12.00	9.63E-05	4.29E-04	0.224
22.00	9.06E-06	1.03E-04	0.088
28.00	2.19E-06	4.38E-05	0.050

*total radioactivity

Table 6.4 Relationship between mean values of ^{123}I-IAZA and total radioactivity dose fractions per mL of blood.

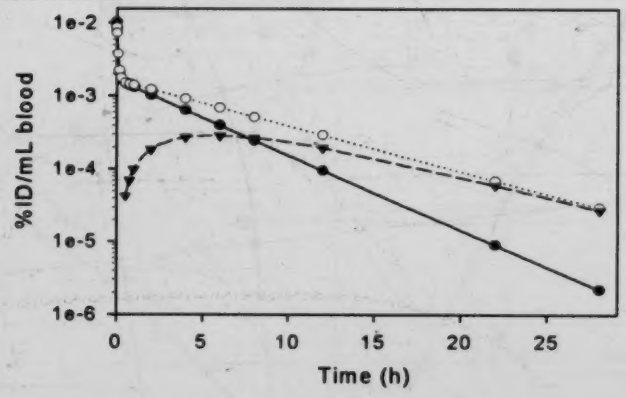

Figure 6.2 Plots of mean disposition of various radioactive components in human volunteers following ^{123}I-IAZA administration. Key: (O) total radioactivity; (●) ^{123}I-IAZA; (▼) radioactive metabolites.

6.3 Discussion

This is the first detailed report of the disposition of ^{123}I-IAZA in humans following preliminary clinical data on the distribution and clearance half-lives for total radioactivity (Parliament *et al.*, 1992). That study reported total radioactivity distribution and elimination phase half-lives of 22.9 ± 8.7 min and 588 ± 246 min, respectively. Differences between the data now reported (^{123}I-IAZA effective $t_{1/2\alpha}$ = 5.3 ± 4.2 min and $t_{1/2\beta}$ = 179 ± 24 min, total radioactivity effective $t_{1/2\alpha}$ = 4.6 ± 2.9 min and $t_{1/2\beta}$ = 294 ± 27 min) and the earlier data can be attributed to three factors. In the early report, i) ^{123}I data were decay corrected to injection time rather than to the actual radioactivity concentration at the time the samples were taken, ii) the terminal phase half-life was reported as an average in three patients, one of whom was renally compromised ($Cr_{Sr} \equiv$ 165 µmol/L) at the time of the study and had an elimination half-life twice as long as the other two patients, and iii) ^{123}I-IAZA was given as a 15 min infusion in the earlier report, however an i.v. bolus model was used in the analysis. When only the two patients with normal renal function in that study are modeled, the effective $t_{1/2\beta}$ of total radioactivity is 262 min (261 and 263 min, respectively), and, therefore, similar to the $t_{1/2\beta}$ of 294 ± 27 min reported in Table 6.2. In addition, the distribution half-lives in the same individuals, when recalculated using a two compartment open model and including a 15 min i.v. infusion, are 1.9 and 6.8 min, respectively, while the $t_{1/2\alpha}$ reported in Table 6.2 is 4.6 ± 2.9 min.

The question of dose-dependent kinetics for MISO (Ash *et al.*, 1979), and the *in vitro* concentration-dependent binding rates for ^{123}I-IAZA can now be addressed for ^{123}I-IAZA in humans. Parliament *et al.* (1992) used a 10 mg chemical dose of IAZA, whereas the dose used in this study ranged from 0.10 to 1.2 mg. After recalculation of the kinetic parameters for the earlier data, it is clear that IAZA has linear pharmacokinetics at least over the range of 0.1 to 10 mg per patient. Furthermore, the relatively small V_{ss} of 0.879 ± 0.241 L/kg for IAZA indicates that although the marker passes freely through biological membranes it undergoes minimal tissue binding.

The issue of decay correction in pharmacokinetic modeling of radiopharmaceuticals has recently been addressed by Williams *et al.* (1995). These authors have criticized the current practice of decay correcting data to injection time prior to pharmacokinetic modeling because of potential problems of non-linearity in kinetics and competition

between the labeled and unlabeled species. ^{123}I-IAZA, however, does not show non-linear kinetics and, since its mode of action does not depend on specific receptor interaction, it is improbable that competition between the labeled and unlabeled species exists *in vivo*. Consequently, the pharmacokinetics of IAZA can be predicted from ^{123}I-IAZA simply by correcting the experimental data for radioactive decay of ^{123}I from the moment of injection. Figure 6.3 illustrates the two plots, where the correction to injection time (open circles) represents IAZA, while the experimental data (solid circles) represents ^{123}I-IAZA. Thus the slope of the concentration curve for ^{123}I-IAZA is always steeper than that for IAZA, because of the overlaying physical decay of the isotope. Such a relationship cannot be determined for radiopharmaceuticals exhibiting non-linear kinetics.

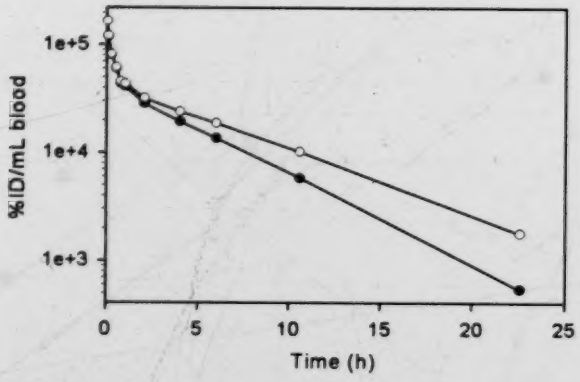

Figure 6.3 Representative concentration vs. time plot for ^{123}I-IAZA (●) and IAZA (O) (based on data from volunteer #2).

However, while only the radioiodinated pharmaceutical can be detected, and thus its parameters must enter all pharmacokinetic, pharmacodynamic or dosimetric modeling, it must be recognized that the fraction of the dose that is actually radioiodinated is very small. For a 5 mCi/1 mg dose only 0.00075 % of IAZA molecules will contain the ^{123}I label. Thus, during the residence of the dose in the body, only 22 % of the molecules in that 0.00075 % of total dose will physically decay to a tellurium labeled component. That particular route of elimination is not available to the reminder of the dose, labeled with the stable ^{127}I isotope. Therefore, the actual dose that the patient receives

consists of two components ^{123}I-IAZA (< 0.01 % of dose), the kinetic parameters of which are presented in Table 6.2 and IAZA (> 99.99 % of dose) the kinetic parameters of which are presented in Table 6.3. In addition, in Table 6.3, the decay corrected total radioactivity parameters represent cumulative kinetic parameters of IAZA and all of its iodinated metabolites.

Similarly, only a very small fraction of the iodinated metabolites will be radioactive. The biological processes involved in the formation of these metabolites are independent of the physical decay of ^{123}I. Under the conditions of linearity assumed and determined in this model, it is improbable that the radiolabeled components should have a different formation rate than the non-radiolabelled iodinated metabolites. In fact, both ^{127}I and ^{123}I labeled metabolites have the same biological formation rate and the same biological elimination rate. The reason for the 100 min shorter apparent formation and elimination half-lives of the radiolabeled metabolic components is that these are the "effective" kinetic parameters, and thus have the 13.2 h physical decay of the ^{123}I isotope superimposed on them.

The very large standard errors estimated during the determination of the metabolite formation and elimination rates stem from the lack of a definite terminal phase in the metabolite concentration *vs.* time plot until IAZA is virtually completely eliminated from the body. In addition, the similar formation and elimination rate constants make it impossible to distinguish from one another. However, initially every metabolic degradation of ^{123}I-IAZA or IAZA will involve the production of an iodinated metabolite, and, therefore, the physiological metabolic clearance of IAZA is actually the "formation clearance" of the iodinated metabolites. Since we know IAZA V_{ss}, Cl_r and its biologic Cl_{TB}, we can estimate the formation rate constant of the iodinated metabolites (β_{met}) using the relationship:

$$Cl_{nr} = Cl_{TB} - Cl_r = V_\beta \times \beta_{met} \qquad (6.2)$$

where Cl_{nr} is the metabolic clearance of IAZA. Based on this equation, the formation half-life of the iodinated metabolites is 322 min, which is within 93 % of the model predicted value of 345 min. Thus the model predicted elimination half-life of the iodinated metabolites can be accepted with similar confidence.

It has recently been suggested that ^{123}I-IAZA, although effective in identifying most hypoxic tumors, is not the "ideal marker" (Biskupiak and Krohn, 1993), because of its long elimination half-life (8-10 h), extensive hepatobiliary excretion leading to accumulation of activity in the lower gastrointestinal tract (GIT), lipophilicity leading to non-specific binding in blood and tissues, and de-iodination leading to thyroid uptake of free radioiodide (Schneider *et al.*,1995; Chapman *et al.*, 1996). Although no attempts were made to quantify the free ^{123}I in the blood or urine of the volunteers, the current elimination data indicate that the extent of de-iodination in man is similar to that reported earlier for a murine model (< 3%) (Mannan, 1991). In clinical practice, accumulation of ^{123}I in the thyroid gland of patients/volunteers does not preclude imaging head and neck tumors after thyroid blocking with Lugol's solution (Parliament *et al.*, 1992).

After accounting for the loss of total radioactivity due to radioactive decay of ^{123}I (37 % of dose), the recovery of 92 % of the remaining radioactive dose in urine within 28 h is conclusive evidence that urinary elimination is by far the principal route of elimination of total radioactivity from the body after ^{123}I-IAZA administration. Since about 97 % of the dose was cleared from the body during the same time, elimination into bile and non-specific retention in the lower GIT are clearly of minor importance.

The 3 h blood elimination $t_{1/2e}$ for ^{123}I-IAZA and the 5 h elimination $t_{1/2e}$ for total radioactivity support a change in imaging protocol to early imaging times after injection. Currently the clinical protocol calls for imaging at 20-24 h after injection, but counting statistics would be much better at 6-8 h after injection, due to the rapid decline of counts because of radioactive decay (13.2 h $t_{1/2p}$) at longer times. The effect of higher background on image resolution at these earlier imaging times would have to be determined.

6.4 References

Ash DV, Smith MR, Bugden RD. Distribution of misonidazole in human tumors and normal tissues. Br J Cancer 1979;39:503-9.

Biskupiak JE, Krohn KA. Second generation hypoxia imaging agents. J Nucl Med 1993;34:411-3.

Casciari JJ, Graham MM, Rasey JS. A modeling approach for quantifying tumor hypoxia with [F-18]fluoromisonidazole PET time-activity data. Med Phys 1995;22:1157-39.

Chapman JD, Coia LR, Stobbe CC, Engelhardt EL, Fenning MC, Schneider RF. Prediction of tumour hypoxia and radioresistance with nuclear medicine markers. Br J Cancer 1996;74(Suppl. 27):S204-S208.

Gibaldi M, Perrier D. Pharmacokinetics. 2nd ed. New York: Marcel Dekker, Inc.; 1982.

Mannan RH, Somayaji VV, Lee J, Mercer JR, Chapman JD, Wiebe LI. Radioiodinated 1-(5-iodo-5-deoxy-β-D-arabinofuranosyl) -2-nitroimidazole (iodoazomycin arabinoside: IAZA), a novel marker of tissue hypoxia. J Nucl Med 1991;32:1764-70.

Mannan RH. Novel non-invasive markers of tumor hypoxia. Edmonton, Alberta, Canada: *PhD. Thesis*, University of Alberta; 1991.

Mercer JR, Mannan RH, Somayaji V V, Lee J, Chapman JD, Wiebe LI. Sugar-coupled 2-nitroimidazoles: novel *in vivo* markers of hypoxic tumor tissue. In Advances in Radiopharmacology, proceedings of the Sixth International Symposium on Radiopharmacology, Maddelena DJ, Snowdon GM, Boniface GR, eds.1990; U Wollongong. Wollongong Writing Services (Australia), 104-113.

Parliament MB, Chapman JD, Urtasun RC, McEwan AJ, Golberg L, Mercer JR, Mannan RH, Wiebe LI. Non-invasive assessment of human tumour hypoxia with ^{123}I-iodoazomycin arabinoside: preliminary report of a clinical study. Br J Cancer 1992;65:90-5.

Schneider RF, Engelhardt EL, Stobbe CC, Brown DQ, Fenning MF, Chapman JD. Nuclear medicine markers of tumor hypoxia and radioresistance (Abstract). The Quarterly Journal of Nuclear Medicine 1995;39:41-2.

Stypinski D, Wiebe LI, Mercer JR. A rapid and simple assay to determine the blood and urine concentration of 1-(5-[$^{123/125}$I]iodo-5- deoxyarabinofuranosyl)-2-nitroimidazole, a marker of tissue hypoxia. Journal of Pharmaceutical and Biomedical Analysis 1997(in Press).

Urtasun RC, Parliament MB, McEwan AJ, Mercer JR, Mannan RH, Wiebe LI, Morin C, Chapman JD. Measurement of hypoxia in human tumours by non-invasive spect imaging of iodoazomycin arabinoside. Br J Cancer 1996;74 (Suppl. 27):S209-S212.

Williams LE, Odom-Maryon TL, Liu A, Chai A, Raubitschek AA, Wong JYC, D'Argenio DZ. On the correction for radioactive decay in pharmacokinetic modeling. Med Phys 1995;22:1619-26.

7. Radiation Dosimetry of ^{123}I-IAZA in Healthy Subjects

7.1 Introduction

Part of the legal requirements for licensure of new radiopharmaceuticals is submission of human dosimetry information. Dosimetry calculations attempt to predict the radiation dose which a patient receiving the radiopharmaceutical would absorb and the relative risk associated with this dose. The absorbed dose is influenced by numerous factors which are either known or must be determined for accurate characterization. These include: a) type of radiation (decay data); b) $t_{1/2p}$ of the isotope; c) amount of activity administered; d) tracer kinetics; e) target organs, specifically their mass, shape and location; and f) fraction of energy emitted by the source organ that is absorbed in the target organ.

Both the decay scheme and $t_{1/2p}$ are physical characteristics of an isotope. The radioactive dose is determined by the protocol goals. Fractional source-to-target energy transfer is determined by the patient's anatomy and the physical characteristics of the radionuclide. The organ-specific products of all these parameters, referred to as the S-values, have been tabulated and published for a variety of human phantoms and radioisotopes in MIRD Pamphlet No. 11 (Snyderet *at al.*, 1975) and are automatically provided by the computer program MIRDOSE® (Stabin, 1996). Thus, only the source organs, which are determined by the tracer's biodistribution, and their tracer kinetics are specific to the pharmaceutical and must be determined from the scintigraphic images prior to absorbed dose calculations.

^{123}I-IAZA is a novel marker of hypoxic cells *in vivo*. ^{123}I is a gamma emitter which decays with a 13.2 h $t_{1/2p}$ to ^{123}Te, according to the scheme shown in Figure 7.1. ^{123}I decays by electron capture with a principal gamma (83%) emitted with 159 keV of energy. Since gamma radiation is penetrating, each source organ will contribute to its own radiation dose and to the radiation doses of target organs other than itself.

The objective of this protocol was to determine ^{123}I-IAZA dosimetry in six healthy volunteers. Tracer kinetics for ^{123}I-IAZA have been described as part of the pharmacokinetic protocol in Chapter 6 of this thesis and in Stypinski *et al.* (1997submitted).

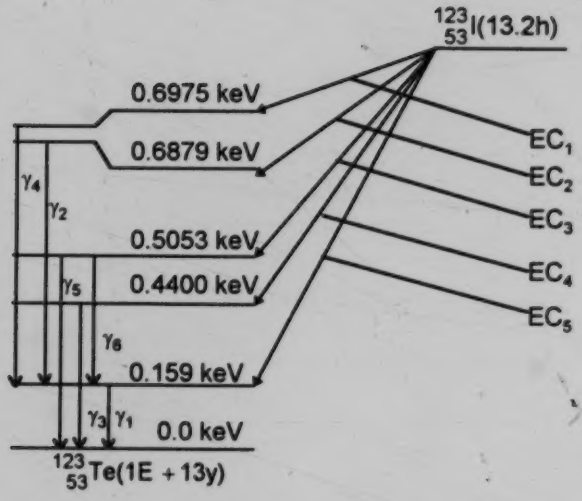

Figure 7.1 Decay scheme for ^{123}I (from: Weber DA, Eckerman KF, Dillman LT, Ryman JC. MIRD: Radionuclide Data and Decay Schemes., Society of Nuclear Medicine, 1989.)

7.2 Experimental

7.2.1 ^{123}I-IAZA Preparation

IAZA was synthesized by Dr. Elena Atrazheva at the Faculty of Pharmacy and Pharmaceutical Sciences, University of Alberta, and radiolabelled by Mr. Ron Schmidt at the Cross Cancer Institute in Edmonton, using published procedures (Mannan, 1991; Mannan *et al.*, 1991).

7.2.2 Clinical Protocol

The research project was conducted in accordance with the tenets of the Declaration of Helsinki (1964) and was approved the Alberta Cancer Board research ethics committee, and by the University of Alberta radiation safety committee. Six healthy volunteers, four males and two females, aged 26 to 54, participated with informed consent. Volunteer demographics are given in Table 6.1 of Section 6.2.2 of this thesis. At the time of injection each volunteer was given an oral dose of 0.6 mL of Lugol's solution (5%, USP) in orange juice to block the thyroid uptake of free radioiodide. Each

subject received a nominal 5 mCi dose of ^{123}I-IAZA administered as a slow (1-3 min) i.v. injection in the arm.

Anterior and posterior whole body images at five different time periods post injection were acquired in each volunteer beginning immediately after injection and at 1-2, 3-4, 6-8, 20-24 h post injection. The images were acquired using a dual-headed, large field of view gamma camera (Picker Odyssey 2000) equipped with a LEAP (low energy all purpose) collimator and interfaced to an Odyssey computer. The 20 % analysis window was set symmetrically over the 159 keV ^{123}I photopeak.

7.2.3 Region of Interest Selection Protocol

The scintigraphic images were exported to a PC equipped with an image analysis package, MEDisplay[4] v 1.32s, capable of automatically measuring the number of counts and pixels in each planar image. The following regions of interest (ROI) were drawn for each volunteer: liver, left kidney, large intestine, urinary bladder, thyroid, gall bladder and the whole body (WB). Since organ dimensions were not available background tissue activity was not corrected. An off-body region drawn to the right of the volunteer's head was used as instrumental background. In addition, several overlapping ROI were included: a region of overlap between the right kidney and liver, a region of left kidney with large intestine overlap, and a region of left kidney where there was no large intestine overlap. The ROI of right kidney and liver overlap was established by drawing two parallel lines through the patient body: one line passing the uppermost point of the left kidney and the other passing through the lowest point of the liver. The left kidney region between the two lines was drawn, flipped around its horizontal axis and dragged to the anatomical position of the right kidney, between the two lines. WB counts were determined by drawing the contours of the entire body of the patient as visible on the image.

All the ROI were drawn on both anterior and posterior images for each volunteer according to the following protocol:

1. First, the large intestine, the thyroid, background and the whole body were drawn on the 20-24 h images.
2. Second, the images in (1) were superimposed on the 3 - 4 h image, and the liver, and left kidney were drawn.

[4] T. Riauka, Copyright 1993.

3. All the ROI were then transposed on the 1 - 2 h image, and the gall bladder was drawn.
4. The ROI were again transposed on the 3 - 4 h image and all the overlap regions were added.
5. At that point, all the ROI were saved and applied to the analysis of each image, with bladder being the only ROI requiring redrawing for each imaging time.
6. For all of the ROI, the count contribution from the blood pool to the organ activity was included as part of the organ activity.

7.2.4 Source Organ Activity

Since no SPECT or CT images were available for the volunteers, assigning activity to organs with overlapping regions as viewed from a planar 2 dimensional image was done based on assumptions which were image-time dependent. The analyses were initially performed manually, and once the protocol was established all calculations were re-analyzed using Microsoft Excel v.7.0 for Windows 95. The calculations performed to determine the anterior and posterior organ counts, together with the assumptions required for these calculations, were as follows:

1: *Immediate, 1-2, 3-4, and 6-8 h images*

a) kidneys

i. only left kidney activity is determined directly from the images
ii. right kidney activity is assumed to be identical to the left kidney activity
iii. no lumen radioactivity in the large intestine
iv. no counts contributed from the large intestine to the region of left kidney and large intestine overlap
v. no overlap between left kidney and liver
vi. 75 % of right kidney area overlaps with liver
vii. both right and left kidney occupy the same horizontal plane
viii. no overlap correction to the left kidney ROI counts

b) liver

i. contributions to liver activity are: gall bladder, large intestine (transverse colon), and right kidney (75 % kidney area)
ii. liver activity was calculated as follows:

(1) gross liver counts per pixel corrected for kidney overlap = (liver counts - 0.75 × right kidney counts) ÷ no. of pixels in liver (7.1)

(2) liver/gall bladder count overlap = gall bladder counts - *(1)* × no. of pixels in gall bladder (7.2)

(3) net liver counts = *(1)* × no. of pixels in liver - *(2)* (7.3)

c) <u>gall bladder</u>

i. gall bladder ROI counts = gall bladder counts - no. of pixels in gall bladder × (net liver counts ÷ no. of pixels in liver) (7.4)

d) <u>large intestine</u>

i. large intestine ROI counts - [(no. of pixels from liver and large intestine overlap × liver net counts per pixel) + (no. of pixels from left kidney and large intestine overlap × left kidney counts) + right kidney overlap counts[5]] (7.5)

2. *20 - 24 h images*

a) <u>large intestine</u>

i. becomes the major source of activity in the abdominal region

ii. no overlap correction to ROI counts

b) <u>liver</u>

i. negligible contribution from kidney and gall bladder

ii. no overlap correction to ROI counts

c) <u>gall bladder</u>

i. negligible contribution (generally less than 1 count per pixel)

ii. calculated as: (gall bladder counts per pixel - liver counts per pixel) × no. of pixels in gall bladder (7.6)

d) <u>right and left kidney</u>

i. major source of overlap counts is the large intestine

ii. assumed that the large intestine counts per pixel contribution is homogeneous

iii. counts in each kidney calculated by subtracting large intestine activity contribution, as determined by the following equations:

[5] assumed to be 25 % of left kidney counts

(1) large intestine count per pixel contribution to the overlap region with kidney = [kidney/intestine overlap region count - (kidney/intestine overlap pixel number × large intestine count per pixel)] ÷ kidney/intestine overlap pixel number (7.7)

(2) counts in kidney = [*(1)* + counts per pixel in the portion of kidney ROI without kidney/liver overlap] × no. of pixels in the kidney ROI (7.8)

Once the posterior and anterior counts in each organ were determined using the above described steps, the counts were further corrected by subtracting instrumental background activity (as count per pixel) from the count per pixel organ activity. Finally, the geometric mean counts for each organ were calculated as:

$$(\text{anterior counts per pixel} \times \text{posterior counts per pixel})^{1/2} \times \text{ROI pixel no.} \quad (7.9)$$

No linear attenuation correction was made for the anterior and posterior tissues (i.e. bone, muscle, fat and skin) above or below the organ of interest.

7.2.5 Total Body and All Body Activity Determination

In order to determine the fractions of radioactivity entering the gut and the bladder, the dosimetry equations include two additional terms: total body (TB) and all body (AB). TB and AB counts were determined from the anterior and posterior images at each acquisition time. TB counts are defined as

$$\text{TB counts} = \text{WB counts} - (\text{GIT counts} + \text{Bladder counts}) \quad (7.10)$$

with the GIT counts consisting of the sum of the geometric mean of counts in the large intestine and the gall bladder. AB counts were determined according to the formula

$$\text{AB counts} = \text{WB counts} - \text{Bladder counts} \quad (7.11)$$

7.2.6 Organ Mean Residence Time Determination

Once the mean counts in an organ were determined for all five imaging times, the mean residence time (MRT) of the radioactivity in the organ was determined using the computer program LAGRAN v. 1.0 D (Eddis and Tam, 1995) by area under the curve integration of ROI count *vs.* time plot. The MRT was calculated for the following organs: large intestine, liver, kidney, thyroid, whole body, all body and total body. Since each image acquisition took 30 min it was assumed that the mean count in an organ corresponded to the mid-time of 15 min after the start of image acquisition. The only exception was the thyroid, for which it was assumed that the mean counts were acquired at 5 min from the image start.

The fractional MRT (MRT_{fr}) was calculated for liver, kidney and the thyroid by multiplying the organ MRT by the fraction of the maximum activity detected in it, according to the formula:

$$MRT_{fr} = \frac{\text{Organ count}_{(\text{immediate})}}{\text{Whole Body count}_{(\text{immediate})}} \times MRT \qquad (7.12)$$

7.2.7 Remainder of the Body Mean Residence Time

The three regions of interest: WB, TB and AB, all include the counts from liver, kidneys and the thyroid. In order to account for the activity in the body that is not in these organs, and has not been excreted into the bladder or the GIT, the remainder of the body (RB) was included as an additional source organ. The MRT_{fr} of this source organ was calculated as:

$$MRT_{fr(RB)} = MRT_{(TB)} - \left[MRT_{fr(liver)} + MRT_{fr(kidneys)} + MRT_{fr(thyroid)}\right] \qquad (7.13)$$

7.2.8 Renal and GIT Excretion Fractions

The fraction of the radioactive dose eliminated via the hepatobiliary system into the intestinal tract was determined from the gamma camera images by first calculating the rate of elimination of radioactivity into the gut (K_{gut}), according to the formula:

$$K_{gut} = \frac{1}{MRT_{(AB)}} - \frac{1}{MRT_{(TB)}} \quad (7.14)$$

Thus, the fraction of radioactive dose eliminated by the gut was determined by the ratio:

$$\text{fraction into gut} = K_{gut} \times MRT_{(TB)} \quad (7.15)$$

Since the only other biological route of excretion from the body available for a radiopharmaceutical is via kidneys, the fraction entering the bladder is

$$\text{fraction into bladder} = 1 - \text{fraction into gut} \quad (7.16)$$

7.2.9 Generation of Radiation Dose Estimates

Radiation dose estimates were performed for all volunteers using the MIRDOSE[6] v.3.1 program. The phantoms used were "reference adult" for the male volunteers and "adult female" for the female volunteers. The model used for analysis included a combination of both ICRP 30 GIT model and the dynamic bladder model (Stabin, 1996). Two sets of estimates were performed for each volunteer, one using a 2 h and one using a 4.8 h bladder void time.

7.3 Results and Discussion

7.3.1 Gamma Camera Imaging

Figure 7.2 shows the typical immediate and 22 h anterior and posterior gamma camera images of one of the volunteers (v # 3). On the earliest images the organs with the highest radioactivity accumulation were the bladder, liver and the kidneys. Some activity accumulation was also visible in the heart and, as it was no longer noticeable on the later images, probably originated from the blood pool. The site of i.v. injection into the right arm was also visible on the immediate images of this volunteer, but the percent of radioactive dose in that area, as determined from image analysis, was

[6] Copyright 1994, Oak Ridge Associated Universities

negligible (< 0.05% of dose) and was not expected to alter the distribution kinetics of the radiopharmaceutical. The injection site was also visible on the immediate images of volunteer # 5, but to a lesser extent.

There was a striking absence of radioactivity in the brains of all the volunteers, as evident on the immediate images, indicating effective exclusion of ^{123}I-IAZA by the blood brain barrier. Later images do show some redistribution of radioactivity into the brain. Immediate, 1-2 h and 3-4 h images also do not show thyroid or large intestine uptake. In fact, these two ROI do not become readily visible until the 20-24 h image acquisition time (Figure 7.2).

During the determination of GIT counts only the large intestine and gall bladder counts were included. The reason for the omission of small intestine activity was that this organ was never clearly distinguishable in any of the images. Since the radioactivity entering the intestinal tract from the gall bladder constituted a small fraction of the dose (< 10 % of biologically eliminated activity), it was only visible when this activity either concentrated in a small area (i.e. in the gall bladder) or 20 h after dose administration, when a substantial portion of the dose was eliminated from the rest of the body. Some concentration of intestinal activity was already visible on the 6-8 h image, however, at this time it was either localized in the junction of the ileum and the ascending colon or already in the initial part of the ascending colon. In each case this activity was included as part of the large intestine ROI.

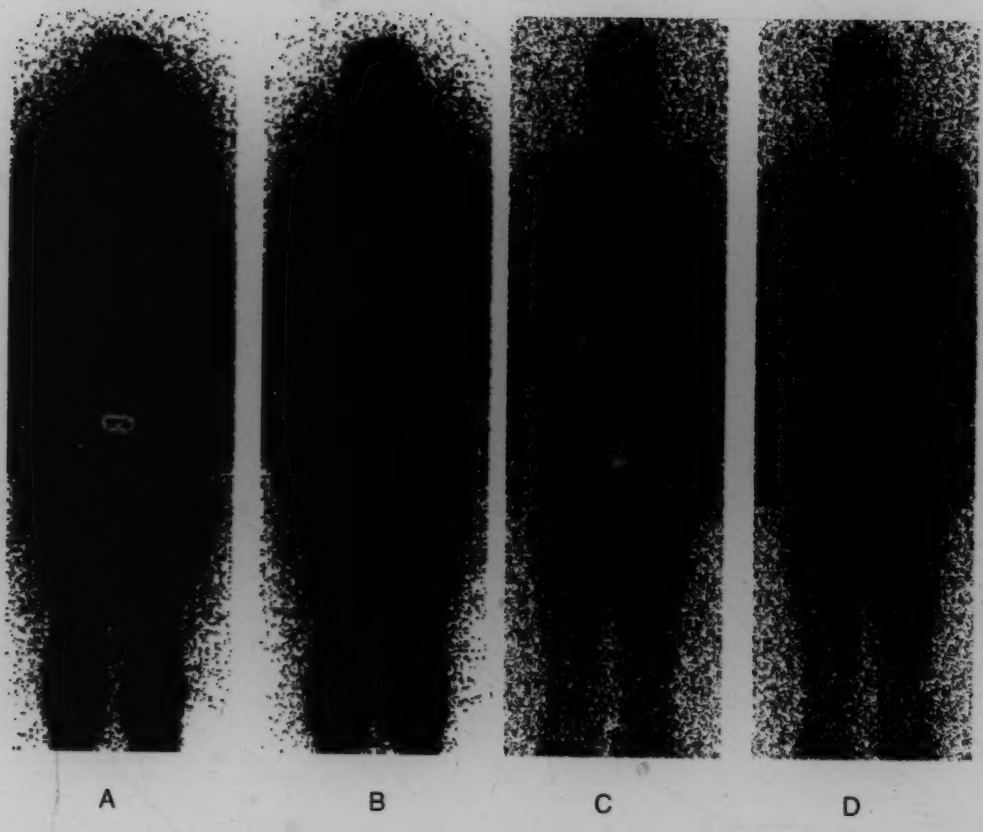

Figure 7.2 Typical immediate anterior (A) and posterior (B) view and 22 h anterior (C) and posterior (D) view images following ^{123}I-IAZA i.v. administration to a volunteer. These images were obtained from volunteer # 3 (27 year old male) following the administration of 5.62 mCi of ^{123}I-IAZA into the right arm.

7.3.2 Volunteer Dosimetry Results

A summary of radiation dose estimates for all volunteers for standard 2 h and 4.8 h bladder void times are shown in Table 7.1 and Table 7.2, respectively. The source organs were: liver, kidneys, thyroid and RB, and the activities in these organs were assumed to be uniformly distributed. The dose to each target organ is expressed in radiation absorbed dose units per mCi of administered activity (rad/mCi). Although the reference adult phantom used for dose estimates in males does predict rad/mCi dose

to the ovaries as well as testis, the adult female phantom does not predict the dose to the testis, and therefore, in both Table 7.1 and 7.2 the dose to the testis has not been entered (N/A) for volunteers # 4 and 6.

These results show that ^{123}I-IAZA appears to be safe with respect to radiation dose when administered in tracer amounts to the volunteers. The urinary bladder wall received the greatest radiation dose, followed by the thyroid, upper and lower large intestinal wall and the kidneys. More than 90 % of physiologically eliminated radioactivity was excreted renally. The radiation dose to the urinary bladder wall could be substantially reduced by encouraging the patients to micturate frequently, especially during the first 8 hours after dose administration.

The radioactivity in the thyroid gland is most likely due to its ability to actively accumulate ^{123}I-iodide generated during metabolic de-iodination of either intact ^{123}I-IAZA or one or more of its radioactive metabolites. Once in the thyroid gland, iodine is incorporated into thyroid hormones and slowly released over a period of several months. Thus, for the purpose of this study, the radioiodine accumulated in the thyroid gland can be considered irreversibly bound, and eliminated with the 13.2 h decay half-life of the isotope. To prevent their thyroids from accumulating radioiodine, the subjects in this study received a dose of Lugol's solution (USP) at the time of injection. Since iodine incorporation into the thyroid gland takes place with a 6 - 8 h half-life, it may be possible to decrease the radiation dose to the thyroid by administering Lugol's solution earlier. Alternatively, a larger dose of Lugol's may be considered, as complete thyroid blockade (> 95 %) requires 135 mg of potassium iodide (Mozley *et al.*, 1996), while the volunteers in this study only received 30 mg. However, the 30 mg dose given at the time of ^{123}I-IAZA administration was sufficient to completely block the thyroid of volunteer # 6, in whom the thyroid gland was virtually undetectable even at the time of the 20 - 24 h image acquisition.

The primary source organ for the majority of target organs listed in Tables 7.1 and 7.2 was the Remainder of the Body. Notable exceptions were the lower large intestinal (LLI) wall, upper large intestinal (ULI) wall, small intestine, kidneys, liver, thyroid and the urinary bladder wall, all of which were their own primary sources and targets. For the urinary bladder, ULI and LLI walls, it was assumed that the source was the organ content and not the organ wall. The uterus and Total Body primary contributors varied with the bladder void time, with either the remainder of the body or the urinary bladder

being the primary contributors for the 2 h and 4.8 h void times, respectively. Similarly, for the Effective Dose (ED) the primary source organ was the colon (2 h bladder void time) or the urinary bladder (4.8 h bladder void time).

The two quantities, Effective Dose Equivalent (EDE) and ED, are given in the two tables in units of "roentgen equivalent, men" per mCi unit dose (rem/mCi). These two radiological effectiveness units have been designed by the International Committee on Radiation Protection (ICRP) to allow representation of the non-uniformly delivered dose to different organs as a single uniformly distributed dose that would result in the same overall risk to the patient (Stabin, 1996). The two parameters incorporate different organ risk factors in risk assessment.

Table 7.3 provides a comparison between ^{123}I-IAZA and several radiopharmaceuticals, which are either commercially available or are being investigated as potential clinically useful imaging agents. Dose estimates are for adults with a 2 h bladder void time. These data emphasize the low doses from ^{123}I-IAZA, since the ^{123}I-IAZA radiation dosimetry is comparable to some ^{99m}Tc-labeled agents. ^{99m}Tc-Sestamibi, for example, is commonly given as a 30 mCi injection, resulting in a total body dose of 0.5 rad, while ^{123}I-IAZA, clinically given as a 10 mCi dose, will produce a total body dose of 0.25 rad.

It has recently been suggested that the reference adult phantom assumption of a 70 kg man leads to an overestimation of the dose to the target organs (Mozley *et al.*, 1996). This overestimation is apparently caused by discrepancy between the organ sizes of a 70 kg "standard" man and an adult male with a higher body mass. In this study, for example, the average body weigh of the male volunteers was 85 kg and thus their organ masses were also proportionally higher. Yet, the dosimetry program assumes that this activity was concentrated in a smaller organ mass, and with shorter in-between organ distances. The same overestimation has taken place for the two female volunteers who weighed 73 and 68 kg, while the adult female phantom assumes a 57 kg female (Stabin, 1996). Some investigators have attempted to compensate for this problem by mathematically adjusting the phantom's weigh for the actual weight of the patient (e.g. Breitz *et al.*, 1995). However, weight distribution could pose an additional problem, as obese individuals may not have as large organs and in-between organ distances as may be predicted from a simple adjustment for total body weight.

Target organ	Total Dose (rad/mCi)							
	Vol # 1	Vol # 2	Vol # 3	Vol # 4	Vol # 5	Vol # 6	Mean	St Dev
Adrenals	2.9E-02	2.5E-02	2.7E-02	3.5E-02	3.2E-02	3.6E-02	3.1E-02	4.3E-03
Brain	1.7E-02	1.4E-02	1.5E-02	1.9E-02	1.8E-02	1.8E-02	1.7E-02	2.0E-03
Breasts	1.4E-02	1.3E-02	1.3E-02	1.7E-02	1.5E-02	1.6E-02	1.5E-02	1.8E-03
Gallbladder Wall	3.8E-02	3.2E-02	3.5E-02	5.0E-02	4.0E-02	4.8E-02	4.1E-02	7.3E-03
LLI Wall	1.4E-01	6.1E-02	1.2E-01	1.9E-01	1.3E-01	1.9E-01	1.4E-01	4.8E-02
Small Intestine	6.0E-02	3.3E-02	5.3E-02	8.4E-02	6.1E-02	8.5E-02	6.3E-02	2.0E-02
Stomach	2.6E-02	2.1E-02	2.3E-02	3.3E-02	2.8E-02	3.2E-02	2.7E-02	4.7E-03
ULI Wall	1.2E-01	5.3E-02	1.0E-01	1.7E-01	1.2E-01	1.7E-01	1.2E-01	4.5E-02
Heart Wall	2.2E-02	2.0E-02	2.0E-02	2.8E-02	2.4E-02	2.6E-02	2.3E-02	3.0E-03
Kidneys	1.3E-01	8.8E-02	1.2E-01	1.1E-01	1.5E-01	1.7E-01	1.3E-01	3.0E-02
Liver	5.0E-02	6.0E-02	5.2E-02	7.9E-02	5.3E-02	6.8E-02	6.0E-02	1.1E-02
Lungs	2.1E-02	1.8E-02	1.9E-02	2.6E-02	2.2E-02	2.4E-02	2.2E-02	3.0E-03
Muscle	2.2E-02	1.8E-02	2.0E-02	2.6E-02	2.3E-02	2.5E-02	2.2E-02	3.1E-03
Ovaries	4.7E-02	3.1E-02	4.2E-02	6.5E-02	4.8E-02	6.4E-02	4.9E-02	1.3E-02
Pancreas	2.9E-02	2.5E-02	2.7E-02	3.6E-02	3.1E-02	3.5E-02	3.0E-02	4.3E-03
Red Marrow	2.2E-02	1.7E-02	2.0E-02	2.6E-02	2.3E-02	2.5E-02	2.2E-02	3.4E-03
Bone Surfaces	3.7E-02	3.1E-02	3.3E-02	4.4E-02	3.9E-02	4.2E-02	3.7E-02	5.0E-03
Skin	1.4E-02	1.2E-02	1.2E-02	1.6E-02	1.5E-02	1.5E-02	1.4E-02	1.6E-03
Spleen	2.6E-02	2.1E-02	2.3E-02	3.0E-02	2.8E-02	3.1E-02	2.6E-02	3.9E-03
Testes	2.1E-02	1.8E-02	2.0E-02	N/A	2.3E-02	N/A	2.1E-02	2.1E-03
Thymus	1.9E-02	1.7E-02	1.7E-02	2.3E-02	2.0E-02	2.1E-02	1.9E-02	2.4E-03
Thyroid	2.0E-01	2.0E-01	2.5E-01	1.5E-01	1.4E-01	1.2E-01	1.8E-01	4.9E-02
Urin.Bladder Wall	1.8E-01	1.8E-01	1.9E-01	2.7E-01	1.8E-01	2.8E-01	2.1E-01	4.8E-02
Uterus	4.4E-02	3.6E-02	4.2E-02	5.7E-02	4.5E-02	5.6E-02	4.7E-02	8.2E-03
Total Body	2.4E-02	2.0E-02	2.2E-02	3.0E-02	2.6E-02	2.9E-02	2.5E-02	3.7E-03
EDE*	6.3E-02	4.7E-02	6.1E-02	8.0E-02	6.3E-02	8.3E-02	6.6E-02	1.3E-02
ED*	6.3E-02	4.8E-02	6.1E-02	7.9E-02	6.0E-02	7.5E-02	6.4E-02	1.1E-02

* units: rem/mCi

Table 7.1 Radiation dose estimates for ^{123}I-IAZA in six volunteers using a 2 h bladder void time. The "reference adult" phantom was used for volunteers 1, 2, 3 and 5 (males). The "adult female" phantom used for volunteers 4 and 6 (females).

Target organ	Total Dose (rad/mCi)							
	Vol # 1	Vol # 2	Vol # 3	Vol # 4	Vol # 5	Vol # 6	Mean	St Dev
Adrenals	2.9E-02	2.6E-02	2.7E-02	3.5E-02	3.2E-02	3.6E-02	3.1E-02	4.3E-03
Brain	1.7E-02	1.4E-02	1.5E-02	1.9E-02	1.8E-02	1.8E-02	1.7E-02	2.0E-03
Breasts	1.4E-02	1.3E-02	1.3E-02	1.7E-02	1.5E-02	1.6E-02	1.5E-02	1.9E-03
Gallbladder	3.8E-02	3.3E-02	3.6E-02	5.1E-02	4.0E-02	4.9E-02	4.1E-02	7.4E-03
LLI Wall	1.4E-01	6.9E-02	1.3E-01	2.0E-01	1.4E-01	2.0E-01	1.5E-01	4.9E-02
Small	6.3E-02	3.6E-02	5.6E-02	8.8E-02	6.3E-02	8.9E-02	6.6E-02	2.0E-02
Stomach	2.6E-02	2.1E-02	2.4E-02	3.3E-02	2.8E-02	3.2E-02	2.7E-02	4.7E-03
ULI Wall	1.2E-01	5.5E-02	1.0E-01	1.7E-01	1.2E-01	1.8E-01	1.2E-01	4.5E-02
Heart Wall	2.2E-02	2.0E-02	2.0E-02	2.8E-02	2.4E-02	2.6E-02	2.3E-02	3.0E-03
Kidney	1.3E-01	8.8E-02	1.2E-01	1.1E-01	1.5E-01	1.7E-01	1.3E-01	3.0E-02
Liver	5.1E-02	6.0E-02	5.2E-02	7.9E-01	5.3E-02	6.8E-02	1.8E-01	3.0E-01
Lungs	2.1E-02	1.8E-02	1.9E-02	2.6E-01	2.2E-02	2.4E-02	6.1E-02	9.8E-02
Muscle	2.3E-02	2.0E-02	2.2E-02	2.8E-01	2.5E-02	2.8E-02	6.7E-02	1.1E-01
Ovaries	5.4E-02	3.8E-02	5.0E-02	7.5E-02	5.5E-02	7.5E-02	5.8E-02	1.4E-02
Pancreas	2.9E-02	2.5E-02	2.7E-02	3.6E-02	3.1E-02	3.5E-02	3.1E-02	4.3E-03
Red	2.3E-02	1.9E-02	2.1E-02	2.8E-02	2.4E-02	2.7E-02	2.3E-02	3.5E-03
Bone	3.8E-02	3.2E-02	3.4E-02	4.5E-02	4.0E-02	4.3E-02	3.9E-02	5.1E-03
Skin	1.4E-02	1.2E-02	1.3E-02	1.7E-02	1.5E-02	1.6E-02	1.4E-02	1.7E-03
Spleen	2.6E-02	2.1E-02	2.3E-02	3.0E-02	2.8E-02	3.1E-02	2.6E-02	4.0E-03
Testes	2.6E-02	2.3E-02	2.5E-02	N/A	2.7E-02	N/A	2.6E-02	1.7E-03
Thymus	1.9E-02	1.7E-02	1.7E-02	2.3E-02	2.0E-02	2.1E-02	1.9E-02	2.4E-03
Thyroid	2.0E-01	2.0E-01	2.5E-01	1.5E-01	1.4E-01	1.2E-01	1.8E-01	4.9E-02
Urin.Bladder	4.0E-01	4.0E-01	4.4E-01	6.2E-01	3.9E-01	6.4E-01	4.8E-01	1.2E-01
Uterus	6.3E-02	5.5E-02	6.4E-02	8.1E-02	6.4E-02	8.2E-02	6.8E-02	1.1E-02
Total	2.6E-02	2.2E-02	2.4E-02	3.2E-02	2.8E-02	3.2E-02	2.7E-02	4.0E-03
EDE*	7.9E-02	6.3E-02	7.9E-02	1.0E-01	7.9E-02	1.1E-01	8.6E-02	1.7E-02
ED*	7.7E-02	6.2E-02	7.8E-02	1.0E-01	7.5E-02	1.0E-01	8.3E-02	1.6E-02

* units:

Table 7.2 Radiation dose estimates for ^{123}I-IAZA in six volunteers using a 4.8 h bladder void time. The "reference adult" phantom was used for volunteers 1, 2, 3 and 5 (males). The "adult female" phantom used for volunteers 4 and 6 (females).

Generic name	ULI (rad/mCi)	LLI (rad/mCi)	Thyroid (rad/mCi)	Urin. Bladder Wall (rad/mCi)	Total Body (rad/mCi)	Reference
^{123}I-IAZA	0.12	0.14	0.18	0.21	0.025	this work
^{123}I-Tropane	0.16	0.17	0.21	0.36	N/A[a] EDE[b] = 0.12	Mozley *et al.*, 1996
^{131}I-iobenguane sulfate	N/A	N/A	0.34	2.96	0.23	^{131}I-MIBG product monograph
^{99m}Tc-Bicisate	0.061	0.047	0.013	0.110	0.0090	Neurolite® product monograph
^{99m}Tc-Sestamibi	0.18	0.13	0.023	0.067	0.017	Cardiolite® product monograph

[a] N/A not provided in the product monograph
[b] EDE units rem/mCi

Table 7.3 Dosimetry estimates comparison between ^{123}I-IAZA and several other radiopharmaceuticals. Dose estimates are for adults with a 2 h bladder void time.

The assumption of uniform distribution of radioactivity in an organ is one of the main limitations of MIRD calculations, especially for organs such as the large intestine, where GIT transit time determines radioactivity localization at the time of image acquisition, and for kidneys, where the highest activity concentration in the kidney following ^{123}I-IAZA administration was visible in the renal pelvis area. Not only will different parts of these organs receive variable radiation doses, but also any overlap ROI calculation involving these organs will introduce errors in the ROI counts determination of all the overlapping organs. Accuracy of ROI drawing has been estimated at ± 10 % based on 5 repeated drawings of the same ROI. Additional sources of error involved in the dose estimates of Tables 7.1 and 7.2 include lack of correction for photon attenuation, backscatter and for tissue background counts. Failure to correct for attenuation has been suggested to introduce as much as 60 % error in the organ MRTfr values calculated (Seibyl *et al.*, 1994). The true error, however, may be overestimated by most attenuation correction methods, and currently no standard correction method exists.

7.3.3 Kinetic and Dosimetric Correlation

The dosimetric total body MRT and the pharmacokinetic MRT are identical in concept and should, theoretically, have the same value. Although determined by completely different technology, they both represent the sum of MRT_{fr} of various organs in the body, with the "remainder of the body" representing the tissues and organs with similar distribution characteristics. By analogy, in pharmacokinetics the organs representing the "remainder of the body" would all comprise one compartment, while organs with different MRTs for total radioactivity could each constitute a separate compartment. Thus, the overall MRT of the tracer in the body is the sum of the MRTs of all these compartments corrected for the fraction of the actual dose given to the patient that will enter each compartment.

During the pharmacokinetic analysis of total radioactivity following ^{123}I-IAZA administration, only two compartments were discernible. Yet, gamma camera scintigraphic images of the whole body have shown at least four compartments with different MRTs, namely liver, kidney, thyroid and "remainder of the body". The reason for the discrepancy is rooted in the different sources of data sampled by each technique.

Classical pharmacokinetic sample acquisition methods generally rely on venous blood samples. Consequently, only identification of quantitatively important compartments with variable MRTs is possible. In the case of ^{123}I-IAZA, for example, the very small fraction of dose accumulated in the thyroid would not be detected, despite the long MRT of activity in this organ. Furthermore, all organs with similar MRTs will be grouped into a single compartment, regardless of the their respective concentrations of radioactivity.

In dosimetric MRT determination, first the organs which have different concentration of activity are identified as separate compartments from the scintigraphic images, and then their MRTs are determined. Table 7.4 illustrates that following ^{123}I-IAZA administration the differences between the various organs' total radioactivity MRT values are actually very small. Furthermore, a one way analysis of variance (power of significance = 0.05) has not been able to detect statistically significant difference in the organ MRTs when compared between the volunteers.

This lack of variable MRTs between organs, as determined from the dosimetric analysis, results in a very short (5 % to the overall AUC) distribution phase of total

radioactivity, as determined from the pharmacokinetic analysis of blood samples. With 30 min image acquisition time, this distribution phase is too short to be discernable with gamma camera scintigraphic techniques. Thus, the source organs are the sources of radioactivity not by a virtue of longer MRTs, but because, compared to other organs, they have higher affinity for the radioactive components resulting in greater volumes of distribution of total radioactivity. The MRT_{fr} values used in dosimetric calculation are not true rate constants, because they incorporate a "fraction of dose" parameter. The higher the dose fraction, the higher will be the quantities such as its MRT_{fr}, its contribution to the total body MRT, and the radiation exposure from this source to all the target organs in the body.

Organ	MRT(h) for Volunteer #							
	1	2	3	4	5	6	Mean	St Dev
Liver	8.00	6.82	6.85	7.12	9.13	6.19	7.35	1.05
Kidney	7.86	5.45	7.39	6.32	8.84	9.29	7.53	1.47
Thyroid	8.29	6.60	7.11	6.31	7.55	5.25	6.85	1.05
RB	6.38	5.68	5.80	6.03	6.82	5.61	6.05	0.47

Table 7.4 MRT estimates for various organs for six healthy volunteers. Values based on whole body scintigraphic image analysis at five time points within a 24 h period after ^{123}I-IAZA administration.

In addition to the estimate of the total body MRT, the two methods also determined the biological elimination routes of total radioactivity from the body. In pharmacokinetic analysis the fraction eliminated in urine was determined directly by collecting and analyzing the urine. The remainder of the dose was assumed to be excreted via the gut (ref. Chapter 6 and Stypinski *et al.*, 1997submitted). Dosimetric analysis proceeds in the opposite order: first the fraction of the activity entering the gut is determined from the images, and then whatever remains is considered to be eliminated in the urine.

Table 7.5 shows estimates of the MRT_{TB} and percent dose eliminated in urine, using the two methods for each of the volunteers in this study. Although the two methods use completely different approaches, include different arrays of assumptions, and have vastly different errors associated with them, the resulting values are strikingly similar. The only exception, where the values calculated by the two methods were outside the

0.9 - 1.1 range, was in the case of volunteer # 2. For this individual, dosimetric analysis underestimated both the MRT_{TB} and the fraction of activity entering the gut. This was most likely due to the physiological make-up of this individual whose height and weight were 164 cm and 95 kg, respectively. Consequently, the actual number of counts in his organs and in the whole body images were probably underestimated because, compared to the other volunteers, there would have been more photon absorption and scatter before reaching the anterior or posterior gamma camera. These problems can be largely overcome using image attenuation correction techniques (Hammond, *et al.*, 1984; Eary, *et al.*, 1989; Mozley *et al.*, 1996; McQuarrie, 1995).

	Dosimetric		Pharmacokinetic* (PK)		PK:Dosimetric	
V#	MRT_{TB} (h)	Urine (%)	MRT_{TB} (h)	Urine (%)	MRT_{TB}	Urine
1	6.69	93.3	7.25	95.3	1.08	1.02
2	5.91	97.6	7.28	85.1	1.23	0.87
3	6.03	94.3	5.95	64.4**	0.99	0.68
4	6.26	91.4	6.52	93.5	1.04	1.02
5	7.20	93.5	7.67	91.2	1.07	0.98
6	5.95	91.2	6.40	97.0	1.08	1.06

* Ref: Chapter 6, Tables 6.2 and 6.3
**Incomplete urine collection (last collection time missed)

Table 7.5 Comparison of dosimetric and pharmacokinetic methods to estimate the effective total body MRT and the percent of total radioactivity eliminated in the urine of six volunteers. Percent dose in urine is based on biological elimination routes only, and does not include clearance due to physical decay of the radionuclide.

It is interesting to note that in the case of volunteer # 3, who has missed one of his urine collection times, the dosimetric analysis was able to estimate a %ID in urine value that was comparable with those of the other five volunteers. Thus a renal clearance of 111 mL/min was determined using dosimetric analysis, whereas it was impossible to determine this value from the pharmacokinetic protocol described in Chapter 6 of this thesis. In this case, dosimetric analysis had the advantage, because it did not need to rely on the subject's compliance.

Based on table 7.5, in general, the dosimetric and pharmacokinetic analysis methods used in this study have validated each other. Although pharmacokinetic

analysis is many times more accurate then the dosimetric analysis, both methods have produced very similar estimates of total body MRT and renally eliminated fraction of radioactivity. Dosimetric estimation of these parameters required correct identification of the total body ROI which, according to equation 7.10, directly relies on the activity estimates in three other ROI's, namely whole body, gut and urinary bladder. However, gut activity determination relies on numerous other ROIs, including large intestine overlap regions with other organs and the organs which overlap with the large intestine (i.e. liver and kidney). Consequently, the excellent correlation between pharmacokinetic and dosimetric estimates in these volunteers has also validated the ROI drawing and overlap resolution procedures described in the experimental section of this chapter.

7.4 References

Breitz HB, Durham JS, Fisher DR, Weiden PL, DeNardo GL, Goodgold HM, Nelp WB. Pharmacokinetics and normal organ dosimetry following intraperitoneal rhenium-186-labeled monoclonal antibody. J Nucl Med 1995;36:754-61.

Eary JF, Appelbaum FL, Durack L, Brown P. Preliminary validation of the opposing view method for quantitative gamma camera imaging. Med Phys 1989;16:382-7.

Eddis C, Tam YK. An interactive computer program for determining areas bounded by drug concentration curves using lagrange interpolation. J Pharmacol Toxicol Methods 1995;34(3):164-8.

Hammond ND, Moldofsky PJ, Beardsley MR, Mulhern CB. External imaging techniques for quantification of distribution of I-131 F(ab')$_2$ fragments of monoclonal antibody in humans. Med Phys 1984;11:778-83.

Mannan RH, Somayaji VV, Lee J, Mercer JR, Chapman JD, Wiebe LI. Radioiodinated 1-(5-iodo-5-deoxy-β-D-arabinofuranosyl) -2-nitroimidazole (iodoazomycin arabinoside: IAZA), a novel marker of tissue hypoxia. J Nucl Med 1991;32:1764-70.

Mannan RH. Novel non-invasive markers of tumor hypoxia. Edmonton, Alberta, Canada: *PhD. Thesis*, University of Alberta, 1991.

McQuarrie SA. The development of a pharmacokinetic and radiation dosimetric model for selected ^{99m}Tc labelled monoclonal antibodies. Edmonton, Alberta, Canada: *PhD. Thesis*, University of Alberta, 1995.

Mozley PD, Stubbs JB, Kim H-J, McElgin W, Kung M-P, Meegalla A, Kung HF. Dosimetry of an iodine-123-labeled tropane to image dopamine transporters. J Nucl Med 1996;37:151-9.

Seibyl JP, Wallace E, Smith EO, Stabin M, Baldwin RM, Zoghbi S, Zea-Ponce Y, Gao Y, Zhang WY, Neumeyer JL, Zubal IG, Charney DS, Hoffer PB, Innis RB. Whole-body biodistribution, radiation absorbed dose and brain SPECT imaging with iodine-123-β-CIT in healthy human subjects. J Nucl Med 1994;35:764-70.

Snyder W, Ford M, Warner G, Watson S. "S" absorbed dose per unit cumulated activity for selected radionuclides and organs. MIRD Pamphlet No. 11. New York: Society of Nuclear Medicine 1975.

Stabin MG. MIRDOSE: personal computer software for internal dose assessment in nuclear medicine. J Nucl Med 1996;37:538-46.

Stypinski D, Wiebe LI, McEwan AJ, Tam YK, Mercer JR. Radiopharmacokinetics of ^{123}I-IAZA in healthy volunteers. 1997(Submitted).

8. Pharmacokinetics and Radiation Dosimetry of ^{123}I-IAZA in Healthy Volunteers Following "Bruce" Treadmill Protocol

8.1 Introduction

Accurate identification and quantification of the severity of myocardial ischemia is essential in view of the morbidity and mortality associated with the partial loss of myocardial function. Since 2-nitroimidazoles bind selectively to hypoxic cells *in vivo*, they are thought to have tremendous potential as selective markers of ischemic but salvageable myocardium. Several 2-nitoimidazoles have been specifically designed and investigated for that purpose: technetium-99m-labeled BMS181321 (DiRocco *et al.*, 1992; Shi *et al.*, 1995; Rumsey *et al.*, 1993; Rumsey *et al.*, 1995; Kusuoka *et al.*, 1994; Rasey *et al.*, 1990; Okada *et al.*, 1996; Stone *et al.*, 1995; Fukuchi *et al.*, 1996), fluorine-18-labeled fluoromisonidazole (Caldwell *et al.*, 1995; Shelton *et al.*, 1988; Cerqueira *et al.*, 1988; Martin *et al.*, 1989; Martin *et al.*, 1992), and iodine-123-labeled idovinylmisonidazole (Biskupiak *et al.*, 1991; Martin *et al.*, 1993).

Since ^{123}I-IAZA has been shown to be capable of clinically detecting hypoxic tissues in tumors (Parliament *et al.*, 1992; Urtasun *et al.*, 1996), in the limbs of diabetic patients with peripheral vascular disease (Al-Arafaj *et al.*, 1994) and in active synovitis of patients with rheumatoid arthritis (McEwan *et al.*, 1996), we are currently interested in this agent's potential as a marker of ischemic myocardium. Although, based on the dosimetry data presented in Chapter 7 of this thesis, there is no evidence that normal, rest-state cardiac tissue retains ^{123}I-IAZA, its retention characteristics in acutely stressed normal myocardium have not been determined. In addition, the volume of distribution, clearance and other tissue-specific parameters may change during cardiac stress-tests, resulting in changes in both the kinetic parameters of ^{123}I-IAZA and in the scintigraphic image characteristics. In this paper, we report the pharmacokinetics and dosimetry of ^{123}I-IAZA following "Bruce" treadmill protocol in healthy volunteers.

8.2 Experimental

8.2.1 Chemicals and reagents

IAZA was synthesized by Dr. Elena Atrazheva at the Faculty of Pharmacy and Pharmaceutical Sciences, University of Alberta, and radiolabelled by Mr. Ron Schmidt

at the Cross Cancer Institute in Edmonton, using published procedures (Mannan, 1991; Mannan *et al.*, 1991).

8.2.2 Clinical protocol

The research project was conducted in accordance with the tenets of the Declaration of Helsinki (1964) and was a modification of a protocol approved by the Alberta Cancer Board research ethics committee and by the University of Alberta radiation safety committee. Three healthy male volunteers participated in the study with informed consent. Prior to the study, blood was drawn for hematology and for hepatic and renal function tests. Volunteer demographic and specific dosage information are given in Table 8.1. Shortly after injection each volunteer was given an oral dose of 0.6 mL of Lugol's solution (USP) to block the thyroid uptake of free radioiodide.

Volunteer #	Sex	Age (years)	Weight (kg)	Height (cm)	Radioactive dose (mCi)	IAZA dose (mg)
CV1	M	42	70	175	3.23	0.80
CV2	M	27	75	186	5.64	1.18
CV3	M	40	73	165	3.05	0.57

Table 8.1 Volunteer demographics and doses for ^{123}I-IAZA cardiac stress test study.

The complete details of the protocol, and the list of instructions given to the volunteer prior to the study are reproduced in Appendix I of this thesis. Briefly, the "Bruce" treadmill protocol was followed, with the volunteer running until the desired heart rate (calculated as 85% of (220 - age) beats/min) for his age group was reached. At one minute prior to achieving this target heart rate, ^{123}I-IAZA was administered as a slow (1-3 min) i.v. injection in the right arm. The volunteer continued running for one more minute, after which time he rested.

Venous blood samples (9 mL) were drawn from an indwelling catheter in the contralateral arm at 1, 5, 15, 30, 45 min and 1, 2, 5, 8, 12, 22, and 28 h. Volunteer # 1 had an additional sample taken at 45 h. Blood samples were collected into SST Vacutainer® tubes containing 30 μg of non-radiolabelled IAZA dissolved in 250 μL of sterile normal saline. The blood was first allowed to clot at room temperature for 30 min and then refrigerated prior to analysis. The samples were analyzed using a

radiometric/HPLC assay described in Chapter 4 of this thesis and in Stypinski, *et al.* (1997in press). Urine samples were not collected in this group of volunteers.

In addition, for each volunteer three SPECT scintigraphs of the chest cavity and five anterior and posterior whole body images for dosimetry determination were collected, starting at 0.75 to 2.35 h until 24 h after ^{123}I-IAZA injection. Volunteer # CV1 had two additional SPECT images acquired, for a total of five. Due to technical problems, two of the images, including the immediate, were missed in Volunteer # CV2. For this volunteer the first image was taken at 2.35 h after dose administration, when some of the dose was already excreted from the urinary bladder.

The images were acquired using a dual-headed, large field of view gamma camera (Picker Odyssey 2000) equipped with a LEAP (low energy all purpose) collimator and interfaced to an Odyssey computer. The 20 % analysis window was set symmetrically over the 159 keV ^{123}I photopeak.

8.2.3 Pharmacokinetic and dosimetric analysis

Blood clearance profiles for ^{123}I-IAZA and total radioactivity were analyzed using the same procedures as described in Section 6.2.3 of this thesis. Dosimetry calculations were done as described in Sections 7.2.3 through 7.2.9 of this thesis. Since only male volunteers were used, the reference adult phantom was used for the radiation dose estimates in all three volunteers. Both the pharmacokinetic and dosimetric data for this study group were compared with the previously reported results in six non-stressed normal volunteers as described in Chapters 6 and 7 of this thesis and in Stypinski, *et al.* (1997submitted).

In order to determine any changes in the disposition of radioactivity in the cardiac and/or skeletal muscles, two additional ROIs were drawn: the heart and a representative thigh section. These ROIs were drawn on images of the three stressed volunteers and on the scintigraphic images of the six rested volunteers whose dosimetry was reported in Chapter 7.

Statistical comparison of the two groups, stressed and rest, was completed using unpaired t-test (SigmaStat[7] v1.01). The tests were conducted at the 0.05 level of significance. All the data are reported as arithmetic mean ± standard deviation.

[7] Copyright 1992-1994 Jandel Scientific.

8.3 Results and Discussion

8.3.1 Pharmacokinetics

The concentration *vs.* time plots for ^{123}I-IAZA and total radioactivity for the three volunteers are shown in Figure 8.1. Both ^{123}I-IAZA and total radioactivity showed a bi-exponential disposition in blood, with a brief distribution phase followed by a much longer elimination phase. The mean distribution phase half-lives for ^{123}I-IAZA and total radioactivity were 1.2 ± 0.15 min and 1.4 ± 0.28 min, respectively. The elimination phase half-lives were 195 ± 34 min and 290 ± 37 min, respectively.

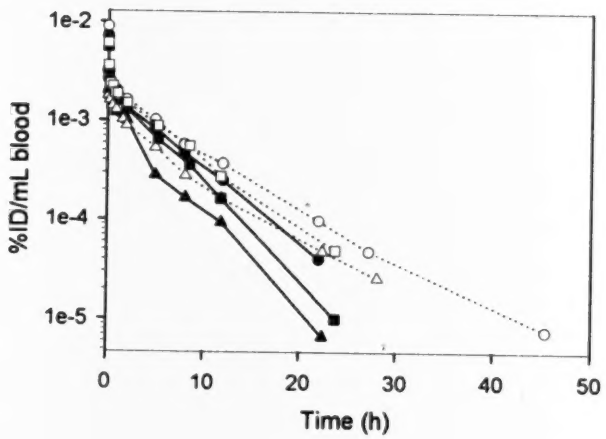

Figure 8.1 Concentration-time profiles of ^{123}I-IAZA (solid symbols) and total radioactivity (open symbols) for volunteers 1 (circles), 2 (triangles) and 3 (squares), following ^{123}I-IAZA administration during "Bruce" treadmill protocol.

Table 8.2 shows the kinetic parameters of both ^{123}I-IAZA and total radioactivity in the three volunteers. For comparison, this table also includes the mean parameters for a group of six normal volunteers who were given a resting (i.e. no "Bruce" treadmill protocol) dose of ^{123}I-IAZA. The complete description of the study and the results for this group of un-stressed volunteers are given in Chapter 6 of this thesis and in Stypinski, *et al.* (1997submitted).

	^{123}I-IAZA				Total Radioactivity			
V #	$t_{1/2\alpha}$ (min)	$t_{1/2\beta}$ (min)	V_{ss} (L/kg)	Cl_{TB} (mL/ min)	$t_{1/2\alpha}$ (min)	$t_{1/2\beta}$ (min)	V_{ss} (L/kg)	Cl_{TB} (mL/ min)
CV1	1.1	234	0.677	145	1.3	328	0.794	104
CV2	1.3	170	0.803	254	1.2	287	0.979	182
CV3	1.1	182	0.541	157	1.8	254	0.581	120
Mean ± SD	1.2 ± 0.12	195 ± 34	0.674 ± 0.13	185 ± 60	1.4 ± 0.32	290 ± 37	0.785 ± 0.20	135 ± 41
rest Mean ± SD[a]	5.3 ± 3.8	179 ± 27	0.716 ± 0.10	239 ± 53	4.6 ± 2.6	294 ± 30	0.746 ± 0.10	145 ± 19

[a] Ref: rest study, Chapter 6 Table 6.2

Table 8.2 Summary of pharmacokinetic parameters of ^{123}I-IAZA and total radioactivity in the three stressed volunteers. Also included are the arithmetic mean ± SD values for the six volunteers whose kinetic parameters have been determined at rest.

Based on the results for these two groups of volunteers, acute strenuous exercise does not appear to dramatically alter the pharmacokinetic parameters of ^{123}I-IAZA or of total radioactivity. These results are not surprising, considering that in normal, un-stressed volunteers ^{123}I-IAZA rapidly distributes into the peripheral tissues, is mainly cleared by metabolic degradation and that, overall, it is a low extraction drug with hepatic clearance mainly dependent on enzyme function (Stypinski, *et al.*, 1997submitted). Exercise mainly affects cardiac output and regional perfusion, with the organ perfusion changes depending on whether vasoconstriction or vasodilatation controls the particular organ (Caru *et al.*, 1992). Since ^{123}I-IAZA metabolism is relatively insensitive to hepatic flow changes, Cl_{nr} would not be expected to alter during acute, strenuous exercise. Increased cardiac output and increased perfusion to tissues which were not normally well perfused resulted in an even faster distribution of ^{123}I-IAZA into peripheral tissue, as is evident in the shorter $t_{1/2\alpha}$ of ^{123}I-IAZA in the cardiac stress test volunteers, although the extent of distribution has not been affected.

Unlabeled IAZA was shown to have a V_{ss} in un-stressed volunteers of close to 90 % that of total body weight. Since this is a fairly lipid-soluble compound (P = 4.98; ref: Mannan, 1991), such a relatively small volume of distribution suggests that it is negligibly bound to extravascular tissues (Gibaldi and Perrier, 1982). IAZA blood protein binding has not been specifically measured, however, it is a conjugated isomer of IAZR, and IAZR plasma protein binding is 20.5 ± 1.6 % (Jette *et al.*, 1986). Assuming that IAZA plasma protein binding is similar, than with its slow elimination half-life IAZA has more than sufficient time to equilibrate well between blood and tissues. Since it is not the rate of drug delivery to the tissue that determines the distribution of IAZA in that tissue, then even a five fold increase in skeletal muscle perfusion between rest and maximal exercise state, as reported by Caru *et al.* (1992), will not have much effect on the volume of distribution of this compound. The only exception to this may be active uptake of ^{123}I-IAZA into regions where hypoxia may develop during exercise, particularly if the uptake and retention are substantial. However, the whole body images of the exercised volunteers have not shown any unusual radioactivity retention characteristics.

Generally, it is assumed that even at maximum exercise the renal blood flow will not decrease by more than 20 % of the resting value in a normal subject (Caru *et al.*, 1992). For both ^{123}I-IAZA and total radioactivity, renal clearance is low, although it is the principal route of elimination for the radioactive metabolites. Thus, renal clearance of ^{123}I-IAZA will also be largely unaffected by exercise.

Since neither renal or hepatic clearance, nor clearance due to physical decay, will be affected by exercise, the plots of ^{123}I-IAZA and total radioactivity for the two groups of volunteers should be similar. Figure 8.2 shows that, in fact, concentration *vs.* time plots for ^{123}I-IAZA for the two study groups will practically superimpose on one another. Figure 8.3 shows ^{123}I-IAZA and total radioactivity disposition in blood of volunteer # CV2, who has participated in both the "Bruce" protocol and the resting study with ^{123}I-IAZA (see Chapter 6, volunteer # 3).

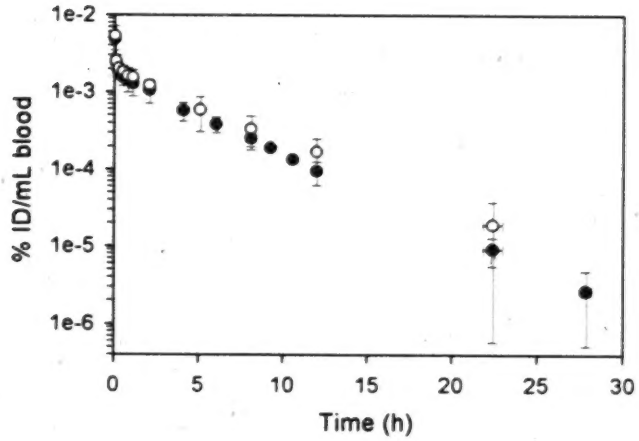

Figure 8.2 ^{123}I-IAZA blood concentration *vs.* time plots for the two groups of volunteers: (O) dose administration during "Bruce" protocol (n = 3); (●) dose administration at rest (n = 6).

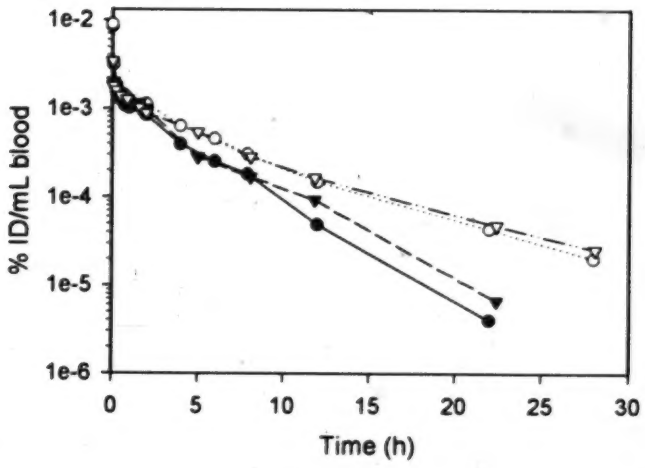

Figure 8.3 Plots of ^{123}I-IAZA (solid symbols) and total radioactivity (open symbols) for volunteer # CV2. ^{123}I-IAZA dose administered at rest (circles) and during "Bruce" treadmill protocol (triangles).

8.3.2 Dosimetry

Whole body scintigraphic images of the three volunteers who participated in this study did not show any apparent differences in the disposition of total radioactivity when compared to the six volunteers who were given ^{123}I-IAZA at rest. The most radioactive, or "hottest" organs, were again the bladder, liver and the kidneys, with thyroid and gut becoming apparent on the later images. The only exception was Volunteer CV1 who had substantial activity uptake into the thyroid, with the gland already becoming visible on the 1.5 h image. In this volunteer, however, the Lugol's solution was not administered until almost 4 h after the ^{123}I-IAZA dose.

There was no apparent increase in uptake of radioactivity by the skeletal muscles in the thigh or in the myocardium. As in the rest study, the myocardium in the stressed volunteers was only visible on the initial whole body and SPECT images, but not on the later ones. This activity most likely originated from the blood pool in the highly perfused cardiac muscle. This is supported by the MRT_{fr} values for the heart, which were 0.16 h and 0.15 h for volunteers CV1 and CV3, respectively. The mean value in the rest study was 0.17 ± 0.02 h. The MRT_{fr} value for volunteer CV2 was not determined because of the missing immediate image. Figure 8.4 shows three representative SPECT image frames (anterior, lateral and posterior) of the chest cavity of volunteer CV2.

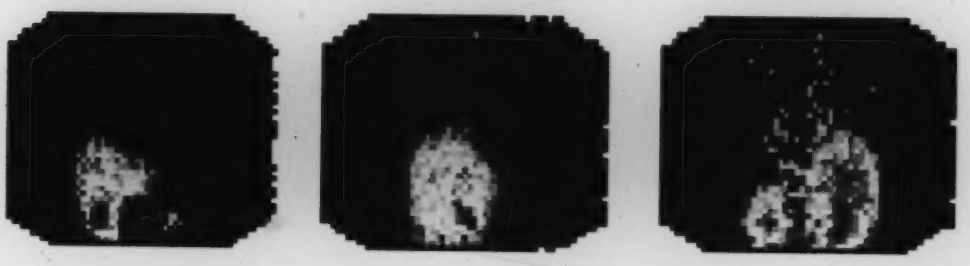

Figure 8.4 Three representative SPECT image frames (numbers 36, 57 and 72, respectively) of the chest cavity in a 27 year old male volunteer (CV2) following 5.68 mCi ^{123}I-IAZA dose given i.v. during "Bruce" treadmill protocol. Images acquired 1.5 h after the radiopharmaceutical administration.

The dose estimates for volunteers CV1 and CV3 are given in Table 8.3 for both the 2 h and the 4.8 h bladder void times. For reference, this table also includes the mean dose estimated for the six volunteers who were given ^{123}I-IAZA at rest. Dosimetry estimates for volunteer CV2 have not been determined because the minimum number of required images were not acquired.

The dose estimates for the two stressed volunteers show that strenuous exercise, such as during the "Bruce" treadmill protocol, does not appear to have any effect on the dosimetry estimates for total radioactivity following ^{123}I-IAZA administration. These results are in complete agreement with the pharmacokinetic results described above, as absence of change in the disposition kinetics of total radioactivity has translated into no change in the dosimetry.

Furthermore, although the urine of the stressed volunteers has not been collected, the ROI analysis has shown that the biologic fraction of activity eliminated in the urine was 0.97 and 0.92 for volunteers CV1 and CV3, respectively. Since in the rest study the mean urinary excretion fraction was 0.94 ± 0.02, the exercise protocol also did not have any apparent effect on the urinary or gut elimination routes.

Target organ	Total Dose (rad/mCi)							
	2 H BLADDER VOID TIME				4.8 H BLADDER VOID TIME			
	Stress Study		*Rest Study (V1-6)*		*Stress Study*		*Rest Study (V1-6)*	
	CV1	**CV2**	**Mean**	**St Dev**	**CV1**	**CV2**	**Mean**	**St Dev**
Adrenals	3.3E-02	3.3E-02	3.1E-02	4.3E-03	3.3E-02	3.3E-02	3.1E-02	4.3E-03
Brain	2.1E-02	1.8E-02	1.7E-02	2.0E-03	2.1E-02	1.8E-02	1.7E-02	2.0E-03
Breasts	1.8E-02	1.6E-02	1.5E-02	1.8E-03	1.8E-02	1.6E-02	1.5E-02	1.9E-03
Gallbladder Wall	3.8E-02	4.5E-02	4.1E-02	7.3E-03	3.8E-02	4.6E-02	4.1E-02	7.4E-03
LLI Wall	8.4E-02	1.6E-01	1.4E-01	4.8E-02	9.2E-02	1.7E-01	1.5E-01	4.9E-02
Small Intestine	4.5E-02	7.1E-02	6.3E-02	2.0E-02	4.8E-02	7.4E-02	6.6E-02	2.0E-02
Stomach	2.9E-02	2.9E-02	2.7E-02	4.7E-03	2.9E-02	2.9E-02	2.7E-02	4.7E-03
ULI Wall	7.3E-02	1.4E-01	1.2E-01	4.5E-02	7.5E-02	1.4E-01	1.2E-01	4.5E-02
Heart Wall	2.7E-02	2.5E-02	2.3E-02	3.0E-03	2.7E-02	2.5E-02	2.3E-02	3.0E-03
Kidney	1.3E-01	1.4E-01	1.3E-01	3.0E-02	1.3E-01	1.5E-01	1.3E-01	3.0E-02
Liver	4.5E-02	7.0E-02	6.0E-02	1.1E-02	4.6E-02	7.0E-02	6.1E-02	1.1E-02
Lungs	2.5E-02	2.3E-02	2.2E-02	3.0E-03	2.5E-02	2.3E-02	6.1E-02	9.8E-02
Muscle	2.5E-02	2.4E-02	2.2E-02	3.1E-03	2.7E-02	2.6E-02	6.7E-02	1.1E-01
Ovaries	4.2E-02	5.3E-02	4.9E-02	1.3E-02	4.9E-02	6.2E-02	5.8E-02	1.4E-02
Pancreas	3.3E-02	3.3E-02	3.0E-02	4.3E-03	3.3E-02	3.3E-02	3.1E-02	4.3E-03
Red Marrow	2.5E-02	2.4E-02	2.2E-02	3.4E-03	2.6E-02	2.5E-02	2.3E-02	3.5E-03
Bone Surfaces	4.4E-02	4.0E-02	3.7E-02	5.0E-03	4.5E-02	4.2E-02	3.9E-02	5.1E-03
Skin	1.7E-02	1.5E-02	1.4E-02	1.6E-03	1.7E-02	1.6E-02	1.4E-02	1.7E-03
Spleen	3.0E-02	2.8E-02	2.6E-02	3.9E-03	3.0E-02	2.8E-02	2.6E-02	4.0E-03
Testes	2.5E-02	2.3E-02	2.1E-02	2.1E-03	3.0E-02	2.9E-02	2.6E-02	1.7E-03
Thymus	2.4E-02	2.1E-02	1.9E-02	2.4E-03	2.4E-02	2.1E-02	1.9E-02	2.4E-03
Thyroid	3.3E-01	1.6E-01	1.8E-01	4.9E-02	3.3E-01	1.6E-01	1.8E-01	4.9E-02
Urin.Bladder Wall	1.8E-01	2.0E-01	2.1E-01	4.8E-02	4.0E-01	4.5E-01	4.8E-01	1.2E-01
Uterus	4.5E-02	5.0E-02	4.7E-02	8.2E-03	6.4E-02	7.1E-02	6.8E-02	1.1E-02
Total Body	2.7E-02	2.7E-02	2.5E-02	3.7E-03	2.9E-02	2.9E-02	2.7E-02	4.0E-03
EDE*	6.1E-02	7.0E-02	6.6E-02	1.3E-02	7.8E-02	8.8E-02	8.6E-02	1.7E-02
ED*	6.3E-02	6.9E-02	6.4E-02	1.1E-02	7.8E-02	8.5E-02	8.3E-02	1.6E-02

*rem/mCi

Table 8.3 Radiation dose estimates for ^{123}I-IAZA in stressed volunteers CV1 and CV2, and mean and standard deviation values from the rest study in a group of six volunteers (Ref; Chapter 7, Tables 7.1 and 7.2).

8.4 References

Al-Arafaj A, Ryan EA, Hutchison K, Mannan RH, Mercer JR, Wiebe LI, McEwan AJB. An evaluation of iodine 123 iodoazomycin arabinoside as a marker of localized tissue hypoxia in patients with diabetes mellitus. Eur J Nucl Med 1994;21(12):1338-42.

Biskupiak JE, Grierson JR, Rasey JS, Martin GV, Krohn KA. Synthesis of an (iodovinyl)misonidazole derivative for hypoxia imaging. J Med Chem 1991;34:2165-8.

Caldwell JH, Revenaugh JR, Martin GV, Johnson PM, Rasey JS, Krohn KA. Comparison of flourine-18-fluorodeoxyglucose and tritiated fluoromisonidazole uptake during low-flow ischemia. J Nucl Med 1995;36:1633-8.

Caru B, Colombo E, Santoro F, Laporta A, Maslowsky F. Regional flow responses to exercise. Chest 1992;101(Suppl.):223S-5S.

Cerqueira M, Martin G, Embree L, Caldwell J, Krohn K, Rasey J. Enhanced binding of fluoromisonidazole in isolated adult rat myocytes during hypoxia. (Abstract). J Nucl Med 1988;29:807.

DiRocco RJ, Bauer A, Kuczynski BL, Pirro JP, Linder KE, Narra RK, Nunn AD. Imaging regional hypoxia with a new technetium-labeled imaging agent in rabbit myocardium after occlusion of the left anterior descending coronary artery. (Abstract). J Nucl Med 1992;33:865.

Fukuchi K, Kusuoka H, Watanabe Y, Fujiwara T, Nishimura T. Ischemic and reperfused myocardium detected with technetium-99m-nitroimidazole. J Nucl Med 1996;37:761-6.

Gibaldi M, Perrier D. Pharmacokinetics. 2nd ed. New York: Marcel Dekker, Inc.; 1982.

Jette DC, Wiebe LI, Flanagan RJ, Lee J, Chapman JD. Iodoazomcin riboside (1-(5'-iodo-5-deoxyribofuranosyl]-2-nitroimidazole), a hypoxic cell marker. 1. Synthesis and *in vitro* characterization. Radiat Res 1986;105:169-79.

Kusuoka H, Hashimoto K, Fukuchi K, Nishimura T. Kinetics of a putative hypoxic tissue marker, technetium-99m-nitroimidazole (BMS181321), in normoxic, hypoxic, ischemic and stunned myocardium. J Nucl Med 1994;35:1371-6.

Mannan RH, Somayaji VV, Lee J, Mercer JR, Chapman JD, Wiebe LI. Radioiodinated 1-(5-iodo-5-deoxy-β-D-arabinofuranosyl) -2-nitroimidazole (iodoazomycin arabinoside: IAZA), a novel marker of tissue hypoxia. J Nucl Med 1991;32:1764-70.

Mannan RH. Novel non-invasive markers of tumor hypoxia. Edmonton, Alberta, Canada: *PhD. Thesis*, University of Alberta; 1991.

Martin GV, Biskupiak JE, Caldwell JH, Rasey JS, Krohn KA. Characterization of iodovinylmisonidazole as a marker for myocardial hypoxia. J Nucl Med 1993;34:918-24.

Martin GV, Caldwell JH, Graham MM, Grierson JR, Kroll K, Cowan MJ, Lewellen TK, Rasey JS, Casciari JJ, Krohn KA. Noninvasive detection of hypoxic myocardium using fluorine-18-fluoromisonidazole and positron emission tomography. J Nucl Med 1992;33:2202-8.

Martin GV, Caldwell JH, Rasey JS, Grunbaum Z, Cerqueira M, Krohn KA. Enhanced binding of the hypoxic cell marker [3H]fluoromisonidazole in ischemic myocardium. J Nucl Med 1989;30:194-201.

McEwan AJB, Skeith KJ, Mannan RH, Davies N, Jamali F, Wiebe LI. ^{123}I-iodoazomycin arabinoside - a possible marker of hypoxia in rheumatoid arthritis. CANM Annual Scientific Meeting1996; Quebec City, PQ.

Okada RD, Nguyen KN, Strauss HW, Johnson III G. Effects of low flow and hypoxia on myocardial retention of technetium-99m BMS 181321. Eur J Nucl Med 1996;23:443-7.

Parliament MB, Chapman JD, Urtasun RC, McEwan AJ, Golberg L, Mercer JR, Mannan RH, Wiebe LI. Non-invasive assessment of human tumour hypoxia with ^{123}I-iodoazomycin arabinoside: preliminary report of a clinical study. Br J Cancer 1992;65:90-5.

Rasey JS, Nelson NJ, Chin L, Evans ML, Grunbaum Z. Characteristics of the binding of labeled fluoromisonidazole in cells *in vitro*. Radiat Res 1990;122:301-8.

Rumsey WL, Cyr JE, Raju N, Narra RK. A novel [99m]technetium-labeled nitroheterocycle capable of identification of hypoxia in heart. Biochem Biophys Res Commun 1993;193:1239-46.

Rumsey WL, Kuczynski B, Patel B, Bauer A, Narra RK, Eaton SM, Nunn AD, Strauss HW. SPECT imaging of ischemic myocardium using a Technetium-99m-nitroimidazole ligand. J Nucl Med 1995;36:1445-50.

Shelton ME, Welch MJ, Dence CS, Hwang D-R, Bergmann SR. [F-18]fluoro-misonidazole: a potential marker of salvageable myocardium. (Abstract). J Nucl Med 1988;29:807.

Shi CQX, Sinusas AJ, Dione DP, Singer MJ, Young LH, Heller EN, Rinker BD, Wackers FJT, Zaret BL. Technetium-99m-nitroimidazole (BMS181321): a positive imaging agent for detecting myocardial ischemia. J Nucl Med 1995;36:1078-86.

Stone CK, Mulnix T, Nickles RJ, Renstrom B, Nellis SH, Liedtke AJ, Nunn AD, Kuczynski BL, Rumsey WL. Myocardial kinetics of a putative hypoxic tissue marker, ^{99m}Tc-labeled nitroimidazole (BMS-181321), after regional ischemia and reperfusion. Circulation 1995;92:1246-53.

Stypinski D, Wiebe LI, McEwan AJ, Tam YK, Mercer JR. Radiopharmacokinetics of ^{123}I-IAZA in healthy volunteers. 1997(Submitted).

Stypinski D, Wiebe LI, Mercer JR. A rapid and simple assay to determine the blood and urine concentration of 1-(5-[$^{123/125}$I]iodo-5- deoxyarabinofuranosyl)-2-nitroimidazole, a marker of tissue hypoxia. Journal of Pharmaceutical and Biomedical Analysis 1997(in Press).

Urtasun RC, Parliament MB, McEwan AJ, Mercer JR, Mannan RH, Wiebe LI, Morin C, Chapman JD. Measurement of hypoxia in human tumours by non-invasive spect imaging of iodoazomycin arabinoside. Br J Cancer 1996;74 (Suppl. 27):S209-12.

9. A Pharmacokinetic-Pharmacodynamic Model to Quantify Tissue Hypoxia with ^{123}I-IAZA

9.1 Introduction

Quantifying the fraction of chronically hypoxic cells in a tissue is of considerable clinical interest. In radiation oncology, especially, this interest stems from a long suspected and recently demonstrated relationship between tumor hypoxia and poor prognosis in cancer patients (Hőckel *et al.*, 1996). In 1995 a model was proposed to determine the extent of tumor hypoxia using ^{18}F-FMISO (Casciari *et al.*, 1995). These authors combined a multicompartmental interstitial physiological kinetic model with an intracellular bioreductive model to simulate the fate of ^{18}F-FMISO in a tumor with radiobiologically hypoxic fraction.

Although physiological pharmacokinetic models are anatomically and physiologically more correct than the classical approaches, they are not practical with the usual clinical study design. More recently, we have suggested that a simpler model based on the classical PK/PD modeling concepts could also be applicable, provided that the PK parameters of the parent compound and of the radioactive metabolites are known (Wiebe and Stypinski, 1996). Such a model would have the advantage of having fewer parameters requiring estimation without compromising its ability to determine percent tissue hypoxia.

We have now further expanded this model by merging the classical pharmacokinetic effect compartment model (Holford and Sheiner, 1981) with organ perfusion concepts applied to physiological pharmacokinetic models. Since the basis of the activity of 2-nitroimidazole imaging agents is their reductive metabolism and intracellular trapping within hypoxic cells, these cells can be represented as an "eliminating organ". By determining the relationships between ^{123}I-IAZA and total radioactivity in blood of human volunteers, and between tissue radioactivity and image intensity in a normoxic region of interest, we can directly substitute the kinetic parameters into the proposed model and derive a kinetic-link model capable of predicting tissue oxygenation status from the scintigraphic image intensity.

9.2 Theoretical Model Development

9.2.1 Physiological Pharmacokinetic Model of the Effect Compartment

The physiological pharmacokinetic model illustrated in Figure 9.1 is a modification of a simple blood flow rate-limited model (Gibaldi and Perrier, 1982). It consists of two eliminating compartments: the hypoxic cells and the remainder of the body, which serves as the drug reservoir. The parameters k_{eo} and K_{el} are the two elimination rate constants of ^{123}I-IAZA associated with the respective compartments, while Q, C_{in}, and C_o denote the blood perfusion to the hypoxic cells, and ^{123}I-IAZA arterial and venous blood concentrations in the hypoxic cell zone, respectively.

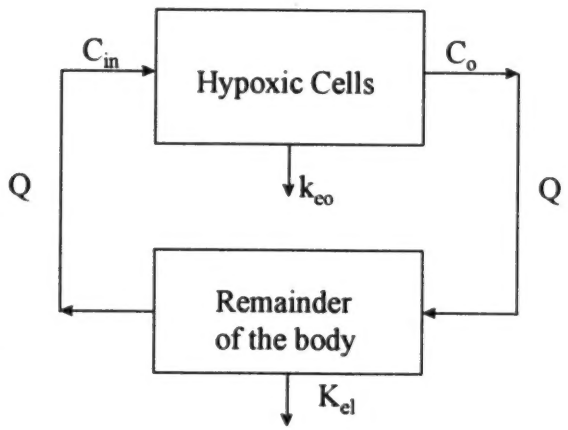

Figure 9.1 A two compartment blood-flow limited physiological pharmacokinetic model of ^{123}I-IAZA. For hypoxia modeling, only the hypoxic cells and the rest of the body need to be considered in this simplest form of the physiological pharmacokinetic model.

The modeling assumptions, based on Gibaldi and Perrier (1982), Holford and Sheiner (1981), and Harashima *et al.* (1985), are as follows:

(1) Only perfusion (Q) and/or transfer rate constant limit ^{123}I-IAZA delivery to the hypoxic cell; neither interstitium nor the cell membrane are rate limiting.

(2) There is instantaneous partition (P) of drug between hypoxic cells and emergent blood ($P = C_h \div C_o$, where C_h is the drug concentration in the hypoxic cells).

(3) ^{123}I-IAZA delivery to the hypoxic cells occurs via the blood only.

(4) Binding of ^{123}I-IAZA in blood is negligible so that the blood free (unbound) fraction of ^{123}I-IAZA available for tissue distribution is equivalent to the total blood concentration of ^{123}I-IAZA .

(5) The amount of radioactive metabolites leaving the effect compartment is negligible and can be disregarded from the overall total body mass balance.

Based on these assumptions, the differential mass balance equation for the amount (X_h) of ^{123}I-IAZA in the hypoxic cells effect compartment can be written as:

$$\frac{dXh}{dt} = Q \times (Cin - Co) - keo \times Xh \qquad (9.1)$$

9.2.2 Classical Pharmacokinetic Model of the Effect Compartment

This classical approach to hypoxia modeling is based on the work first described by Jusko (1971) for drugs undergoing covalent binding at the site of action. The irreversibility of the reductive metabolism of ^{123}I-IAZA, and the subsequent intracellular binding of these reduced metabolites in the hypoxic cells necessitate the assumption that the amount of drug in the effect compartment is negligible and does not affect the mass balance of the total drug in the body. Since the effect compartment acts as a "sink" for ^{123}I-IAZA, it is essential that the transfer rate constant into the effect compartment (k_{1e}) be very small, otherwise this assumption will not hold. All other assumptions for this model have been defined previously in section 9.2.1.

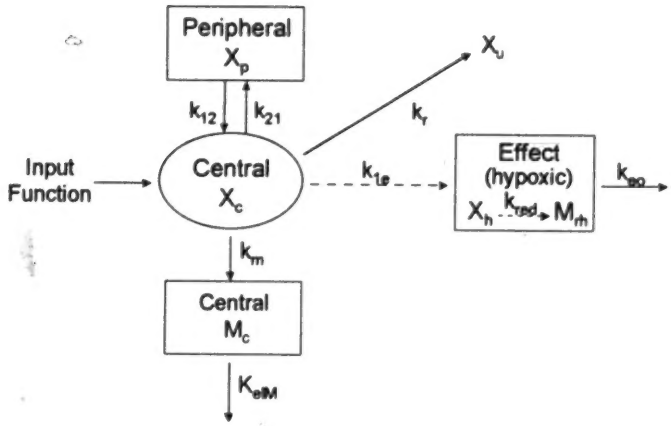

Figure 9.2 Classical PK/PD model to describe the profile of radioactivity in the hypoxic cells effect compartment following ^{123}I-IAZA administration.

Figure 9.2 is an expansion of the PK/PD model developed by Holford and Sheiner (1981). It permits the evaluation of the radioactivity profile in the hypoxic cells effect compartment following ^{123}I-IAZA administration. Since the blood profile of ^{123}I-IAZA after its i.v. administration can be described by a biexponential equation, the central and peripheral compartments for this drug are included in the model, with X_c and X_p representing their respective amounts of ^{123}I-IAZA. The single compartment containing radioactive metabolites (M_c) produced outside of the hypoxic effect compartment was included in the model to account for the contribution of these radioactive species to the background radioactivity against which the scintigraphic image intensity of the tumor will be compared. The only two species contributing to the effect compartment image intensity include ^{123}I-IAZA in that compartment (X_h) and the products of its reductive metabolism (M_{rh}). During image acquisition X_c, X_p and M_c only contribute to background radioactivity. The amount of drug in the urine (X_u) is not normally considered as part of the body, however, together with renally eliminated radioactive metabolites, it may be visible during imaging depending on bladder voiding time. The following rate constants are found in the model: k_{21} and k_{12} are the first order transfer rate constants between the central and peripheral compartments of ^{123}I-IAZA; k_m and k_u refer to ^{123}I-IAZA metabolic and renal elimination rate constants, respectively, and constitute K_{el} defined

in section 9.2.1; K_{elM} is the sum of renal and biliary excretion rate constants of the radioactive metabolites out of the system; k_{eo} is the elimination rate constant of the reduced metabolites of ^{123}I-IAZA from the effect compartment; k_{red} is the reductive rate constant of ^{123}I-IAZA in the hypoxic cells.

Based on the model in Figure 9.2, the following mass balance can be written for the amount of ^{123}I-IAZA in the effect compartment:

$$\frac{dXh}{dt} = k1e \times Xc - keo \times Xh \tag{9.2}$$

9.2.3 Merging of the Classical and Physiological Models

Although equation 9.1 and equation 9.2 have been derived from different modeling approaches, they each describe the differential mass balance for the amount of ^{123}I-IAZA in the effect compartment. Furthermore, each equation contains the term $k_{eo} \times X_h$. Combining the two equations

$$Q \times Cin - Q \times Co = k1e \times Xc \tag{9.3}$$

allows one to define the input function of ^{123}I-IAZA into the effect compartment in terms of its extraction (E) by the hypoxic cells, and thus to determine ^{123}I-IAZA clearance by these cells (Cl_{hy})

$$Clhy = \frac{Q \times (Cin - Co)}{Cin} = Q \times E \tag{9.4}$$

By directly substituting equation 9.4 into equation 9.3 it follows that

$$k1e \times Xc = Clhy \times Cin \tag{9.5}$$

As stated above, the main assumption of the link-model is that the amount of ^{123}I-IAZA removed by the hypoxic cells is negligible. C_{in} can, therefore, be estimated by the

blood ^{123}I-IAZA concentration at the venous sampling site in the arm. Since blood ^{123}I-IAZA represents the concentration in the central compartment, then

$$C_{in} = \frac{X_c}{V_c} \tag{9.6}$$

where V_c is the volume of distribution of ^{123}I-IAZA in the central compartment. Equation 9.5 can be further simplified to

$$Cl_{hy} = k_{1e} \times V_c \tag{9.7}$$

However, if assumption (2) from section 9.2.1 is true and there is instantaneous partition of drug between hypoxic cells and emergent blood, then at equilibrium the two transfer rates between the central and hypoxic cells compartment will be equal (Gabrielsson and Weiner, 1994), giving

$$k_{1e} \times X_c = k_{eo} \times X_h \tag{9.8}$$

Thus, equation 9.7 can be also expressed as

$$Cl_{hy} = k_{eo} \times V_h \tag{9.9}$$

Now that the two transfer rate constants can be expressed in terms of Cl_{hy}, or, more specifically, in terms of the product of Q and E, equation 9.2 can be rearranged to give

$$\frac{dX_h}{dt} = Q \times E \times \left(\frac{X_c}{V_c} - \frac{X_h}{V_h} \right) \tag{9.10}$$

Solving equation 9.10 produces the following relationship describing the change in the amount of ^{123}I-IAZA in the hypoxic cells with time:

$$Xh = \frac{Xo \times Q \times E}{Vc} \times \left[\frac{(k21-\alpha) \times e^{-\alpha \times t}}{(\beta-\alpha) \times \left(\frac{Q \times E}{Vh} - \alpha\right)} + \frac{(k21-\beta) \times e^{-\beta \times t}}{(\alpha-\beta) \times \left(\frac{Q \times E}{Vh} - \beta\right)} + \frac{\left(k21 - \frac{Q \times E}{Vh}\right) \times e^{-\left(\frac{Q \times E}{Vh} \times t\right)}}{\left(\alpha - \frac{Q \times E}{Vh}\right) \times \left(\beta - \frac{Q \times E}{Vh}\right)} \right] \quad (9.11)$$

where X_o is the radioactive dose, and the parameters V_c, α (distribution rate constant) and β (elimination rate constant) have been determined for ^{123}I-IAZA in healthy volunteers (ref: Chapter 6 of this thesis and Stypinski *et al.*, 1997submitted). All of the kinetic parameters are based on real data (no physical decay correction between sample collection and the time of injection), and therefore represent the effective kinetic parameters. Of the remaining parameters, it may be possible to determine Q with nuclear medicine imaging protocols, however, E and V_h are both cell-phenotype specific and require *in vitro* determination.

9.2.4 In Vitro Data

Hypoxic cells reductively metabolize ^{123}I-IAZA. It is therefore theoretically possible to determine their intrinsic clearance (Cl_{int}) *in vitro* and to use this information to predict their *in vivo* behavior (Houston, 1994). Studies of the initial binding rate of ^{125}I-IAZA to suspensions of EMT-6 tumor cell line (Mannan, 1991) and [^{3}H]FMISO uptake into V79 cell monolayers and spheroids (Casciari and Rasey, 1995) have been published. Since the uptake of these 2-nitroimidazoles is time dependent, the initial binding rate to the acid-insoluble fraction is probably the best estimate of the rate of irreversible removal (elimination) of IAZA from circulation by these cells.

The initial binding rate of ^{125}I-IAZA to the EMT-6 tumor cell line was reported by Mannan (1991) at four different ^{125}I-IAZA concentrations. Using these data, the Michaelis-Menten plot in Figure 9.3 was constructed. Although the plateau was never reached, a relatively good fit of the data was achieved with V_{max} of 650 pmol/10^6 cells/h and K_m of 26 μmol/L, respectively. Using the relationship

$$Clint = \frac{Vmax}{Km} \quad (9.12)$$

Cl_{int} was determined to be 0.000417 mL/10^6 cells/min (0.417 mL/min per 1 g of hypoxic cells, assuming 1 g contains 10^9 cells).

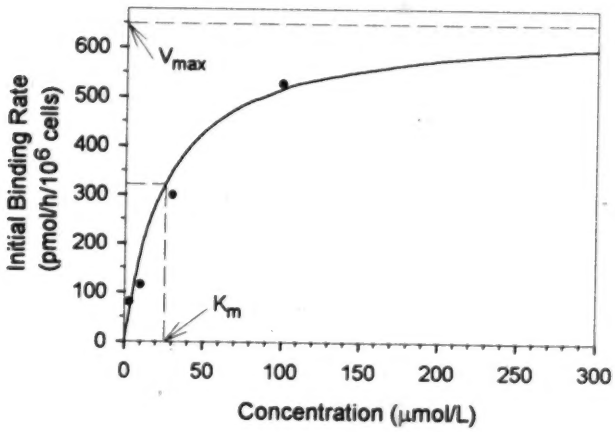

Figure 9.3 Michaelis-Menten plot of the initial binding rate of ^{125}I-IAZA to the EMT-6 tumor cell line. The maximum rate V_{max} is fixed at 650 pmol/10^6 cells/h while the Michaelis constant K_m is fixed at 26 μmol/L.

The tumor perfusion value used in the simulation was chosen as 0.2 mL/min/g, which is the mean of the 0.03 to 0.73 mL/min/g range reported by other investigators (Kallinowski *et al.*, 1991; Endrich *et al.*, 1979; Casciari *et al.*, 1995). Since we have assumed negligible binding of ^{123}I-IAZA in blood, then the hypoxic cells extraction ratio, determined by

$$E = \frac{Clint}{Q + Clint} \qquad (9.13)$$

was estimated to be 0.67 for the 0.2 mL/min/g blood flow, but could vary from 0.93 to 0.36 through the 0.03 to 0.73 mL/min/g range of perfusion values. Substitution of the median values of Q and E into equation 9.4 gives a Cl_{hy} value of 0.135 mL/min/g of hypoxic cells.

Efflux of radioactivity from the EMT-6 hypoxic cell line is the final parameter which determines the V_h of this cell line. Although efflux in this cell line has not been measured for ^{125}I-IAZA, it has been determined for [^{3}H]FMISO in V79 cell monolayers (Casciari and Rasey, 1995). There are indications that at least for [^{3}H]FMISO there may be some differences in the efflux of activity between the two cell lines (Rasey *et al.*, 1990), however, for the purpose of the simulation the assumption was made that in respect to this characteristic the two cell lines and the two compounds behave identically. Consequently, the efflux is bi-phasic with 36 % of activity irreversibly bound and eliminated with a 13.2 h half-life of the ^{123}I isotope, while the remaining 64 % diffuses out of the cells with a 50 min effective half-life.

9.3 Computer Simulations

All computer simulations were generated using transform functions (SigmaPlot[8] v.3). Modeling of the effect compartment was performed using equation 9.11 with the E and Q values as determined in section 9.2. The parameters V_c, α and β of ^{123}I-IAZA have been determined in healthy volunteers (Stypinski *et al.*, 1997submitted), and are assumed to be unchanged in patients with hypoxic tissue. Since the hypothetical tumor mass modeled was 200 g, the activity in a 200 mL blood pool was used as a reference for normal (i.e. no hypoxia) radioactivity disposition profile. The %ID activity in this 200 mL blood pool was determined based on the disposition characteristics of total radioactivity in blood of healthy volunteers following ^{123}I-IAZA administration.

Figure 9.4 shows three simulations of expected percent injected dose uptake into three identical 200 g tumors varying only in the homogeneous hypoxic fraction. In these examples it is assumed that radioactivity partitions into the normoxic remainder of the tumor cells to the same extent as it does in the blood, making a 200 mL blood pool the reference point for hypoxia uptake. Thus, the scintigraphic image intensity of a tumor at any time after dose administration is determined only by the number of hypoxic cells in that tumor volume.

By using a convenient imaging time, such as eight hours after ^{123}I-IAZA administration, the percent hypoxia in the tumor can be determined by its relative uptake of radioactivity. Figure 9.5 shows that, in an ideal scenario, the relationship between these two parameters will be linear. Theoretically, a range of values between

[8] Copyright 1986-1995 Jandel Corporation

0 to 100 % hypoxic fraction can be accommodated by the model, since even at 100 %, the fundamental assumption of negligible dose uptake into the effect compartment still holds.

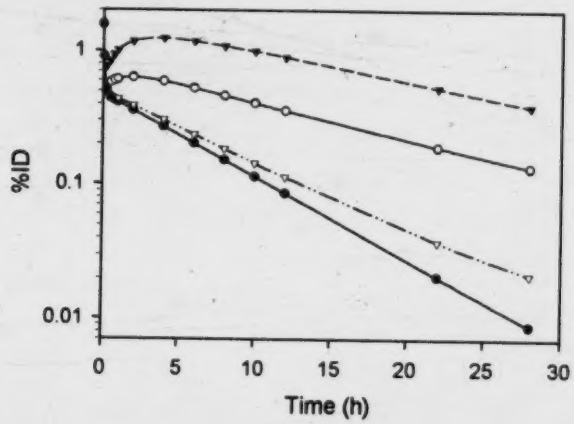

Figure 9.4 Temporal change in the percent injected dose in a 200 mL blood pool (●) and in three hypothetical 200 g tumors with varying hypoxic fractions: (▽) 1 %, (O) 10 % and (▼) 30 % of tumor cells are hypoxic. Partitioning of activity between normoxic cells and blood is assumed to be one.

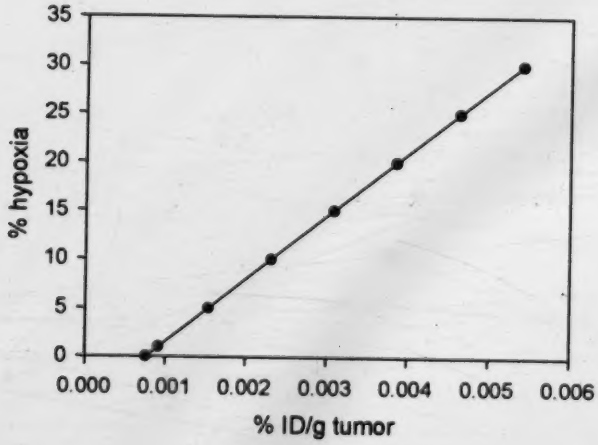

Figure 9.5 Graded response intensity (●) in a hypothetical homogeneous tumor at eight hours after ^{123}I-IAZA administration to the patient.

9.4 Discussion

The compartmental link-model of ^{123}I-IAZA transport and retention described above is general enough to be applicable to a variety of conditions characterized by vascular insufficiencies. The pivotal point of the model is that only the uptake in the hypoxic cells is modeled and not the entire ROI (i.e. tumor). The goal is to predict the maximum potential uptake (maximum potential image intensity) in a completely hypoxic ROI (100 % hypoxic fraction), and then downgrade the fraction of hypoxic cells in the ROI based on the actual image intensity. The other major characteristic is that the real kinetic parameters of ^{123}I-IAZA serve as the input function into the hypoxic cell compartment, as opposed to reliance on total radioactivity kinetics. Since total radioactivity includes the radiopharmaceutical and all of its radioactive metabolites, total radioactivity can only be used as the input function in two instances: when there is either no metabolism or no accumulation of radioactive metabolites.

Since the reference region in this model is the blood pool, a blood sample must be collected at mid-point of the image acquisition. Alternatively, a non-accumulating normoxic ROI (i.e. muscle) may be substituted, provided its PK profile can be shown to parallel that of blood. The advantages of using this technique would include no need to collect and analyze the patient's blood sample and, for a compound with V_{ss} < TBW, the tumor-to-normoxic tissue ratio will be higher than the T:B ratio.

Although radioactive metabolites of ^{123}I-IAZA have been shown to have an elimination half-life comparable to that of ^{123}I-IAZA, resulting in some metabolite accumulation in the patient, the kinetics of ^{123}I-IAZA are linear and, therefore, the relationship between ^{123}I-IAZA, its metabolites, and total radioactivity can be predicted as seen in Table 6.4 of this thesis. Consequently, regional T:B comparison can be made directly once pixel activity in a scintigraphic image is correlated to DPM. This can be done either by *in vitro* imaging of a known amount of ^{123}I activity followed by aliquot gamma well-counting, or directly in the patient by whole body imaging immediately after dose administration.

One of the assumptions of this effect compartment model is that neither the tumor vascular endothelium nor cell membrane pose permeability barriers for ^{123}I-IAZA. Casciari *et al.* (1995) have included separate cellular and interstitial compartments in their model. Since Cl_{int} for our model was determined in intact EMT-6 cancer cells, cellular permeability did not pose a major concern. However, tumor vascular

endothelium is a major obstacle to various treatments and is becoming a target of novel strategies in cancer research (Molema *et al.*, 1997). While tumor blood vessels are generally more porous and permeable than normal tissues, tumor vascular pressures tend to be lower and interstitial pressures often higher than in normal tissues. Furthermore, these pressure gradients are not uniform throughout the tumor. Tumor vasculature is currently considered to be of particular concern for the development of novel macromolecular drug delivery systems, however, there are no indications that it poses a permeability barrier for 2-nitoimidazoles. In addition, ^{123}I-IAZA has a relatively long elimination half-life, and, with its blood concentration decreasing slowly, any concentration gradients between blood and tissue should be minimal. There is evidence, however, that for certain 2-nitroimidazoles pH-gradients between cells and interstitium may exist (Stratford, 1992). For example, for the basic radiosensitizer pimonidazole, the acidic intracellular environment of hypoxic cells resulted in cellular trapping and an intracellular:extracellular concentration ratio of 3 (Dennis *et al.*, 1985).

In the PK/PD model defined in Figure 9.2, both X_h and M_{rh} contribute to the scintigraphic image intensity. However, in equation 9.11 we have only modeled ^{123}I-IAZA without any reference to its cellular biotransformation rate (k_{red}) or the radioactive metabolites (M_{rh}) themselves. The reason for the omission of these parameters from the mass balance of radioactivity in the effect compartment stems from equation 9.4 and the well-stirred model of organ clearance. According to the well-stirred model, E can be defined as the ability of the hypoxic cells to extract ^{123}I-IAZA. Thus, we are only concerned with ^{123}I-IAZA going into (C_{in}) and out of (C_o) the effect compartment, plus any radioactive metabolic degradation products of ^{123}I-IAZA leaving the hypoxic effect compartment at a measurable rate $X_h \times k_{eo}$. Therefore, the cellular bioreduction and binding dynamics are irrelevant, for as long as there is a signal from the hypoxic cell, it is immaterial from which reductive metabolite it originates. Although physiologically the intracellular M_{rh} products exist as separate entities, mathematically their radioactivity contribution can still be considered a part of X_h until they diffuse out of the hypoxic cell. Equation 9.11 actually describes the uptake and bioreductive retention of radioactivity following ^{123}I-IAZA administration, and the term X_h, which can be directly determined from the scintigraphic image intensity, may be more appropriately defined as the fraction of the radioactive dose retained by the tumor volume.

As bioreduction and intracellular binding determine k_{eo} and can both be phenotype-specific, they can potentially lead to unacceptable variability in tumor response that may not originate from variability in oxygen concentration alone. Different cell lines have been shown to have variable uptake and efflux characteristics for 2-nitroimidazoles (Mannan, 1991; Casciari and Rasey, 1995; Rasey *et al.*, 1990). It is also well known that tumors tend to acquire more chromosomal aberrations as they progress (Buick and Tannock, 1992). Mutation can lead to the formation of subclones with variable activities of bioreductive enzymes and/or altered types and concentrations of intracellular components to which reduced 2-nitroimidazoles can bind. As a result, the hypoxic cells derived from different subclones would have different retention characteristics for agents such as ^{123}I-IAZA and its reduced metabolites. The variable levels of enzymes and intracellular components involved in biotransformation and intracellular binding may, in part, explain the noticeable differences in retention of hypoxic cell markers in tumors of different origins, or even between the primary tumor and its different metastases, as shown through numerous examples in the literature (Urtasun *et al.*, 1996; Parliament *et al.*, 1992; Koh *et al.*, 1991; Koh *et al.*, 1995).

The potential problem associated with variable tumor metabolic factors unrelated to oxygenation status have also been recognized by other investigators (e.g. Raleigh *et al.*, 1996; Casciari *et al.*, 1995). Casciari *et al.* (1995) have attempted to derive a perfusion and permeability independent "global reaction rate constant" (K_A) which would be a function of intracellular oxygen concentration. Those authors have suggested that K_A provides a much better indicator of tumor oxygenation status than the tumor to blood ratio, and therefore it is "K_A parametric imaging" that will be the basis of quantitative estimates of radiobiologically hypoxic fraction. However, while theoretically attractive, upon closer examination K_A is actually nothing more than "formation" intrinsic clearance (i.e. the negative of Cl_{int}) as defined in equation 9.12. The Michaelis-Menten constant, K_M, originates from the schematic model of boireductive reaction shown in Figure 9.6 and is derived as

$$K_M = \frac{k2 + k3}{k1} \qquad (9.14)$$

Since k_2 is the constant directly influenced by the intracellular oxygen concentration; a doctrine on which the whole theory of the selectivity of 2-nitroimiadazoles for hypoxic cells rests, clearly Cl_{int} is related to the intracellular oxygen concentration as well. Not only does this make K_A a function of cellular reductive potential, which these same investigators have already shown to be phenotype-specific (Rasey *et al.*, 1990; Casciari and Rasey, 1995), but it also makes it extremely unlikely that K_A, like Cl_{int}, would be readily estimated *in vivo* (Houston, 1994), especially in the heterogeneous environment found in tumors.

$$RNO_2 \underset{k_2}{\overset{k_1}{\rightleftharpoons}} RNO_2^{\cdot-} \xrightarrow{k_3} RNHOH$$

Figure 9.6 A simplified scheme of the first major reversible and irreversible steps in the 2-nitroimidazole bioreductive pathway.

One significant issue addressed in the papers by Casciari *et al.* (1995) and Ng *et al.* (1995) deals with the differences in intracellular reduction of 2-nitroimidazoles within the range of oxygen concentrations defining the cell as hypoxic. While an ideal hypoxia marker would have a binding rate independent of oxygen concentration over a wide range of hypoxia (Wiebe and Stypinski, 1996), all hypoxia markers currently under investigations appear to bind at a rate dependent on oxygen concentration. Fortunately, it has been shown that the reductive potential of ^{123}I-IAZA, as determined by its initial binding rate (Mannan, 1991), is relatively consistent at least up to the 0.5 % oxygen concentration, at which it is generally accepted that the oxygen effect is at half of its maximum sensitizing effect (Hill, 1992). Such is not the case for hypoxic myocardium uptake of the ^{99m}Tc-labeled BMS-18132, where the authors have reported a sigmoidal relationship between perfusate oxygen level and the fractional tissue retention of the marker (Ng *et al.*, 1995).

However, the goal is to determine the fraction of hypoxic cells that are below a certain oxygen concentration in a region of a tumor. Considering the current imaging technology it is unlikely that we will be able to correlate the signal intensity to the oxygen concentration in a single cell in the near future. Thus, until an all-or-none type

of hypoxia marker is discovered, at best we can determine the mean volume of distribution of the imaging agent in the tissue of interest. From that, it will have to be decided whether the %ID accumulated in excess of that expected in a normoxic tissue is localized in a few very hypoxic cells or in many slightly hypoxic cells. This decision could be based on correlation studies between hypoxia marker uptake and oxygen electrode measurements in accessible tumors.

Another problem associated with hypoxia modeling relates to perfusion measurements in the hypoxic area. Generally, tumor perfusion measurement performed in the past in patients (e.g. Groshar *et al.*, 1993) are targeted at determining problems in vascular supply, as opposed to the measurement of the value of Q, which is defined as the blood flow through a region divided by the volume (or weight) of the region (Lassen and Henriksen, 1983). While estimates of tumor volume can be made by combining transverse images from computed tomography (Hammond *et al.*, 1984; Koh *et al.*, 1995), the erratic tumor vasculature which is responsible for the development of hypoxic regions necessitates making individual measurements of vascular density and blood flow in each patient. Such measurements have been made in experimental tumors in animals (Endrich *et al.*, 1979; Kallinowski *et al.*, 1991). Although simple in theory (Peters, 1993), they are too invasive and impractical in a clinical setting. Microvasculature density measurements of biopsy samples in humans (Raleigh *et al.*, 1996) can potentially be used as indicators of regional distribution of flow through the tumor. Unfortunately, such estimates may be of limited value in view of both the significant blood flow inhomogeneity in tumors (Endrich *et al.*, 1979) and the apparent lack of correlation between vascular density and hypoxia marker uptake (Cline *et al.*, 1994).

The interdependence of parameters Q, E and V_h, combined with their instability, particularly in tumors, makes it highly improbable that the actual relationship of tumor hypoxic fraction will be as "clean" as that shown in Figure 9.5. At best, we can hope that at least for tumors with the same tissue of origin the phenotype-specific intracellular variability in respect to bioreductive metabolic pathways will be minimal, allowing for *in vitro* determined Cl_{int} to serve as a good predictor of Cl_{int} *in vivo*. A reasonable relationship should then be possible, and would further improve with more accurate determination of the intra-tumor blood flow rate, and the presence and size of necrotic zones, intra-tumor abscesses or bone.

Depending on the cellular K_m value, large doses of low specific activity imaging agent may result in less of the radioactive dose entering the tumor than predicted by the effective compartment model. This would come as a consequence of non-linearity in the rate of removal of the agent by hypoxic cells at higher ^{123}I-IAZA blood concentrations. Linear conditions prevail only when C_{in} << Km, usually by 10 % or less. For IAZA and EMT-6 cells, where K_m is 26 μmol/L = 9.2×10^6 pg/mL, the concentration in blood would have to be higher than 9.2×10^5 pg/mL for non-linear transfer into the tumor to be taking place. Based on the ^{123}I-IAZA concentration in the 2 min blood sample in 6 healthy volunteers, the minimum dose required to give such concentration would be 14 mg of IAZA. In the case of IAZA, which has a very rapid distribution phase, such concentrations would not persist for long, and linear transfer conditions into the hypoxic cells would be established very quickly. However, for hypoxic cell lines with much lower K_m values, non-linear uptake conditions may occur at lower concentrations and persist for much longer, especially if they continue into the agent's elimination phase in blood. For IAZA concentrations considerably greater than K_m, the rate of removal of the drug by the hypoxic cells will occur at a constant rate V_{max} and be independent of IAZA blood concentration. In such cases a better signal may be elicited from the tumor hypoxic cells by giving a smaller chemical dose (higher specific activity) of ^{123}I-IAZA.

Although we have discussed mainly tumor hypoxia, as mentioned above, the model is applicable all types of tissue hypoxia. In fact, the relationship shown in Figure 9.5 may be far easier to derive in non-cancerous hypoxic tissue. These cells will be phenotypically stable, have more consistent mass and will be present in an environment where it is easier to determine perfusion. This would allow for much less variability in Cl_{int} and Q, giving a better defined E, leading to a stable predicted V_h for a completely hypoxic tissue. Once the V_h in a 100 % hypoxic tissue can be predicted, and the volume of distribution of ^{123}I-IAZA under normoxic conditions (0 % hypoxia) is known, we can determine the actual volume of distribution of ^{123}I-IAZA by determining the %ID in the target tissue, and from that the fraction of cells with the V_h volume of distribution.

The final consideration in hypoxia modeling is the choice of the optimal imaging time for the diagnosis. The limits are always set by the two competing elimination routes of a radiopharmaceutical, namely, the physiologic elimination of the radioactive

components and the physical decay of the isotope. The general assumption is that for both an optimal tumor to blood ratio and the best counting statistics, the determination should be made after a minimum of three elimination $t_{1/2b}$ (Parliament *et al.*, 1992), but within one $t_{1/2p}$ of the radiolabel. This means that either the radiopharmaceutical must have a very short elimination half-life of total radioactivity, or that a radiolabel with a long decay half-life is needed. Neither scenario is ideal, as the former drives the input function into the effect compartment while the latter increases the radiation dose to the patient.

In fact, the generally accepted three biologic elimination half-lives rule is probably too stringent. The reason for waiting the $3 \times t_{1/2b}$ before imaging comes from the expectation that by that time the transfer of the radiopharmaceutical from blood into the effect compartment will become negligible. Thus, by that time, the accumulation in the effect compartment will plateau, and, with only about 12.5 % of the chemical dose still remaining in the body, the expected blood concentration should be sufficiently low to give a good T:B ratio. However, in our model, in the hypothetical 10% hypoxic tumor in Figure 9.4, a T:B ratio of 3 was already achieved within 8 hours of ^{123}I-IAZA administration. Yet, the elimination $t_{1/2b}$ of total radioactivity following ^{123}I-IAZA administration is 7.8 ± 1.3 h. The reasons for the discrepancies between the assumed and modeled imaging T:B fractions are rooted in the parameters describing both the input and elimination from the effect compartment, and in the total radioactivity kinetics determining the background radiation:

1. The efflux parameter (k_{eo}) determines the extent of accumulation in the effect compartment, and it is the difference between the α and β parameters and k_{eo}, that actually determines the T:B ratio. Thus, the smaller the k_{eo} the greater the degree of accumulation, however, since k_{eo} is determined by the parameters Q, E and V_h, tumor to tumor variability can be expected. If the efflux characteristics assumed in the model overestimate the actual fraction forming irreversibly bound reductive adducts, then the predicted T:B ratios would be artificially high.
2. Only radioactivity can be measured, and a plateau of radioactivity in the effect compartment does not exist. Figure 9.7 illustrates what happens when a first order physical decay of the isotope is superimposed on the time activity data in a hypothetical tumor from which there is no biologic efflux of radioactivity. The Q and E parameters are the same as those defined for the simulation in Figure 9.4;

the only parameter that does change with inclusion of physical decay is V_h. Further comparison between Figures 9.4 and 9.7 shows that the inclusion of biologic efflux parameters further decreases both the maximum %ID in the effect compartment and the time required to reach it. Since V_h depends on the effective value of k_{eo}, it is, again, the efflux from hypoxic cells that determines the T:B ratio.

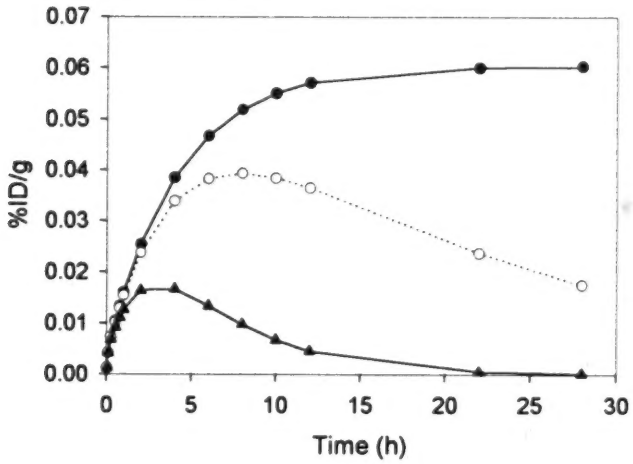

Figure 9.7 Effect of physical decay on the accumulation of radioactivity in a hypothetical 1 g mass of hypoxic EMT-6 tumor cells following ^{123}I-IAZA dose to a patient. Input parameters into the effect compartment are defined in the text. Biological efflux of radioactivity is assumed to be zero. Key: (●) no physical decay in the effect compartment; (O) 13.2 h decay of ^{123}I in the effect compartment; (▲) 1.83 h decay of ^{18}F in the effect compartment.

The final determinant of %ID/g is, of course, the hypoxic fraction of the tumor. While it may be possible to image tumors with higher hypoxic fractions earlier, low degree of hypoxia may not become apparent until at least three biologic half-lives of total radioactivity have passed. Consequently, while 8 h imaging may be an acceptable standard imaging protocol with ^{123}I-IAZA for most tumors, tumors with no accumulation at 8 h should probably be re-imaged at 24 h to eliminate the possibility of the presence of low hypoxic fraction.

9.5 References

Buick RN, Tannock IF. Properties of malignant cells. In: The basic science of oncology. Tannock IF, Hill RP (editors). 2nd ed. New York: McGraw-Hill, Inc.; 1992. pp. 139-53.

Casciari JJ, Graham MM, Rasey JS. A modeling approach for quantifying tumor hypoxia with [F-18]fluoromisonidazole PET time-activity data. Med Phys 1995;22:1157-39.

Casciari JJ, Rasey JS. Determination of the radiobiologically hypoxic fraction in multicellular spheroids from data on the uptake of [^{3}H]fluoromisonidazole. Radiat Res 1995;141:28-36.

Cline JM, Thrall DE, Rosner GL, et al. Distribution of the hypoxia marker CC1-103F in canine tumors. Int J Radiat Oncol Biol Phys 1994;28:921-33.

Dennis MF, Stratford MRL, Wardman P, Watts ME. Cellular uptake of misonidazole and analogues with acidic or basic functions. Int J Radiat Biol 1985;47:629-43.

Endrich B, Reinhold HS, Gross JF, Intaglietta M. Tissue perfusion inhomogeneiety during early tumor growth in rats. J Natl Cancer Inst 1979;62:387-93.

Gabrielsson J, Weiner D. Pharmacokinetic and pharmacodynamic data analysis. Concepts and applications. 1st. ed. Stockholm, Sweden: Apotekarsocieteten Swedish Pharmaceutical Press; 1994.

Gibaldi M, Perrier D. Pharmacokinetics. 2nd ed. New York: Marcel Dekker, Inc.; 1982.

Groshar D, McEwan AJB, Parliament MB, Urtasun RC, Golberg LE, Hoskinson M, Mercer JR, Mannan RH, Wiebe LI, Chapman JD. Imaging tumor hypoxia and tumor perfusion. J Nucl Med 1993;34:885-8.

Höckel M, Schlenger K, Mitze M, Schäffer U, Vaupel P. Hypoxia and radiation response in human tumors. Seminars in Radiation Oncology 1996;6:3-9.

Hammond ND, Moldofsky PJ, Beardsley MR, Mulhern CB. External imaging techniques for quantification of distribution of I-131 F(ab')$_2$ fragments of monoclonal antibody in humans. Med Phys 1984;11:778-83.

Harashima H, Sawada Y, Sugiyama Y, Iga T, Hanano M. Analysis of nonlinear tissue distribution of quinidine in rats by physiologically based pharmacokinetics. J Pharmacokinet Biopharm 1985;13:425-40.

Hill RP. Cellular basis of radiotherapy. In: The basic science of oncology. Tannock IF, Hill RP (editors). 2nd ed. New York: McGraw-Hill, Inc.; 1992. pp. 259-75.

Holford NHG, Sheiner LB. Understanding the dose-effect relationship: clinical application of pharmacokinetic-pharmacodynamic models. Clin Pharmacokinet 1981;6:429-53.

Houston JB. Utility of *in vitro* drug metabolism data in predicting *in vivo* metabolic clearance. Biochem Pharmacol 1994;47:1469-79.

Jusko WJ. Pharmacodynamics of chemotherapeutic effects: dose-time-response relationships for phase-nonspecific agents. J Pharm Sci 1971;60:892-5.

Kallinowski F, Wilkerson R, Moore R, Strauss W, Vaupel P. Vascularity, perfusion rate and local tissue oxygenation of tumors derived from *ras*-restransformed fibroblasts. Int J Cancer 1991;48:121-7.

Koh W-J, Bergman KS, Rasey JS, Peterson LM, Evans ML, Graham MM, Grierson JR, Lindsley KL, Lewellen TK, Krohn KA, Griffin TW. Evaluation of oxygenation status during fractionated radiotherapy in nonsmall cell lung cancers using [F-18]fluoromisonidazole positron emission tomography. Int J Radiat Oncol Biol Phys 1995;33:391-8.

Koh W-J, Rasey JS, Evans ML, Grierson JR, Lewellen TK, Graham MM, Krohn KA, Griffin TW. Imaging hypoxia in human tumors with [F-18]fluoromisonidazole. Int J Radiat Oncol Biol Phys 1991;22:199-212.

Lassen NA, Henriksen O. Tracer studies of peripheral circulation. In: Lecture notes in biomathematics. Tracer kinetics and physiologic modeling: theory to practice. Levin S, Lambrecht RM, Rescigno A (editors). 1983; St, Louis, Missouri. Berlin, Germany: Springer-Verlag; 1983. pp. 235-97.

Mannan RH. Novel non-invasive markers of tumor hypoxia. Edmonton, Alberta, Canada: *PhD. Thesis*, University of Alberta; 1991.

Molema G, de Leij LFMF, Meijer DKF. Tumor vascular endothelium: barrier or target in tumor directed drug delivery and immunotherapy. Pharm Res 1997;14:2-10.

Ng CK, Sinusas AJ, Zaret BL, Soufer R. Kinetic analysis of technetium-99m-labeled nitroimidazole (BMS-181321) as a tracer of myocardial hypoxia. Circulation 1995;92:1261-8.

Parliament MB, Chapman JD, Urtasun RC, McEwan AJ, Golberg L, Mercer JR, Mannan RH, Wiebe LI. Non-invasive assessment of human tumour hypoxia with ^{123}I-iodoazomycin arabinoside: preliminary report of a clinical study. Br J Cancer 1992;65:90-5.

Peters AM. A unified approach in quantification by kinetic analysis in nuclear medicine. J Nucl Med 1993;34:706-13.

Raleigh JA, Dewhirst MW, Thrall DE. Measuring tumor hypoxia. Seminars in Radiation Oncology 1996;6:37-45.

Rasey JS, Nelson NJ, Chin L, Evans ML, Grunbaum Z. Characteristics of the binding of labeled fluoromisonidazole in cells *in vitro*. Radiat Res 1990;122:301-8.

Stratford MRL. Pharmacokinetics and subcellular localization of radiosensitizers. Br J Cancer 1992;Suppl 24:100-4.

Stypinski D, Wiebe LI, McEwan AJ, Tam YK, Mercer JR. Radiopharmacokinetics of ^{123}I-IAZA in healthy volunteers. 1997(Submitted).

Urtasun RC, Parliament MB, McEwan AJ, Mercer JR, Mannan RH, Wiebe LI, Morin C, Chapman JD. Measurement of hypoxia in human tumours by non-invasive spect imaging of iodoazomycin arabinoside. Br J Cancer 1996;74 (Suppl. 27):S209-12.

Wiebe LI, Stypinski D. Pharmacokinetics of SPECT radiopharmaceuticals for imaging hypoxic tissues. Quarterly Journal of Nuclear Medicine 1996;40:270-84.

10. General Discussion and Conclusions

It was recognized prior to the present investigation that in both humans and animals some metabolism of $^{123/125}$I-IAZA is taking place, however, its extent went undetermined. The initial analysis of tracer kinetics following ^{123}I-IAZA administration in three cancer patents (Parliament *et al.*, 1992) resulted in overestimation of both the distribution and elimination half-lives, thyroid uptake and the fraction eliminated by hepatobiliary excretion. In addition, it was estimated that due to the long $t_{1/2b}$, the optimal imaging time for patients was ≥ 24 h after ^{123}I-IAZA administration, by which time the count rate was so low that the image quality was compromised. This combination of long elimination half-life and poor image quality are considered serious problems for a diagnostic radiopharmaceutical. This current study was initially based on the observation that in the Parliament study (Parliament *et al.*, 1992) the single patient with cancer who was renally compromised (S_{cr} = 165 μmol/L) at the time of imaging with ^{123}I-IAZA had an elimination half-life more than twice that of the other two patients who had normal renal function. Thus, it was hypothesized that the contribution of hepatobiliary excretion to total body clearance may have been overestimated, and since the data for this patient had been included in the published mean elimination half-life of ^{123}I-IAZA (Parliament *et al.*, 1992; Urtasun *et al.*, 1996), the actual elimination half-life may be, in fact, much shorter.

The study began by first developing a sensitive, specific and convenient assay which would allow quantification of ^{123}I-IAZA in blood and urine samples. The assay was based on the addition of non-radiolabelled IAZA (internal standard) to the blood and urine samples containing $^{123/125}$I-IAZA, allowing for UV identification of the appropriate HPLC peak, followed by highly sensitive gamma radiometry of the radiolabelled species. Although dependent on the specific activity of the administered dose, in this study the lowest ^{123}I-IAZA concentration detected by the assay within the set statistical confidence limits was 7.46 pg (21 fmol) per mL of serum.

Once the assay was developed, its performance was first evaluated in an animal model. Sprague-Dawley rats were chosen, since this strain has been used in the pre-clinical imaging protocols with ^{125}I-IAZA (McEwan *et al.*, 1996). Due to the routine use of anesthetics to restrain animals during imaging, the study was designed to evaluate the effects of methoxyflurane anesthesia on tracer kinetics and ^{123}I-IAZA

pharmacokinetics. The results were somewhat surprising, in that while there were no discernable differences in tracer kinetics, the total body clearance of ^{125}I-IAZA was almost 3.5 times lower in the anaesthetized animals than in the recovered group, with no apparent change in the V_{ss}. In rats, ^{125}I-IAZA has perfusion-dependent clearance which is sensitive to changes in perfusion and cardiac output induced by anesthetics. Total radioactivity elimination, on the other hand, is capacity-limited, and insensitive to perfusion changes. While the anesthetic-dependent decrease in the clearance of ^{125}I-IAZA will result in a longer exposure of the anaesthetized animal to the parent compound, tracer kinetics would give no indication that any such change is taking place. These striking differences in the pharmacokinetic profiles of ^{125}I-IAZA between anaesthetized and non-anaesthetized animals brings into question the current practices of anaesthetizing animals during pre-clinical imaging studies, as false positive diagnoses may result. It should be pointed out, that in species with low total body clearance of radiolabeled IAZA, such as in humans, both tracer and IAZA clearance will be capacity-limited and the anesthetic effect should be insignificant. Moreover, patients are not routinely anesthetized during nuclear medicine procedures.

The findings of the human ^{123}I-IAZA pharmacokinetic and dosimetry studies are even more important:

1. The elimination half-life of ^{123}I-IAZA was shown to be three times lower than the original estimate, with the total radioactivity elimination half-life (4.90 ± 0.45 h) being exactly half of the originally predicted value.
2. Excretion into the bile and the GIT was found to be a minor route of elimination, accounting for approximately 8 % of the biological and 5 % of the radioactive doses in the volunteers who had collected their entire 28 h cumulative urine samples.
3. Thyroid uptake of radioiodine was negligible, and, in fact, in one of the volunteers the thyroid gland was not well outlined even on the 24 h image.
4. The radiation dosimetry from a clinical dose of ^{123}I-IAZA was very low, comparable to some routinely used ^{99m}Tc-labeled agents.
5. Despite its lipophilic nature, IAZA had a V_{ss} of about 88 % of total body weight, indicating that in humans it neither undergoes excessive non-specific binding in tissues nor in plasma, a concern which has been raised by some investigators (Chapman, *et al.*, 1996; Nunn *et al.*, 1995).

6. In humans both ^{123}I-IAZA and total radioactivity have capacity-limited clearance, and therefore exercising during ^{123}I-IAZA administration, a protocol which may become necessary for hypoxia imaging in cardiac patients, will not alter ^{123}I-IAZA pharmacokinetics nor tracer kinetics.

The pharmacokinetic and dosimetric data were also combined to develop a physiologically realistic kinetic link-model to predict tissue oxygenation status from the radioactivity level in a scintigraphic image of a tumor containing a radiobiologically hypoxic fraction. The model was general enough to be applicable to a variety of conditions characterized by vascular insufficiencies, and could also be used to determine the optimal imaging time for the diagnosis of tissue hypoxia. Based on the simulations, this model justifies a change in the current imaging protocol from 26 h (2 × $t_{1/2p}$ of ^{123}I) to 6.5 - 8 h (0.5 - 0.6 × $t_{1/2p}$ of ^{123}I), giving superior image quality and better counting statistics.

Based on its favorable dosimetry and biodistribution in humans, ^{123}I-IAZA has been shown to be a far more suitable contender for an "ideal" hypoxia diagnostic imaging agent than initially assumed. In fact, it is has much more suitable pharmacokinetic characteristics in humans than in the animal model used during its pre-clinical evaluation. Currently, further clinical studies are planned with ^{123}I-IAZA in cancer patients and in cardiac patients, and a study is being planned to validate the kinetic link-model proposed in this thesis. The tracer elimination characteristics also warrant a future study of the effect of renal insufficiencies on tracer kinetics, since ^{123}I-IAZA has potential applicability as a marker of diseases more commonly affecting the elderly segment of the population.

References

Chapman JD, Coia LR, Stobbe CC, Engelhardt EL, Fenning MC, Schneider RF. Prediction of tumour hypoxia and radioresistance with nuclear medicine markers. Br J Cancer 1996;74(Suppl. 27):S204-S208.

McEwan AJB, Skeith KJ, Mannan RH, Davies N, Jamali F, Wiebe LI. Hypoxia-targeted ^{123}I-iodoazomycin arabinoside imaging of the adjuvant arthritis in rat model. CANM Annual Scientific Meeting1996; Quebec City, PQ.

Nunn A, Linder K, Strauss WH. Nitroimidazoles and imaging hypoxia. Eur J Nucl Med 1995;22:265-80.

Parliament MB, Chapman JD, Urtasun RC, McEwan AJ, Golberg L, Mercer JR, Mannan RH, Wiebe LI. Non-invasive assessment of human tumour hypoxia with ^{123}I-iodoazomycin arabinoside: preliminary report of a clinical study. Br J Cancer 1992;65:90-5.

Urtasun RC, Parliament MB, McEwan AJ, Mercer JR, Mannan RH, Wiebe LI, Morin C, Chapman JD. Measurement of hypoxia in human tumours by non-invasive spect imaging of iodoazomycin arabinoside. Br J Cancer 1996;74 (Suppl. 27):S209-12.

11. Appendices

Appendix 1: Whole blood concentrations of total radioactivity, ^{125}I-IAZA and radioactive metabolites in anesthetized and non-anesthetized rats after ^{125}I-IAZA administration.

Time (min)	Total Rtadioactivity (%ID/g blood)						^{125}I-IAZA (%ID/g blood)					
	Rat #						Rat #					
	1.1	1.2	1.3	1.4	Mean	St Dev	1.1	1.2	1.3	1.4	Mean	St Dev
1	4.13E-01	2.82E-01	3.34E-01	2.67E-01	3.24E-01	6.59E-02	3.26E-01	2.45E-01	2.90E-01	2.25E-01	2.71E-01	4.52E-02
1.5	3.18E-01	2.40E-01	2.79E-01	2.61E-01	2.74E-01	3.32E-02	2.76E-01	2.13E-01	2.86E-01	2.07E-01	2.45E-01	4.15E-02
2	2.98E-01	2.37E-01	2.74E-01	2.48E-01	2.64E-01	2.70E-02	2.54E-01	1.84E-01	2.30E-01	1.94E-01	2.16E-01	3.24E-02
2.5	2.60E-01	2.28E-01	2.70E-01	2.34E-01	2.48E-01	2.01E-02	2.29E-01	1.80E-01	2.42E-01	1.93E-01	2.11E-01	2.93E-02
3	2.42E-01	2.19E-01	2.56E-01	2.33E-01	2.37E-01	1.58E-02	1.91E-01	1.74E-01	2.14E-01	1.82E-01	1.90E-01	1.69E-02
4	2.38E-01	2.32E-01	2.26E-01	2.13E-01	2.27E-01	1.04E-02	1.83E-01	1.76E-01	1.95E-01	1.79E-01	1.84E-01	8.34E-03
5	2.11E-01	2.08E-01	2.25E-01	1.92E-01	2.09E-01	1.34E-02	1.73E-01	1.61E-01	1.80E-01	1.71E-01	1.71E-01	8.01E-03
7	1.88E-01	1.90E-01	1.96E-01	1.80E-01	1.88E-01	6.57E-03	1.51E-01	1.47E-01	1.40E-01	1.63E-01	1.50E-01	9.71E-03
10	1.83E-01	1.62E-01	1.70E-01	1.71E-01	1.71E-01	8.56E-03	1.45E-01	1.31E-01	1.39E-01	1.55E-01	1.43E-01	1.02E-02
15	1.44E-01	1.50E-01	1.48E-01	1.35E-01	1.45E-01	6.75E-03	1.24E-01	1.24E-01	1.18E-01	1.27E-01	1.23E-01	3.56E-03
20	1.40E-01	1.50E-01	1.18E-01	1.38E-01	1.36E-01	1.35E-02	1.27E-01	1.11E-01	9.68E-02	1.26E-01	1.15E-01	1.44E-02
30	1.15E-01	1.42E-01	1.11E-01	1.32E-01	1.25E-01	1.40E-02	1.09E-01	1.14E-01	8.32E-02	1.07E-01	1.03E-01	1.37E-02
45	1.05E-01	1.34E-01	1.00E-01	1.13E-01	1.13E-01	1.48E-02	9.73E-02	9.43E-02	7.48E-02	9.49E-02	9.03E-02	1.05E-02
60	9.20E-02	1.20E-01	9.27E-02	1.10E-01	1.04E-01	1.37E-02	8.45E-02	8.18E-02	6.88E-02	9.34E-02	8.21E-02	1.02E-02
90	7.15E-02	1.06E-01	7.91E-02	9.21E-02	8.72E-02	1.51E-02	6.25E-02	7.94E-02	6.24E-02	6.22E-02	6.66E-02	8.55E-03
120	6.70E-02	9.77E-02	7.60E-02	8.84E-02	8.23E-02	1.35E-02	5.32E-02	6.00E-02	5.03E-02	5.68E-02	5.51E-02	4.23E-03

Table 11.1 Individual and mean concentrations of total radioactivity and ^{125}I-IAZA in anesthetized rats (group 1). All values represent percent injected dose per g of whole blood.

Time (min)	Total Rtadioactivity (%ID/g blood) Rat # 2.1	2.2	2.3	Mean	St Dev	^{125}I-IAZA (%ID/g blood) Rat # 2.1	2.2	2.3	Mean	St Dev
2.5	2.71E-01	2.73E-01	3.05E-01	**2.83E-01**	**1.91E-02**	2.22E-01	1.89E-01	2.17E-01	**2.09E-01**	**1.74E-02**
5	2.15E-01	2.03E-01	2.13E-01	**2.11E-01**	**6.48E-03**	1.38E-01	1.37E-01	1.44E-01	**1.39E-01**	**3.71E-03**
10	1.74E-01	1.52E-01	1.65E-01	**1.64E-01**	**1.10E-02**	1.12E-01	9.06E-02	1.09E-01	**1.04E-01**	**1.16E-02**
20	1.29E-01	1.16E-01	1.16E-01	**1.20E-01**	**7.79E-03**	7.04E-02	6.43E-02	6.91E-02	**6.79E-02**	**3.18E-03**
30	1.18E-01	9.74E-02	9.08E-02	**1.02E-01**	**1.39E-02**	6.36E-02	4.76E-02	5.06E-02	**5.40E-02**	**8.50E-03**
45	8.98E-02	7.94E-02	7.31E-02	**8.08E-02**	**8.43E-03**	4.40E-02	3.19E-02	3.26E-02	**3.62E-02**	**6.80E-03**
60	8.42E-02	7.04E-02	5.85E-02	**7.10E-02**	**1.29E-02**	3.42E-02	2.61E-02	2.34E-02	**2.79E-02**	**5.63E-03**
90	ND*	6.21E-02	4.25E-02	**5.23E-02**	**1.39E-02**	ND	1.43E-02	1.14E-02	**1.29E-02**	**2.06E-03**
120	5.37E-02	4.82E-02	3.54E-02	**4.58E-02**	**9.39E-03**	8.99E-03	9.72E-03	5.82E-03	**8.18E-03**	**2.07E-03**
210	2.92E-02	3.45E-02	2.61E-02	**2.99E-02**	**4.25E-03**	9.40E-04	1.97E-03	1.15E-03	**1.35E-03**	**5.44E-04**
300	2.50E-02	3.01E-02	ND	**2.76E-02**	**3.61E-03**	1.20E-04	4.40E-04	2.30E-04	**2.63E-04**	**1.63E-04**

*ND not determined

Table 11.2 Individual and mean concentrations of total radioactivity and ^{125}I-IAZA in non-anesthetized rats (group 2). All values represent percent injected dose per g of whole blood.

Group 1 Time (min)	Tot RA* (%ID/g)	^{125}I-IAZA (%ID/g)	Metab (%ID/g)	Group 2 Time (min)	Tot RA* (%ID/g)	^{125}I-IAZA (%ID/g)	Metab (%ID/g)
1	3.24E-01	2.71E-01	5.27E-02	2.5	2.83E-01	2.09E-01	7.38E-02
1.5	2.74E-01	2.45E-01	2.90E-02	5	2.11E-01	1.39E-01	7.13E-02
2	2.64E-01	2.16E-01	4.86E-02	10	1.64E-01	1.04E-01	5.99E-02
2.5	2.48E-01	2.11E-01	3.67E-02	20	1.20E-01	6.79E-02	5.21E-02
3	2.37E-01	1.90E-01	4.70E-02	30	1.02E-01	5.40E-02	4.79E-02
4	2.27E-01	1.84E-01	4.34E-02	45	8.08E-02	3.62E-02	4.46E-02
5	2.09E-01	1.71E-01	3.76E-02	60	7.10E-02	2.79E-02	4.32E-02
7	1.88E-01	1.50E-01	3.78E-02	90	5.23E-02	1.29E-02	3.94E-02
10	1.71E-01	1.43E-01	2.85E-02	120	4.58E-02	8.18E-03	3.76E-02
15	1.45E-01	1.23E-01	2.12E-02	210	2.99E-02	1.35E-03	2.86E-02
20	1.36E-01	1.15E-01	2.11E-02	300	2.76E-02	2.63E-04	2.73E-02
30	1.25E-01	1.03E-01	2.16E-02				
45	1.13E-01	9.03E-02	2.27E-02				
60	1.04E-01	8.21E-02	2.16E-02				
90	8.72E-02	6.66E-02	2.05E-02				
120	8.23E-02	5.51E-02	2.72E-02				

* total radioactivity

Table 11.3 Mean concentrations of total radioactivity, ^{125}I-IAZA and radioiodinated metabolites in anesthetized (group 1) and non-anesthetized (group 2) rats. All values represent percent injected dose per g of whole blood.

Appendix 2: Blood sample collection times and corresponding concentrations of ^{123}I-IAZA and total radioactivity in volunteers 1 through 6.

Sample #	Target Time (h)	Actual Time (h) V#1	V#2	V#3	V#4	V#5	V#6
1	0.017	0.040	0.046	0.027	0.049	NC*	NC
2	0.083	0.106	0.089	0.089	0.096	0.10	0.15
3	0.25	0.26	0.26	0.26	0.26	0.28	0.25
4	0.50	0.51	0.53	0.51	0.52	0.52	0.56
5	0.75	0.76	0.77	0.75	0.78	0.86	0.79
6	1.0	1.0	1.0	1.0	1.0	1.2	0.99
7	2.0	2.0	2.1	2.0	2.0	2.7	2.0
8	4.0	4.1	4.0	4.0	4.0	4.1	4.4
9	6.0	6.1	6.0	6.0	6.1	6.1	6.0
10	8.0	8.1	10.6	7.9	8.0	9.3	8.1
11	12.0	12.3	NC	12.0	12.0	12.1	12.0
12	22.0	22.0	22.6	22.0	22.2	22.8	22.0
13	28.0	28.0	27.8	28.0	28.0	27.7	28.0

*NC sample not collected

Table 11.4 Target and actual blood sample collection times for volunteers 1 – 6.

Sample #	^{123}I-IAZA (%ID/mL) V#1	V#2	V#3	V#4	V#5	V#6
1	2.97E-03	3.84E-03	8.40E-03	4.09E-03	NC*	NC
2	2.16E-03	2.77E-03	3.15E-03	2.40E-03	1.65E-03	2.30E-03
3	1.56E-03	1.86E-03	1.59E-03	2.18E-03	1.49E-03	2.07E-03
4	1.27E-03	1.38E-03	1.25E-03	2.08E-03	1.37E-03	1.81E-03
5	1.20E-03	9.99E-04	1.06E-03	1.89E-03	1.26E-03	1.87E-03
6	1.00E-03	9.44E-04	1.02E-03	1.79E-03	1.13E-03	1.74E-03
7	SD**	6.55E-04	8.44E-04	1.38E-03	9.34E-04	1.47E-03
8	5.20E-04	4.45E-04	3.93E-04	7.99E-04	5.77E-04	6.83E-04
9	3.84E-04	3.13E-04	2.52E-04	4.39E-04	4.24E-04	4.93E-04
10	2.71E-04	1.34E-04	1.81E-04	3.13E-04	1.90E-04	2.47E-04
11	7.97E-05	NC	4.90E-05	1.26E-04	1.23E-04	9.44E-05
12	9.00E-06	1.25E-05	4.00E-06	1.12E-05	1.22E-05	5.60E-06
13	4.80E-06	1.30E-06	7.00E-07	5.00E-06	3.70E-06	3.00E-07

*NC sample not collected
**SD sample damaged during processing

Table 11.5 ^{123}I-IAZA concentrations in blood samples of volunteers 1 – 6 following i.v. administration of ^{123}I-IAZA.

Sample #	Total Radioactivity (%ID/mL)					
	V#1	V#2	V#3	V#4	V#5	V#6
1	3.19E-03	4.96E-03	8.96E-03	4.07E-03	NC*	NC
2	2.57E-03	3.61E-03	3.23E-03	2.49E-03	1.75E-03	2.06E-03
3	1.64E-03	2.25E-03	1.85E-03	2.17E-03	1.52E-03	1.94E-03
4	1.61E-03	1.67E-03	1.50E-03	2.10E-03	1.33E-03	1.66E-03
5	1.46E-03	1.50E-03	1.38E-03	1.97E-03	1.23E-03	1.65E-03
6	1.38E-03	1.38E-03	1.23E-03	1.91E-03	1.27E-03	1.81E-03
7	1.32E-03	1.18E-03	1.12E-03	1.64E-03	1.01E-03	1.32E-03
8	8.63E-04	8.06E-04	6.31E-04	1.10E-03	8.95E-04	7.45E-04
9	6.68E-04	5.70E-04	4.55E-04	7.29E-04	6.23E-04	5.40E-04
10	5.46E-04	2.83E-04	3.03E-04	4.83E-04	4.93E-04	3.89E-04
11	2.40E-04	NC	1.49E-04	2.43E-04	2.42E-04	1.78E-04
12	7.49E-05	6.80E-05	4.34E-05	6.78E-05	7.70E-05	5.65E-05
13	4.08E-05	4.65E-05	2.03E-05	3.62E-05	4.07E-05	2.60E-05

*NC sample not collected

Table 11.6 Total radioactivity concentrations in blood samples of volunteers 1 – 6 following i.v. administration of ^{123}I-IAZA.

Appendix 3: Blood sample collection times and corresponding concentrations of ^{123}I-IAZA and total radioactivity in volunteers CV1, CV2 and CV3.

CV1			CV2			CV3		
Time (h)	123I-IAZA	Tot Rad	Time (h)	123I-IAZA	Tot Rad	Time (h)	123I-IAZA	Tot Rad
0.026	7.11E-03	8.94E-03	0.039	3.34E-03	3.39E-03	0.044	5.59E-03	6.09E-03
0.080	2.59E-03	3.27E-03	0.080	1.99E-03	1.78E-03	0.086	2.95E-03	3.59E-03
0.25	2.14E-03	2.45E-03	0.22	1.76E-03	1.59E-03	0.26	2.13E-03	2.36E-03
0.53	1.86E-03	2.12E-03	0.48	1.47E-03	1.38E-03	0.53	2.12E-03	2.21E-03
0.79	1.66E-03	1.88E-03	0.87	1.20E-03	1.27E-03	0.76	1.98E-03	1.89E-03
1.0	1.57E-03	1.76E-03	1.6	1.14E-03	1.02E-03	1.0	1.89E-03	1.86E-03
2.0	1.32E-03	1.60E-03	2.0	9.92E-04	8.85E-04	2.0	1.31E-03	1.49E-03
5.0	8.25E-04	1.00E-03	5.0	2.82E-04	5.35E-04	5.3	6.50E-04	8.74E-04
8.0	4.68E-04	5.70E-04	8.1	1.68E-04	2.82E-04	8.5	3.64E-04	5.58E-04
12.0	2.51E-04	3.69E-04	11.8	9.32E-05	1.64E-04	11.8	1.65E-04	2.74E-04
22.0	3.99E-05	9.72E-05	22.4	6.70E-06	4.79E-05	23.7	1.00E-05	4.91E-05
27.2		4.77E-05	28.1		2.57E-05			
45.4		7.60E-06						

Table 11.7 Total radioactivity and ^{123}I-IAZA concentrations in blood samples of volunteers CV1, CV2 and CV3 following i.v. administration of ^{123}I-IAZA during Bruce treadmill protocol.

Appendix 4: Fractional mean residence times used for calculation of dosimetry estimates in healthy volunteers after i.v. administration of ^{123}I-IAZA.

	MRTfr (h)									
Organ	V#1	V#2	V#3	V#4	V#5	V#6	CV1	CV3	**Mean**	**St Dev**
LLI	0.349	0.125	0.297	0.449	0.341	0.459	0.176	0.430	**0.328**	**0.124**
Small intestine	0.221	0.0793	0.188	0.284	0.216	0.291	0.112	0.273	**0.208**	**0.079**
ULI	0.428	0.153	0.364	0.549	0.418	0.561	0.216	0.527	**0.402**	**0.152**
Kidneys	0.340	0.220	0.324	0.231	0.392	0.421	0.322	0.374	**0.328**	**0.072**
Liver	0.518	0.686	0.555	0.666	0.546	0.548	0.439	0.762	**0.590**	**0.105**
Thyroid	0.0497	0.0496	0.0615	0.0286	0.0337	0.0229	0.0811	0.0369	**0.0455**	**0.0192**
RB	5.79	4.95	5.15	5.33	6.23	4.96	7.36	6.20	**5.75**	**0.83**

Table 11.8 Fractional mean residence times of total radioactivity in source organs and in the remainder of the body ROI following ^{123}I-IAZA administration.

Appendix 5: Consent form given to each volunteer prior to ^{123}I-IAZA administration.

Protocol Title

Blood and Urine Sample Analysis and Dosimetry After Intravenous Administration of ^{123}I-IAZA to Volunteers

(A Study to Measure the Distribution in the Body of a New Compound for Assessing the Amount of Oxygen in Tumors)

CONSENT FORM

This consent form, a copy of which has been given to you, is only a part of the process of informed consent. It should give you the basic idea of what the research project is about and what your participation will involve. If you would like more detail about something mentioned here, or information not included here, you should feel free to ask. Please take the time to read this carefully and to understand any accompanying information.

BACKGROUND INFORMATION

Doctors are currently testing a new scanning agent which they believe may be able to measure the levels of oxygen that are found in cancers. It is important to be able to measure these levels as it is believed that cancers which have very low levels of oxygen within them respond poorly to radiotherapy and to chemotherapy. This new scanning agent has so far been used in a number of patients, and has been shown to be effective in indicating those patients with very low levels of oxygen within them.

The scanning agent is a chemical compound that binds and becomes fixed in areas that have very low oxygen concentration. It is tagged with a small amount of a radioactive tracer which allows images to be taken in the same way as bone scans. The radioactive tracer, Iodine-123, is the same tracer that is used routinely in many nuclear medicine tests. Because IAZA is only concentrated in sites where oxygen concentrations are low, it is not expected that there will be any abnormal accumulation of this tracer in volunteers who have no disease.

The doctors involved with the development of this compound now wish to proceed to investigate how well this compound works in a much larger number of patients. To do this they are required to have the compound licensed by the Health Protection Branch in Ottawa.

PURPOSE OF STUDY

This is a research project which is designed to provide the additional information which is required for this submission to HPB. It is designed to calculate the precise dose of radiation that is delivered to the body following the injection of the compound, and to

measure the breakdown products of the compound directly from the blood and the urine. You have been asked to volunteer for this project as the information is required to be obtained from people who have no past history of cancer.

STUDY DESIGN

If you agree to participate in this study, you will be asked to attend the Cross Cancer Institute on 2 separate days. Hospitalization is not required.

At your first visit, usually on a Wednesday morning, you will have your age, weight and height recorded and will be asked several questions regarding your past medical history, and any medications that you have been or are currently taking. A blood sample (approximately 2 teaspoons) will be taken for laboratory testing. You will be given a drink of Lugol's solution, which is an agent to prevent your thyroid gland from receiving any of the injected substance. After going to the Day Care Unit to have an intravenous (I.V.) line set up, you will return to Nuclear Medicine, receive an injection of IAZA, and will have images taken on a special imaging machine immediately after the agent is administered.

You will be required to remain at the Cross Cancer Institute for approximately 9 hours on the first visit. During this time, additional images will be taken in Nuclear Medicine at 1-2, 3-4 and 6-8 hours after the administration of the imaging agent. Blood samples will be taken at the following time periods during the day:

1 minute	1 hour
5 minutes	2 hours
15 minutes	4 hours
30 minutes	6 hours
45 minutes	8 hours

A blood sample will also be taken at 9 p.m. that evening.

On the second visit, usually a Thursday morning, the last series of images will take place and a blood sample taken. On the evening of the second day, a blood sample will be taken.

As well, you will be asked to collect your urine in a special container provided to you for 36 hours after the injection.

Each of the series of images that are taken will take approximately 30 minutes.

COSTS

Parking at the Cross Cancer Institute is available in the attached parkade at a daily rate of $6.00 or $0.75 per half hour. These costs, as well as any meals or snacks or transportation to and from the hospital, will be your responsibility. If this is a problem

transportation to and from the hospital, will be your responsibility. If this is a problem for you, please notify the research team of your situation and alternatives may be arranged on your behalf. There will be no additional costs regarding the tests. You will be provided with an honorarium of $250.00 for participating in this study.

RISKS ASSOCIATED WITH THE STUDY

The amount of radioactivity with which you will be injected is considered safe; it is equivalent to the amount used in many routine nuclear medicine tests and is approximately equivalent to the amount of background radiation to which you would be exposed over a year from naturally occurring sources of radiation such as cosmic rays.

I-123 IAZA has now been safely used in over 40 patients at the Cross Cancer Institute with no adverse effects. Due to the experimental nature of this study, there is the potential for unknown side effects. You will also be provided with an information sheet about nuclear medicine tests. The nature of these tests is that the radioactive tracers leave the body by normal secretion and also by radioactive decay.

BENEFITS

Participation in this study will be of no personal benefit to you. However, based on the results of this study, it is hoped that, in the long term, larger clinical studies can be conducted and patient care can be improved.

If any new information becomes available during your participation in the study this will be explained to you by the investigator.

CONFIDENTIALITY

The IAZA has been developed by scientists and doctors at the Cross Cancer Institute and the Faculty of Pharmacy at the University of Alberta. Your records pertaining to this study at the Cross Cancer Institute will be made available to the Canadian Health Protection Branch, and to the Food And Drug Administration in the U.S.A. for quality control. Amersham International plc, a radiopharmaceutical company associated with our research may also be provided with the results of the dosimetry calculations and metabolic studies as it may help in the development of second generation compounds which we shall be developing with them. Strict confidentiality will be maintained. Any information used for scientific purposes will not reveal your identity. You will not be identified in any report or publication resulting from this study.

All material and data obtained from this study will be stored and may be used for future analysis without obtaining further consent from you. However, each study arising as a result of information obtained in this study will be submitted for ethics approval.

UNDERSTANDING OF PARTICIPANTS

My signature on this form indicates that I have understood to my satisfaction the information regarding my participation in the research project, and agree to participate as a subject. In no way does this waive my legal rights nor release the investigators, sponsors, or involved institutions from their legal and professional responsibilities.

I am free to withdraw from the study at any time. My continued participation will be as informed as my initial consent, so I am free to ask for clarification or new information throughout my participation.

I understand that Dr. A.J.B. McEwan may be reached during office hours at 492-8524 or 492-6907 and will answer any additional questions that I have about this research project. The Research Nurse assigned to this study, Ms. Gail Amyotte, can be reached at 492-7542. After working hours, the telephone number of the Cross Cancer Institute is 492-8771.

If at any time during the course of the study I feel that I have been inadequately informed of the risks, benefits, or alternatives, or that I have been encouraged to continue in this study beyond my wish to do so, I may contact the Chairman of the Alberta Cancer Board Research Ethics Committee (403) 482-9366.

A copy of this consent form will be given to me to keep for my records and future reference.

_____	_____
Name of Subject	Signature of Subject
_____	_____
Name of Witness	Signature of Witness
_____	_____
Name of Investigator	Signature of Investigator
_____	
Date	

Appendix 6: Instruction sheet supplied to each volunteer prior to the cardiac stress test study.

PROTOCOL FOR ^{123}I-IAZA STUDY FOR VOLUNTEERS
(CARDIAC STRESS EFFECT ON CLEARANCE PROFILE)

June-July 1996
by
Daria Stypinski
Home phone # 4817373
Office phone # 4924959
Lab phone # 4924494

Please note that this is an informal description of the protocol for the study of ^{123}I-IAZA biodistribution following exercise. This information is just to help you, the volunteer, to have a better understanding of what will be taking place, as the Consent Form which you were given describes a slightly different study. This current study is a continuation of the one described in the Consent Form, but with the following modifications:

TUESDAY (day before the study)

1. On Tuesday you will be required to register at the Cross Cancer Institute (CCI). Please bring your Alberta Health Care number, Social Insurance number and address. You will have to first register at the main reception desk, which is the big desk right in front of the main entrance to the CCI (from the University Avenue). If the receptionist has any difficulties finding you on her computer, please tell her that you are here for a drug study which will be taking place the next day in Nuclear Medicine.
2. Once you will get your red plastic ID card, proceed to the Nuclear Medicine department, which is located on the same floor as the main reception desk. There, you will need to pick up forms for your lab work, and these will be waiting for you in the Nuclear Medicine department (hopefully) at their main desk.
3. With the lab forms, you will next go to the Laboratory Medicine department, hand the forms to one of the lab techs and get your blood sample taken for CBC and total blood chemistry. Once this is done you are finished for the day.

WEDNESDAY (1st day of the study)

1. On this day I will meet with you at a designated time (before 9 AM) and at a location which is convenient and known to both of us. We will then proceed to a meeting with Dr. A. McEwan at the University of Alberta Hospitals in the Department of Radiology and Diagnostic Medicine. His office number at the U of A Hospitals is 2A2.42 and his telephone number is 492-6907. This meeting is scheduled to take place at 9 AM, and is intended to answer any questions you might have about the IAZA study. Please bring the Consent Form with you.
2. After this meeting we will go the Department of Cardiology at the hospital, which is just across from Radiology and Diagnostic Medicine. There, you will again be asked you for your Alberta Health Care number, Social Insurance number and address.
3. Next, in the Department of Cardiology, a technician will insert two IV lines into your arms (one in each arm). One of these lines will be temporary, and will be used to inject ^{123}I-IAZA. It will be removed right after the injection. The second line will be

used for the multiple blood sample collection, and will hopefully last for the next 36 hours. I will take a "blank" blood sample from this line right after it is inserted just to make sure that it is not resting against a valve.

4. While the technician is inserting the IV lines, she will also put cardiac leads on your chest. This means that you will have to remove your shirt, as the leads have to be placed directly on your skin.
5. While she is doing that, please remind her to give you a dose of Lugol's solution to block your thyroid from taking up free ^{123}I.
6. Once the IV lines and the cardiac leads are in place, your blood pressure will be measured, and you will be started on the treadmill. The protocol which will be followed is called "Bruce" protocol. Essentially, the speed of the treadmill will increase in three minute intervals until the desired heart rate for your age group is reached. At that time ^{123}I-IAZA will be injected, you will continue running for 1 more minute, and than you will stop and rest. All the leads will be taken off your chest, the temporary IV line will be removed and you will get ready to go over to the CCI for imaging.
7. The imaging protocol is a little different from the one described in the Consent Form. As soon as you will arrive at the department of Nuclear Medicine at the CCI, a SPECT image of your heart will be taken. This image is taken by two cameras which rotate around your chest while you are lying on the table. This procedure takes about 36 min.
8. Right after the SPECT imaging is finished a whole body image will be taken. This image is taken by the same machine, but the two cameras are positioned one right above you and one right below you, and they slowly slide along the length of your body. This procedure takes 30 min.
9. Once both imaging protocols are finished you will probably have a short break, but the technician will tell you the exact time when you will have to be back for the next series of images.
10. The next series of images will also include a SPECT and a whole body image. These will take the same amount of time as before. After they are finished, you will only have two more whole body (each 30 min) images on that day, and no more SPECT. Again the technician will tell you at what time to come back for imaging.
11. Through all these procedures I will also take some blood samples from you to determine the exact clearance of ^{123}I-IAZA and total radioactivity from your body. The blood samples will be taken at the following times after the injection of ^{123}I-IAZA: 1, 5, 15, 30 and 45 min, and 1, 2, 5, 8, 12, 22, 28 and 36 h. The 1 min sample will be taken by the cardiology technician while you are still on the treadmill. The 5 and 15 min samples will be taken by me at the U of A Hospitals. After the 15 minute sample we will walk over to the CCI together, where I will take the rest of the samples up to the 2 hour one.
12. The 5 hour sample will be taken by one of the Nuclear Medicine technicians, as by that time I will return to the Faculty of Pharmacy to start analyzing the earlier blood samples. Since the technicians are always very busy you will have to remind them to take your blood sample. Once I will know the exact time of injection of ^{123}I-IAZA, I will prepare a sheet for you with the times for all of the blood samples. I will also show you where all the Vaccutainer tubes for your blood samples are kept. These tubes must be used in the proper order since they all contain an internal standard and are pre-weighed. Each tube is numbered and also has the time (i.e. 5 h) for the sample to be taken written on it. The tubes are refrigerated prior to blood collection and 30 min after blood collection. If by any chance a sample is not taken at the

specified time, just put the exact time of the day (hour and minute) that the sample was taken right on the tube.

13. The 8 h and 12 hour blood samples will be taken by me at the Faculty of Pharmacy that evening.

THURSDAY (2nd day of the study)

1. In the morning you will proceed to the CCI where a 22 hour blood sample will be taken and the last (5th) 30 min whole body image will be taken.
2. After that, I will only need to see you to take 2 more blood samples that day; one at 28 hours and one at 36 hours post injection. Provided that the IV line still works, I will take these samples at the Faculty of Pharmacy.

FRIDAY

1. Sometime on Friday you will have to go back to the CCI to the Laboratory Medicine department for another blood test. We are required to do both a pre- and post-study blood analysis. There is no specific time for this, and the requisition forms will already be on file with the Laboratory Medicine department. After this you are completely finished with the study.

Here are few suggestions which you may find helpful:

a) bring something to read, since after the first very busy couple of hours you will have long breaks between imaging times.
b) it appears from our earlier study, that total radioactivity is eliminated from the human body with a half-life of 4.8 hours, and practically entirely in urine. This means that frequent voiding of the bladder, especially in the first several hours after injection will quickly decrease the radiation dose to your body, and especially to the bladder.
c) for the treadmill, you may want to wear comfortable shoes.
d) for imaging you will be asked to remove all jewelry and any pieces of clothing which contain metal, including belt buckles and pants with metal zippers. There are "hospital" clothes available at the CCI into which you will be asked to change, but if you prefer to wear your own things sweatpants may be a good idea.

This is as complete a description of the protocol as I can provide you with. If you have any other questions please contact me at one of the numbers on the top of the 1st page of this document.

Thanks,

Dana

Appendix 7: Summary of all the currently available effective pharmacokinetic parameters of ^{123}I-IAZA and total radioactivity in patients and volunteers.

	^{123}I-IAZA				Total Radioactivity			
Study Type	$t_{1/2e\alpha}$ (min)	$t_{1/2e\beta}$ (h)	V_{ss} (L/kg)	Cl_{TB} (mL /min)	$t_{1/2e\alpha}$ (min)	$t_{1/2e\beta}$ (h)	V_{ss} (L/kg)	Cl_{TB} (mL /min)
normal v. n = 6	5.3 ± 4.2	2.98 ± 0.4	0.716 ± 0.088	239 ± 48	4.6 ± 2.9	4.90 ± 0.45	0.746 ± 0.091	145 ± 17
cardiac stress v. n = 3	1.2 ± 0.15	3.26 ± 0.57	0.669 ± 0.14	185 ± 60	1.4 ± 0.28	4.83 ± 0.62	0.780 ± 0.21	135 ± 41
cancer p. n = 2[a,b]	-	-	-	-	6.83 ± 1.04	4.37 ± 0.02	0.810 1.34[c]	147 285[c]
cancer p. (pilot)[d] n = 1	12.2	2.28	1.01	310	26.5	4.82	1.04	150

[a] original data source: Parliament *et al.*, personal communications. Based on tracer kinetic analysis published in: Parliament MB, Chapman JD, Urtasun RC, McEwan AJ, Golberg L, Mercer JR, Mannan RH, Wiebe LI. Non-invasive assessment of human tumour hypoxia with ^{123}I-iodoazomycin arabinoside: preliminary report of a clinical study. Br J Cancer 1992;65:90-5.

[b] patient number 2 excluded due to insufficient renal function at the time of imaging (S_{cr} = 165 μmol/L).

[c] estimates for patients 6 and 9 provided separately due to large variability. Estimates for patient # 9 based on 213 MBq dose.

[d] data source: Stypinski *et al.* (unpublished), based on a pilot study in a single cancer patient, with blood samples collected at 0.11, 0.24, 0.51, 0.77, 1.16, 2.02, 3.17, 21.25, 23.17 and 25.25 h after ^{123}I-IAZA administration, and analyzed according to the procedure described in Chapter 4 of this thesis.

Table 11.9 Summary of all the currently available pharmacokinetic parameters of ^{123}I-IAZA and total radioactivity in patients with cancer (n = 3) and in healthy volunteers (n = 9). Parameters are based on effective half-life determinations (i.e. no decay correction).